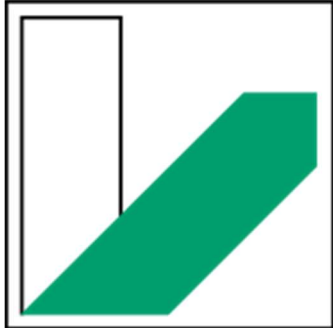


UNIVERSITÄT BAYREUTH
FACULTY OF BIOLOGY, CHEMISTRY AND GEOLOGY



**UNIVERSITÄT
BAYREUTH**

**Automated Oxystat Cultivation and
Transcriptomic Analysis of
Magnetosome Biosynthesis in
*Magnetospirillum gryphiswaldense***

zur Erlangung des akademischen Grades eines
Doktors der Naturwissenschaften (Dr. rer. nat.)
der Fakultät für Biologie, Chemie und Geowissenschaften

der Universität Bayreuth

vorgelegt von

Cornelius Nicolas Riese
aus Bünde

Bayreuth, Oktober 2022

Die vorliegende Doktorarbeit wurde in der Zeit von November 2016 bis November 2022 in Bayreuth am Lehrstuhl für Mikrobiologie unter Betreuung von Herrn Professor Dr. Dirk Schüler angefertigt.

Vollständiger Abdruck der von der Fakultät für Biologie, Chemie und Geowissenschaften der Universität Bayreuth genehmigten Dissertation zur Erlangung des akademischen Grades eines Doktors der Naturwissenschaften (Dr. rer. nat.).

Art der Dissertation: kumulative Dissertation

Dissertation eingereicht am: 13.03.2023

Zulassung durch die Promotionskommission: 05.04.2023

Wissenschaftliches Kolloquium: 09.11.2023

Amtierender Dekan: Prof. Dr. Cyrus Samimi

Prüfungsausschuss:

| | |
|-------------------------|-------------|
| Prof. Dr. Dirk Schüler | (Gutachter) |
| Prof. Dr. Matthias Noll | (Gutachter) |
| Prof. Dr. Klaus Ersfeld | (Vorsitz) |
| Prof. Dr. Ruth Freitag | |

„Am Anfang steht der Größenwahn, am Ende die Demut.“

-Julian Schnabel

Index

| | |
|--|------------|
| List of Publications | 5 |
| Manuscripts comprised in this thesis | 5 |
| Additional co-authored manuscripts originated during this study | 6 |
| Contributions to publications | 7 |
| Abbreviations | 8 |
| Abstract..... | 9 |
| Zusammenfassung | 11 |
| 1 Introduction..... | 13 |
| 1.1 <i>Magnetospirillum gryphiswaldense</i>: A model organism for magnetosome biomineralization | 13 |
| 1.2 Genetic and biochemical control of magnetosome biosynthesis in <i>M. gryphiswaldense</i> | 14 |
| 1.3 Genomic and transcriptional organization and regulation of magnetosome genes 16 | |
| 1.3.1 The Magnetosome Island (MAI) | 16 |
| 1.3.2 Generic pathways involved in magnetosome biosynthesis..... | 18 |
| 1.3.3 Regulation of magnetosome biosynthesis..... | 18 |
| 1.4 Magnetosomes in biotechnology: applications and production | 19 |
| 1.4.1 Potential applications of magnetosomes in biotechnology and biomedicine..... | 19 |
| 1.4.2 Cultivation of <i>M. gryphiswaldense</i> and production of magnetosomes: Previous approaches and their limitations..... | 20 |
| 1.5 Scope of this thesis..... | 22 |
| 2 Synopsis..... | 24 |
| 2.1 Chapter 1: An automated oxystat fermentation regime for microoxic cultivation and magnetosome production in <i>Magnetospirillum gryphiswaldense</i> | 26 |
| 2.2 Chapter 2: The complex transcriptional landscape of magnetosome gene clusters in <i>Magnetospirillum gryphiswaldense</i>..... | 28 |
| 2.3 Chapter 3: The transcriptome of <i>Magnetospirillum gryphiswaldense</i> during magnetosome biomineralization | 30 |
| 2.4 Chapter 4: Establishment of a T7-based expression system | 33 |
| 2.5 Conclusion and Outlook | 35 |
| 3 References..... | 38 |
| 4 Publications and manuscripts..... | 50 |
| Danksagung | 101 |
| (Eidesstattliche) Versicherungen und Erklärungen | 103 |

List of Publications

Manuscripts comprised in this thesis

Manuscript 1

An automated oxystat fermentation regime for microoxic cultivation of

Magnetospirillum gryphiswaldense

Cornelius N. Riese, René Uebe, Sabine Rosenfeldt, Anna S. Schenk, Valérie Jérôme,
Ruth Freitag and Dirk Schüler.

Microbial Cell Factories (2020) 19:206

doi: 10.1186/s12934-020-01469-z

Manuscript 2

The complex transcriptional landscape of magnetosome gene clusters in

Magnetospirillum gryphiswaldense

Marina Dziuba*, Cornelius N. Riese*, Lion Borgert, Manuel Wittchen, Tobias Busche,
Jörn Kalinowski, René Uebe and Dirk Schüler.

mSystems (2021) 6:e0089321

doi: org/10.1128/mSystems.00893-21

*These authors contributed equally

Manuscript 3

The transcriptomic landscape of *Magnetospirillum gryphiswaldense* during
magnetosome biomineralization

Cornelius N. Riese, Manuel Wittchen, Valérie Jérôme, Ruth Freitag, Tobias Busche,
Jörn Kalinowski and Dirk Schüler

BMC Genomics (2022) 23:699

doi: 10.1186/s12864-022-08913-x

Additional co-authored manuscripts originated during this study

Manuscript 4

Probing the nanostructure and arrangement of bacterial magnetosomes by small-angle
X-ray scattering

Sabine Rosenfeldt*, Cornelius N. Riese*, Frank Mickoleit, Dirk Schüler and Anna S.
Schenk.

Applied and Environmental Microbiology (2019) 85:e01513-19

doi: 10.1128/AEM.01513-19

*These authors contributed equally

Manuscript 5

Sesbanimide R, a novel cytotoxic polyketide produced by magnetotactic bacteria
Ram P. Awal, Patrick A. Haack, Chantal D. Bader, Cornelius N. Riese, Dirk Schüler
and Rolf Müller

mBio (2021) 12:e00591-21

doi: 10.1128/mBio.00591-21

Contributions to publications

Manuscripts 1: CNR, RU, VJ, RF and DS conceived and designed research. CNR, RU and SR performed experiments. CNR and RU performed seed-train standardization, oxystat fermentations and analyzed the data. SR performed SAXS measurements and CNR together with SR and ASS analyzed the data. CNR and DS analyzed the whole dataset and wrote the paper. All authors provided critical feedback and helped to shape the research, analysis and manuscript. All authors read and approved the final manuscript.

Manuscript 2: DS, MD and CNR conceived the study and designed the experiments. CNR, MW, TB, JK carried out the transcriptome analysis, MD and RU designed vectors for the bioluminescence reporter assay, MD generated plasmids and carried out the promoter evaluation. MD designed the promoter mutagenesis experiment, MD and LB generated and analyzed the promoter knockout mutants. MD analyzed the sequence conservation. MD, CNR and DS wrote the manuscript. All authors read and approved the final manuscript.

Manuscript 3: DS and CNR conceived the study. CNR, RF and VJ designed and performed the fermentation experiments for sample preparation. CNR, MW, TB, JK carried out the transcriptome analysis. CNR and DS wrote the manuscript. All authors read and approved the final manuscript.

Abbreviations

| | |
|-----------------|--|
| AAS | Atomic absorption spectroscopy |
| dO ₂ | Dissolved oxygen concentration |
| Feo | Magnetosome specific Fe ²⁺ transport system |
| Fnr | Fumarate and nitrate reduction regulator |
| GFP | Green fluorescent protein |
| IPTG | Isopropyl-β-D-thiogalactopyranoside |
| kb | kilobase pairs |
| MagOP | putative Magnetosome operon |
| MAI | Magnetosome island |
| Mam | Magnetosome membrane (gene and protein) |
| MgFnr | <i>Magnetospirillum gryphiswaldense</i> specific Fnr |
| MM | Magnetosome membrane |
| Mms | Magnetosome membrane specific (gene and protein) |
| MTB | Magnetotactic bacterium |
| OD | Optical density |
| PCR | Polymerase chain reaction |
| pO ₂ | Oxygen partial pressure |
| RBS | Ribosome binding site |
| RT-PCR | reverse transcription polymerase chain reaction |
| SAXS | Small-angle X-ray scattering |
| TEM | Transmission electron microscopy |
| TSS | Transcription start site |
| TTS | Transcription termination site |
| UTR | Untranslated region |
| WTSS | Whole transcriptome shotgun sequencing |

Abstract

In order to find their preferred growth conditions, the so called magnetotactic bacteria (MTB) evolved the ability to biomineralize membrane-enveloped magnetic nanoparticles for navigation along the Earth's magnetic field lines. Because of their unprecedented uniformity in size and shape, chemical purity of the magnetite crystal magnetosomes have become a model for bacterial organelle biosynthesis, biotechnology and synthetic biology. The investigation of the alphaproteobacterium *Magnetospirillum gryphiswaldense* as a model organism for the complex process of magnetosome biosynthesis led to the identification of >30 genes organized in five putative operons all located in the genomic magnetosome island, which exert tight control of magnetite biomineralization. However, the transcriptional organization and regulation of magnetosome gene clusters during magnetosome biosynthesis is only poorly understood. In addition, the influence of auxiliary metabolic processes and the effect of growth conditions on magnetosome formation and magnetite crystal maturation remains elusive.

To address these questions, highly controlled growth conditions are needed to ensure reproducible magnetosome biosynthesis. Hence, during the first part of this thesis, an automatic oxystat cultivation regime in a 3 L bioreactor was developed. The programmed automated cascade regulation enabled highly reproducible growth and analysis of magnetosome biosynthesis over a wide range of precisely controlled oxygen concentrations. The precise oxygen control resulted in improved properties as demonstrated by a combination of complementary analytical techniques including quantitative transmission electron microscopy (TEM) and small-angle X-ray scattering (SAXS). Additionally, based on the precise analysis of substrate consumption, fed-batch fermentation processes will result in higher cell and magnetosome yields.

The established oxystat regime was then utilized in the second part of the study for the comparative investigation of the global transcriptome during magnetosome formation. Up-to-date RNA-sequencing techniques including Cappable-sequencing, whole transcriptome shotgun sequencing and 3' end sequencing revealed (i) a much more complex architecture of the large magnetosome operons (MagOPs) and (ii) internal transcription start sites (TSS) originating from biologically meaningful promoters drive their proper transcription. Although different oxygen concentrations led

to differences in TSS detection, most of the magnetosome biosynthesis specific genes were expressed constitutively.

Furthermore, transcriptome-wide analysis showed that genes with direct or indirect function in respiratory processes were highly upregulated under magnetosome formation conditions, and a complex interplay between generic metabolic processes such as intracellular redox control and denitrification, and magnetosome biosynthesis was uncovered. The first global and comparative promoter analysis in an MTB during this study revealed that the transcriptional complexity of the magnetosome gene clusters depended on the applied oxygen conditions. Altogether, the results demonstrate that the transcriptional organization of magnetosome gene clusters is more complex than previously assumed.

In future, the gathered insights could be used for rational reengineering of synthetic magnetosome gene clusters for enhanced as well as inducible expression for higher magnetosome yields in homologous and potentially in heterologous hosts.

Zusammenfassung

Magnetotaktische Bakterien (MTB) haben die Fähigkeit entwickelt, entlang des Erdmagnetfeldes zu navigieren, um Sedimentzonen zu erreichen, die ihnen optimale Wachstumsbedingungen bieten. Dieses magnetotaktische Verhalten ist auf membranumhüllte magnetische Nanopartikel, die Magnetosomen, zurückzuführen. Aufgrund ihrer Uniformität, Monodispersität, chemischen Reinheit des Magnetitkristalls sowie ihres großen Potenzials in der biomedizinischen Anwendung sind Magnetosomen zu einem Modell für die Biosynthese bakterieller Organellen in der Biotechnologie und synthetischen Biologie geworden.

Als einer dieser Organismen wurde das Alphaproteobakterium *Magnetospirillum gryphiswaldense* zum Modellorganismus zur Erforschung des komplexen Prozesses der Magnetosomenbiosynthese. Es wurde ein hohes Maß an Regulation durch mehr als 30 Gene identifiziert, die in fünf mutmaßlichen Operons auf der chromosomalen Magnetosomeninsel organisiert sind. Die transkriptionelle Organisation und Regulation der Magnetosomenbiosynthese ist jedoch nur unzureichend verstanden, wodurch auch der Einfluss von Stoffwechselprozessen und Wachstumsbedingungen auf die Biomineralisation unbekannt bleibt.

Um diese offenen Fragen zu beantworten, ist eine reproduzierbare Magnetosomenbiosynthese notwendig, die nur durch hochgradig kontrollierte Wachstumsbedingungen zu gewährleisten ist. Daher wurde im ersten Teil dieser Arbeit zunächst ein automatisches Oxystat-Kultivierungsregime in einem 3 L-Bioreaktor mithilfe einer Sauerstoffkaskade entwickelt. Dies ermöglichte die Kontrolle des Sauerstoffs in einem weiten Sauerstoffbereich und damit ein reproduzierbares Wachstum. Durch Kombination komplementärer Analysetechniken, wie quantitativer Transmissionselektronenmikroskopie (TEM) und Kleinwinkel-Röntgenstreuung (SAXS) wurde gezeigt, dass die präzise Sauerstoffkontrolle zu einem homogenen Magnetitpartikeldurchmesser führte. Weiterhin könnten basierend auf der präzisen Analyse des Substratverbrauchs *fed-batch*-Fermentationsprozesse entwickelt werden, die in höheren Zell- und Magnetosomenausbeuten resultieren würden.

Das etablierte Oxystat-Regime wurde dann im zweiten Teil der Studie zur vergleichenden Untersuchung des globalen Transkriptoms während der Magnetosomenbildung genutzt.

Modernsten RNA-Sequenzierungstechniken, einschließlich *Cappable*-Sequenzierung, *Whole transcriptome shotgun sequencing* und 3'-Endsequenzierung, zeigten (i) eine komplexere Architektur von Magnetosomen-Operons (MagOPs) sowie (ii) Operon-interne *Transcription Start Sites* (TSS), die von aktiven Promotoren stammen. Obwohl die betrachteten Sauerstoffkonzentrationen zu Unterschieden im TSS-Nachweis führten, wurden die meisten Magnetosomenbiosynthese-spezifischen Gene konstitutiv exprimiert. Weiterhin zeigte die transkriptomweite Analyse, dass Gene mit direkter oder indirekter Funktion in Atmungsprozessen unter Magnetosomenbildungsbedingungen stark hochreguliert waren. Hier wurde ein komplexes Zusammenspiel zwischen Stoffwechselprozessen wie der intrazellulären Redoxkontrolle sowie der Denitrifikation und Magnetosomenbiosynthese aufgedeckt.

Die erste globale und vergleichende Promotoranalyse, die während dieser Studie in einem MTB durchgeführt wurde, zeigte, dass die transkriptionelle Komplexität der Magnetosom-Gen-Cluster von den Sauerstoffbedingungen abhängig sind. Zusammenfassend zeigen die Ergebnisse, dass die transkriptionelle Organisation und Regulation komplexer ist als bisher angenommen. In Zukunft könnten aufgrund der gesammelten Daten synthetische Magnetosomenoperons mit verbesserter und induzierbarer Expression entwickelt werden, die zu höheren Magnetosomenausbeuten in homologen und auch heterologen Wirtsorganismen führen könnte.

1 Introduction

1.1 *Magnetospirillum gryphiswaldense*: A model organism for magnetosome biomineralization

The magneto-responsive behavior of some aquatic bacteria, first described by Salvatore Bellini in 1963¹ and rediscovered in 1975 by Richard Blakemore², is based on the presence of membrane-enveloped magnetite (Fe₃O₄) or greigite (Fe₃S₄) crystals called magnetosomes. These are formed by all members of the highly diverse polyphyletic group of magnetotactic bacteria (MTB) for orientation along the Earth's magnetic field to find the favorable oxic-anoxic transition zone of their natural aquatic habitats^{3,4}. MTB are ubiquitously found in many freshwater and marine sediments, however they are difficult to cultivate in laboratory environments³. Among the few strains grown in axenic cultures are mostly members of the Alphaproteobacteria including the three best studied organisms *Magnetospirillum magneticum* AMB-1⁵, *M. magnetotacticum* MS-1⁶ and *M. gryphiswaldense* MSR-1⁷. Because of its rather simple cultivation, genetical accessibility, its relatively fast growth and high magnetosome yields, *M. gryphiswaldense* has emerged to the best studied model organism for magnetosome biosynthesis⁸. *M. gryphiswaldense* (Figure 1 A) was isolated from the muddy sediments of the small river Ryck near Greifswald⁷ and has a helical cell shape with a single flagellum at each pole^{7,9}. It can be grown chemoorganoheterotrophically by utilizing short organic acids as carbon and electron sources⁹ to relatively high cell densities under anoxic and microoxic conditions¹⁰. Although, *M. gryphiswaldense* is a microaerophilic organism, it exhibits relatively high oxygen tolerance and utilizes oxygen as electron acceptor for respiration and energy generation¹⁰. In the absence of oxygen, nitrate can be utilized for anaerobic respiration by denitrification¹¹. Nitrate is stepwise reduced to nitrite, nitrous oxide and nitrogen by the periplasmic nitrate reductase (NapAB), the Fe²⁺-nitrite oxidoreductase (NirS) and the nitric oxide reductase (NorBC), respectively.

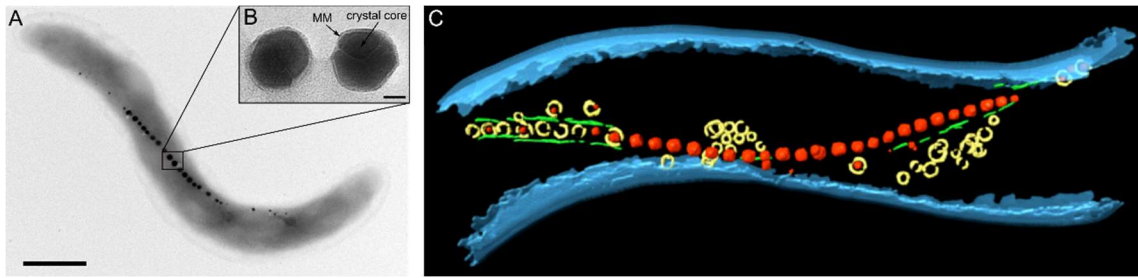


Figure 1: A) Transmission electron microscopy of *M. gryphiswaldense* B) Detailed view on two Magnetosomes with the Magnetosome Membrane (MM) and the magnetite crystal core indicated by black arrows (Article 4 modified). C) 3D rendering of a cell examined by cryo-electron tomography with the MM (yellow) surrounding the magnetite crystal core (red). The linear configuration of the magnetosomes is facilitated by the MamK filament (green) ¹².

Up to 60 magnetosomes per cell with monocrystalline chemically pure magnetite cores are synthesized under microoxic to anoxic conditions as explained below (see 1.2) (Figure 1 B + C) ^{3,10}. Their diameter can vary between 20 – 50 nm depending on the oxygen concentration ^{8,10,13}.

1.2 Genetic and biochemical control of magnetosome biosynthesis in *M. gryphiswaldense*

Magnetosome biosynthesis is a complex, stepwise process starting with the formation of a dedicated magnetosome vesicle, followed by uptake of iron into the lumen and biomineralization of chemically pure magnetite monocrystals with defined size and shape ^{8,14}. This process has been found to be orchestrated by Mam (magnetosome membrane), Mms (magnetosome particle membrane-specific) and Feo (magnetosome specific Fe^{2+} transport system) proteins. Magnetosome vesicle formation begins by introducing curvature into the cytoplasmic membrane caused by a network of distinct Mam proteins (Figure 2). Interactions between MamBEILMOQ, where MamB serves as essential landmark protein, are thought to be responsible for rapid magnetosome membrane invagination to form the magnetosome lumen ^{8,15,16}. Ferrous iron (Fe^{2+}), taken up from the environment by the import systems FeoAB1 and 2, is subsequently transported into the magnetosome vesicles ^{17,18}. This process is then facilitated by the magnetosome specific ferrous iron transporters MamB and MamM ^{16,19}. MamH and MamZ are thought to oxidize ferric iron (Fe^{3+}) from the cytoplasm and release Fe^{2+} into the magnetosome vesicle ²⁰. MamE, MamT, MamP, MamX and

MamZ, which are located in the magnetosome membrane, are thought to provide the environment for magnetite nucleation^{20,22,24}.

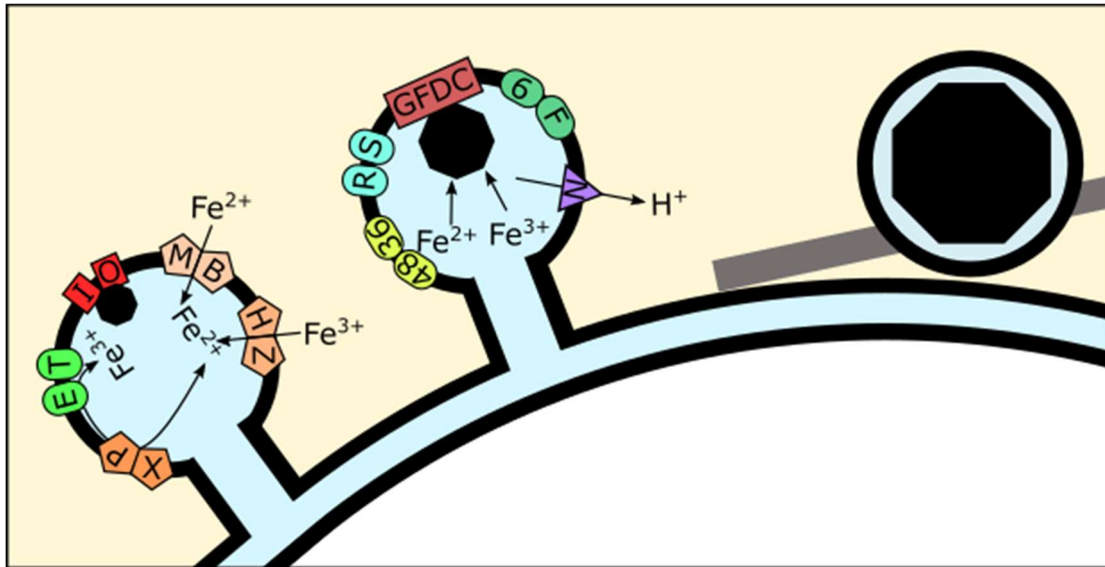


Figure 2: Overview of the magnetosome biosynthesis in *M. gryphiswaldense*. Precipitation of iron that is imported into the magnetosome membrane vesicle is probably mediated by proteins that are located on the magnetosome membrane, such as MamO and MamI. The Fe²⁺/Fe³⁺ ratio inside magnetosome membrane vesicles is regulated by MamE, MamP, MamT and MamX. Magnetite crystal maturation is regulated by MamG, MamF, MamD, MamC, MamS, MamR, MamN, Mms6, MmsF, Mms36 and Mms48.

Since the formation of magnetite, as a mixed-valence iron oxide, is highly dependent on a stable redox condition for biomineralization, minor perturbations caused by high oxygen levels or highly oxidized carbon sources were found to disturb the strictly needed 2/1 Fe²⁺/Fe³⁺ ratio and result in smaller and disformed magnetite crystals^{10,11,23}. Additionally, generic respiratory processes such as denitrification were found to participate in magnetosome biomineralization probably by contributing to oxidation of ferrous iron to ferric iron under oxygen-limited conditions thereby^{11,23}. Mutants of *M. gryphiswaldense* that lack enzymes of the denitrification pathway, such as the periplasmic nitrate reductase (NapAB), Fe²⁺-nitrite oxidoreductase (NirS) or nitric oxide reductase (NorBC) were severely impaired in magnetite biomineralization^{11,23}. Fusion experiments of *gusA*, which encodes a β -glucuronidase, with the denitrification genes as transcriptional reporters revealed that except for the nitrate reductase *nap*, highest expression of the denitrification genes coincided with conditions permitting maximum magnetite synthesis^{11,23}. In a follow up study, a *fumarate and nitrate reduction* regulator (Fnr) -like protein was identified in *M. gryphiswaldense*, which was

named MgFnr²⁴. In *Escherichia coli* and other bacteria, Fnr proteins are known to be global anaerobic regulators in controlling the switch between microoxic and oxic metabolism^{25,26}. Beside this function, MgFnr was found to repress expression of the denitrification genes under aerobic conditions putatively by an MTB-Fnr specific amino acid residue²⁴. Overproduction and deletion of this regulator resulted in fewer magnetosomes and less regular shaped crystals²⁴. A similar phenotype was also observed by deletion of the high affinity, terminal *cbb3*-type oxygen reductase, which putatively functions as an oxygen sensor and redox control²⁷.

After nucleation, which is probably initiated by MamO and MamI^{13,21,28}, the complex interplay of various proteins including Mms36, Mms48, MamG, MamF, MamD and MamC exerts strict control over the growth of the crystal, and their arrangement into well-ordered chains^{8,13,29,30}. Furthermore, MamA is suggested to form a proteinaceous scaffold surrounding the magnetosome membrane and “activate” the magnetosomes for magnetite biomineralization^{31,32}.

To efficiently function as a cellular “compass needle”, magnetosomes are assembled mid-cell into a chain. This process is controlled by the actin-like MamK, which polymerizes into dynamic, cytoskeletal filaments that are connected to magnetosomes through the acidic MamJ and MamY protein to form the magnetoskeleton. To ensure equal organelle inheritance during cytokinesis, magnetosome chains are directed to the cell division site by MamK filaments. Equal splitting of magnetosome chains to the daughter cells occurs with high accuracy, and particle chains undergo rapid intracellular repositioning towards midcell to the new-born daughter cells by pole-to-midcell treadmill growth of MamK filaments³³.

1.3 Genomic and transcriptional organization and regulation of magnetosome genes

1.3.1 The Magnetosome Island (MAI)

All *mam*- and *mms*-genes described above are encoded in five major putative polycistronic operons (MagOPs), namely *mamABop* (16.4 kb), *mamGFDCop* (2.1 kb), *mms6op* (3.6 kb), *mamXYop* (5 kb) and *feoAB1op* (2.4 kb)^{12,16,19,33} within the larger genomic magnetosome island (MAI) that extends over ~110 kb (Figure 3)^{16,35}.

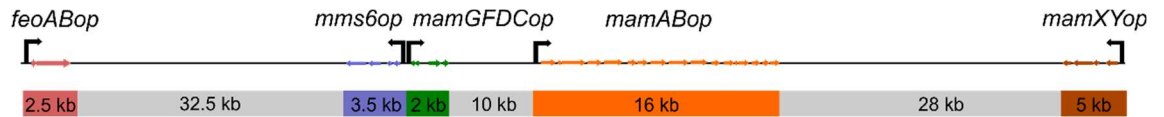


Figure 3: A simplified overview of the magnetosome island (MAI) of *M. gryphiswaldense* comprising the five major magnetosome operons with their respective size. Known promoters, which were identified in previous studies, are indicated by arrows.

The precise spatiotemporal control of the expression and targeting of magnetosome proteins at proper stoichiometry is required for the biosynthesis of such an intricate organelle. For example, copy numbers were found to range from 2 (e.g. MamX and MamZ) to 100 or 121 copies (Mms6 and MamC, respectively) per magnetosome particle in the magnetosome membrane³⁶. To orchestrate proper expression, one fundamental layer of regulation is the level of gene transcription. The large *mamABop* with its 17 genes is the longest operon (16.4 kb) and harbors all essential genes for magnetosome biosynthesis. The other four MagOPs encode genes with accessory roles in magnetite crystal size control, magnetosome chain formation and intracellular positioning^{12,13,15}. The transfer of all these MagOPs from *M. gryphiswaldense* resulted in magnetosome biosynthesis in other different hitherto nonmagnetic host organisms, which underlines the key roles of this gene set^{37,38}. Recently, an additional putative operon was identified namely *mms5op*, which comprises the two genes *mms5* and *mmxF*. Both genes are thought to be involved in crystal size control during magnetite biomineralization^{39,40,41}.

Previous studies focused on the elucidation of operon architecture including transcription start sites (TSS) as well as operon organization. Schübbe and colleagues demonstrated by reverse transcription-PCR (RT-PCR) that genes from the three magnetosome gene clusters known at the time, *mamABop*, *mms6op*, and *mamGFDCop*, are co-transcribed and thus represent genuine operons in *M. gryphiswaldense*³⁴. Additionally, the study also identified a single transcription start site for each transcript by primer extension analysis, which suggested that each operon is transcribed as a single unit driven by a primary promoter residing upstream of the first gene of each operon³⁴. Although internal promoters within the investigated operons, especially in the 16.4 kb long *mamABop*, were assumed, no additional promoters could be found. However, the presence of such were not ruled out based on the gathered data. Later, the

activity of a primary promoter (*PmamY*) upstream of the newly discovered *mamXYop* was demonstrated by a green fluorescent protein (GFP) reporter, whereas no additional promoters were identified²⁰. In *feoAB1op*, a primary promoter (*PfeoA1*) was revealed by a LacZ reporter gene fusion in *M. gryphiswaldense*¹⁷.

1.3.2 Generic pathways involved in magnetosome biosynthesis

Although many studies underlined the key role of the MagOPs in the process of magnetosome biosynthesis, an increasing interest in auxiliary genes encoding generic cellular functions outside of the MAI were addressed during a genome-wide transposon mutagenesis screen. Here, Silva *et al* identified genes with auxiliary function in magnetosome biosynthesis including cytochrome c maturation, sulfate assimilation, oxidative protein folding and nitrate respiration⁴². Consistently, Li and colleagues showed in several studies a linkage between anaerobic as well as microoxic respiration and magnetosome biosynthesis^{11,22,23,26}. The deletion of the essential enzymes of the denitrification pathway such as the periplasmic nitrate reductase (*NapAB*), Fe²⁺-nitrite oxidoreductase (*NirS*) or nitric oxide reductase (*NorBC*) resulted in a prohibited anaerobic growth of *M. gryphiswaldense* cells with nitrate as electron acceptor as well as severely impaired magnetosome biosynthesis^{11,22}. However, the operon architecture and transcriptional organization of genes involved in magnetosome biosynthesis outside the MAI has remained unknown.

1.3.3 Regulation of magnetosome biosynthesis

The most crucial factor influencing magnetosome biosynthesis was found to be the dissolved oxygen concentration (dO_2)¹⁰. However, the molecular mechanisms and determinants of oxygen regulation on transcription and magnetite biomineralization have remained poorly understood. Several studies observed only weak effects of MagOP transcription by oxygen based on qRT-PCR and microarray experiments^{34,43}. Furthermore, empty magnetosome vesicles and nearly unchanged abundances of magnetosome proteins such as MamC were detected between oxicly cultivated non-magnetic and microoxically grown magnetic cells^{15,34}. By investigation of the transcriptome of *M. gryphiswaldense* cells cultured under magnetosome forming microoxic (dO_2 0.5% of air saturation) conditions in comparison to non-magnetic semi-oxic (30% dO_2 of air saturation) conditions by RNA-sequencing, Wang and colleagues

⁴⁴ essentially confirmed the findings of the previous studies that *mam*- as well as *mms*-genes were constitutively expressed and not directly regulated by oxygen. The identified 77 genes, which were significantly upregulated under microoxic conditions, are involved primarily in various cellular processes as microoxic respiration, transport and regulation ⁴⁴.

Despite preliminary insights granted by the previous studies, the majority of the transcriptional landscape including TSS and operon architecture as well as the role of oxygen in transcriptional regulation are still poorly understood. Since *M. gryphiswaldense* advanced to a well-established model organism for bacterial organelle biosynthesis and biomineralization, detailed knowledge about transcriptional organization and global regulatory features such as promoter structure beyond the MAI is highly required. This can be achieved by high-resolution RNA-sequencing techniques such as the novel Cappable-sequencing technique, which is based on the enrichment of the triphosphorylated primary transcripts for determination of TSS with single base resolution ⁴⁵. Here, instead of processed transcripts depletion, the primary transcripts are capped by the Vaccinia capping enzyme and subsequently enriched by streptavidin beads resulting in an increase of mapping resolution. Since an intricate transcriptional regulation seems more common for large polycistronic operons such as the *mamABop*, MagOP landscape may be more complex than previously thought. Thus, a detailed reassessment focused on transcriptional regulatory elements would increase the understanding of magnetosome biosynthesis. Furthermore, previous studies focused on microoxic conditions, which support fastest growth but already show impaired magnetosome phenotypes concerning uniform size and shape ^{10,44}. Additionally, defined growth conditions are required for uniform magnetosome biosynthesis. Therefore, the application fermenter systems would enable strictly controlled standardized culturing regimes, which are needed for reproducibility of magnetosome biosynthesis.

1.4 Magnetosomes in biotechnology: applications and production

1.4.1 Potential applications of magnetosomes in biotechnology and biomedicine

The strict control during the complex magnetosome biosynthesis results in highly uniform magnetite particles regarding their size, shape, magnetic properties and crystallinity, exceeding synthetically produced magnetic nanoparticles ^{46,47,48}. Furthermore, purified magnetosomes exhibit a relatively low toxicity ⁴⁹. In the last

decades, magnetosomes have become of increasing interest for biotechnological and biomedical applications. Consequently, magnetosomes have already been tested in biomedical approaches including hyperthermia ^{50,51}, phototherapy ⁵² and radiosensitization ⁵³, as contrast agents for magnetic particle imaging ^{54,55} and magnetic resonance imaging ⁵⁶ or in particle-based immunoassays ^{30,57,58}, in which they outperformed the routinely used reference techniques. Additionally, magnetosomes were functionalized by genetic or chemical coupling of additional functional moieties to magnetosome membrane targeted anchor proteins, such as enzymes for immobilization of enzymatic cascades ⁵⁹⁻⁶², fluorophores, antibodies for diagnostic purposes e.g. Immuno- polymerase chain reaction (PCR) ^{61,63-65} or immunostimulatory ligands ⁶⁶. The potential biocompatibility of magnetosomes can be further enhanced by coating of the membrane with silica ⁶⁷ or expression of spider silk peptides ⁶⁸. Very recently, magnetosomes have been successfully applied to mouse hippocampal neurons to stimulate axonal outgrowth by mechanically induced stretch-growth ⁶⁹. This might enable future applications of bacterial magnetosomes even in regeneration of nerves. However, practical applications of magnetosomes have among other reasons been limited by their poor availability, which is due to the lack of precise techniques for highly controlled large-scale production with defined process parameters. Since many of the described applications depend on the characteristics and membrane composition, it is crucial to know how magnetosome gene clusters are organized and regulated on the transcriptional level, which enables future reconstitution, engineering, and tuning by synthetic biology approaches in homologous and heterologous hosts.

1.4.2 Cultivation of *M. gryphiswaldense* and production of magnetosomes: Previous approaches and their limitations

Despite application of magnetosomes in various fields is constantly expanding, limitations arise caused by their poor availability. The development of precise techniques for highly controlled large-scale production in bioreactors so far has been hampered by the fastidious microaerophilic to anoxic lifestyle of *M. gryphiswaldense* and related MTB ³. Whereas fastest growth occurs at low dO₂ concentrations of 0.1 – 1% of air saturation (equivalent to oxygen partial pressures (pO₂) of 0.25 – 2 mbar), optimal magnetosome biosynthesis is achieved under denitrifying conditions with nitrate as the only electron acceptor for respiration in the entire absence of oxygen

^{10,11,24,27,70}. However, anoxic shaking flask cultivation is ineffective with respect to high-yield cultivation with highest OD₅₆₅ of about 0.3 ¹¹. Hence, many studies focused on the cultivation of *M. gryphiswaldense* under microoxic conditions, where oxygen and nitrate respiration overlap ^{10,11,24,27,70}. However, stable control of microoxic conditions with dO₂ concentrations below 10% required for magnetosome biosynthesis is technically demanding and requires the use of fermentation systems, which is often customized for this special application. There are two major strategies to achieve optimal dO₂ adjustment: First, by programming an automatic control cascade for dynamical response to the culture's changing oxygen requirements or second, by empirical testing and manual adjustment of the process parameters such as agitation or gas rate. The first strategy was only used in two studies so far. In the first systematic study, Heyen and Schöler ¹⁰ achieved stable oxygen control in a 4 L bioreactor at various dO₂ concentrations from 0.1 to 100% of air saturation (pO₂ 0.25 – 212 mbar) using an automated oxygen regulation with pO₂ measurement and gas supply setup. They could show a clear correlation between lower pO₂ tensions and magnetite formation ¹⁰. During this study, a customized changes in the bioreactor setup as well as the pO₂-probe for signal amplification were made. The second study used an automated cascade during the analysis of oxygen dependent gene expression in a 1 L bioreactor. dO₂ concentration was adjusted by gas mixing of nitrogen and air, whereas gas flow rate and agitation speed were kept constant ⁷¹. Limitations of this cascade was reached at set dO₂ values above 15% leading to a steady decrease in oxygen concentration during the cultivation ⁷¹.

The second strategy, where dO₂ is adjusted manually, was used in the majority of all other studies so far. During fed-batch oxystat fermentations of *M. gryphiswaldense*, Sun *et al* kept the dO₂ concentration permanently below the dO₂-probe's sensitivity to achieve microoxic conditions by variable agitation speed with a fixed airflow in a 42 L bioreactor ⁷². In this study, the stirrer speed was manually increased independently of the measured dO₂ concentration in increments of 40 rounds per minute (rpm), whenever the growth rate decreased significantly. This regime was then used in follow-up studies by Liu *et al* ⁷³ and Zhang *et al* ⁷⁴, where the feeding strategy was further improved. Similar approaches were used by Fernandez-Castané *et al* as well as Berny *et al* ^{75,76}, where the dO₂ was adjusted by manually increasing both the airflow rate and the agitation speed to keep the dO₂ below the probe's sensitivity in

a 5 L bioreactor. Although these studies improved fermentation of *M. gryphiswaldense* resulting in OD₅₆₅ from 16 to 42 and magnetosome yields higher than 35 mg magnetite per L^{74,77}, the manually and thereby discontinuous dO₂ control based on highly specific, empirically determined parameters impede application independent of the bioreactor system used in the respective study as well as scale-up of the fermentation regime. Consequently, an automated dO₂ adjustment would overcome these limitations enhancing reproducibility and handling by standardization of the complete process including preculture from stock to inoculation (i.e. the ‘seed-train’) as important but so far neglected aspect. This enables detailed analysis of oxygen impact on gene expression as well as magnetite crystal growth during magnetosome biosynthesis. Moreover, previous studies focused on the characterization and optimization of growth parameters rather than magnetosome characteristics, despite the well-known effect of oxygen on magnetosome size and shape. Magnetosome formation was typically investigated by the C_{mag} (i.e. a light-scattering parameter for the semiquantative estimation of average magnetic alignment of cells⁷⁸), the intracellular iron content and qualitative transmission electron microscopy (TEM). Although these techniques are well established, they do not provide information about magnetite particle size, shape and number within the cell. Taken together, application of the previous cultivation regimes has been hampered by the discontinuous dO₂ control throughout cultivation. This in turn makes scale-up and transfer of protocols to other fermenter systems difficult, due to the highly specific, empirically determined parameters optimized for the particular type of bioreactor used in these studies.

1.5 Scope of this thesis

In summary, major parts of the regulation of magnetosome biosynthesis on the transcriptional as well as on the particle level are only poorly understood. Addressing these questions are needed to provide valuable insights into transcriptional regulation of prokaryotic biosynthesis of organelles as intricate as the magnetosome. This advances future synthetic biology approaches on reconstitution and tuning of the magnetosome biosynthesis in homologous as well as heterologous hosts.

The major goal of this study was the elucidation of the transcriptional organization and regulation of magnetosome biosynthesis in *M. gryphiswaldense*. To this end, magnetosome formation was studied by under various defined oxygen

conditions, which enable or inhibit magnetite biomineralization. Since the available techniques for cultivation under defined oxygen concentration were not suitable for controlled and dynamic dO_2 adjustment, the first part of the thesis was dedicated to the establishment of an automated cascade regulation for precise control of dO_2 concentration.

The second part the thesis was devoted to the elucidation of the transcriptional architecture of the major magnetosome gene clusters by a unique combination of RNA-sequencing techniques including TSS detection by Cappable-sequencing ⁴⁵, whole transcriptome shotgun sequencing (WTSS) and 3'-end sequencing for mapping of termination sites ⁷⁹. The identified known and unknown promoter regions of the mapped TSS were further characterized by bioluminescence reporter assay as well as promoter knockouts for their biological significance. Furthermore, transcriptional profiles of cells grown under oxygen conditions either favoring or inhibiting magnetosome biomineralization were compared.

2 Synopsis

To address the open questions of magnetosome biosynthesis regulation on the transcriptional as well as magnetite particle level, up-to-date techniques involving strictly controlled fermentation processes, high-throughput analytics and high-resolution transcriptomics were explored. In chapter 1, a standardized oxystat fermentation regime was established including a characterized seed-train procedure from stock to inoculation, which resulted in stable oxygen regulation for a wide range of dO_2 concentrations (1 – 95% of air saturation). Subsequently, magnetosome biosynthesis was investigated under three oxygen concentrations (dO_2 0%, 1% and 95% of air saturation). This is described in detail in Manuscript 1. Significant differences in substrate consumption of the carbon source lactate as well as the alternative electron acceptor nitrate under the three oxygen conditions were observed. Additionally, particle uniformity increased during fermenter growth compared to uncontrolled oxygen conditions in shaking flasks.

Chapter 2 summarizes the investigation of the magnetosome operon architecture under routinely used microoxic shaking flask cultivation by exploring novel RNA-sequencing techniques (e.g. Cappable-sequencing ⁴⁵), as described in detail in Manuscript 2. In addition to the already known primary promoters upstream of the first gene of the five *mam*-operons, new transcription start sites (TSS) within the operons were identified resulting in a new layer of magnetosome biosynthesis gene expression. One key finding of this study is the discovery of the secondary promoter P(*mamH*) residing within the coding sequences of *mamABop*, which drives the expression of essential genes for biomineralization.

In chapter 3, the transcriptomic landscape under conditions enabling magnetosome formation was investigated for the determination of key and auxiliary cellular functions involved in magnetosome biosynthesis. Here, a complex interplay between generic metabolic processes (e.g. aerobic and anaerobic respiration), cellular redox control, and the biosynthesis of specific magnetosome structures was observed. This is described in detail in Manuscript 3. Here, we found that transcription of about 300 genes was significantly increased under anaerobic magnetosome forming conditions, where 41 were found particularly highly upregulated, most of which have functions key magnetosome forming functions in the cell. However, specific *mam* and *mms*-genes directly controlling magnetosome biosynthesis were found among the most

highly transcribed genes in the cell but their regulation was very poor across growth conditions.

Chapter 4 shortly summarizes preliminary data of the establishment of the bacteriophage T7-based expression system in *M. gryphiswaldense*. The successful expression of the T7-RNA polymerase and a codon optimized version codon optimized version of *gfp* (*oegfp*) was shown by fluorescence microscopy and Western blot experiments. Although this is the first time that the functionality of the induced T7-expression system is shown in *M. gryphiswaldenes*, only low amounts of the reporter were detected. However, this system shows great potential for future induced expression of large DNA cassettes.

2.1 Chapter 1: An automated oxystat fermentation regime for microoxic cultivation and magnetosome production in *Magnetospirillum gryphiswaldense*

The first research article addresses the development of a well characterized, automated oxystat fermentation regime summarized in Figure 4, which enables both highly reproducible cultivation of *M. gryphiswaldense* over a wide range of oxygen conditions as well as highly uniform magnetosome biosynthesis (Article 1). First, a seed-train was established starting with two passages of initial subcultivation followed by a stepwise scale-up under suboxic conditions. This procedure resulted in highly viable cells as judged by their motility for inoculation. Next, we developed an oxystat batch fermentation regime for microoxic cultivation of *Magnetospirillum gryphiswaldense* in a 3 L bioreactor. Subsequently, a cascade was designed, which maintained the cell culture's requirements for low oxygen concentrations by keeping stirrer speed and airflow rate at low levels at the beginning and increased them in a stepwise manner to sustain the cells at growing densities. The cascade proved to stably control oxic (95% dO₂) and microoxic (1 – 10% dO₂) conditions. In the case of 95% and 10% dO₂ concentrations, stable control was achieved throughout the process, whereas only sporadic fluctuations during the main growth phase in dO₂ occurred at a set value of 1% dO₂. Since these fluctuations most likely caused by a combination of dO₂ probe sensitivity, and cascade reactivity might result in unstable oxygen conditions, the cascade was not further tested at lower dO₂ values below 1%. The application of the described regime in batch fermentations at 95%, 1% and 0% dO₂ concentration in biological triplicates resulted in highly consistent growth behavior, which confirmed the stability of the process (Figure 5 A). In addition, consumption of lactate as the carbon source and nitrate as alternative electron acceptor were monitored during cultivation. While nitrate became growth limiting during anaerobic growth, lactate was the growth limiting factor during microoxic cultivation. However, achievable, maximal cell densities are limited by the accumulation of toxic metabolic intermediates during denitrification ²⁴, which inhibits increasing the initial nitrate concentration for prolonging the growth phase.

Analysis of microoxic magnetosome biomineralization by TEM and SAXS revealed magnetosomal magnetite crystals were highly uniform in size and shape characteristic for the respective oxygen concentration. Additionally, particle uniformity

increased during fermenter growth, whereas uncontrolled oxygen conditions in shaking flasks resulted in a much wider distribution in particle diameter (Figure 5 B).

In summary, the streamlined seed-train and automated oxystat regime presented in our study provides well characterized and stable culturing environments for reproducible magnetosome biosynthesis. Furthermore, the process can be used to produce ‘tailored’ magnetite particles with distinct sizes for the desired application by adjustment of the oxygen concentration.

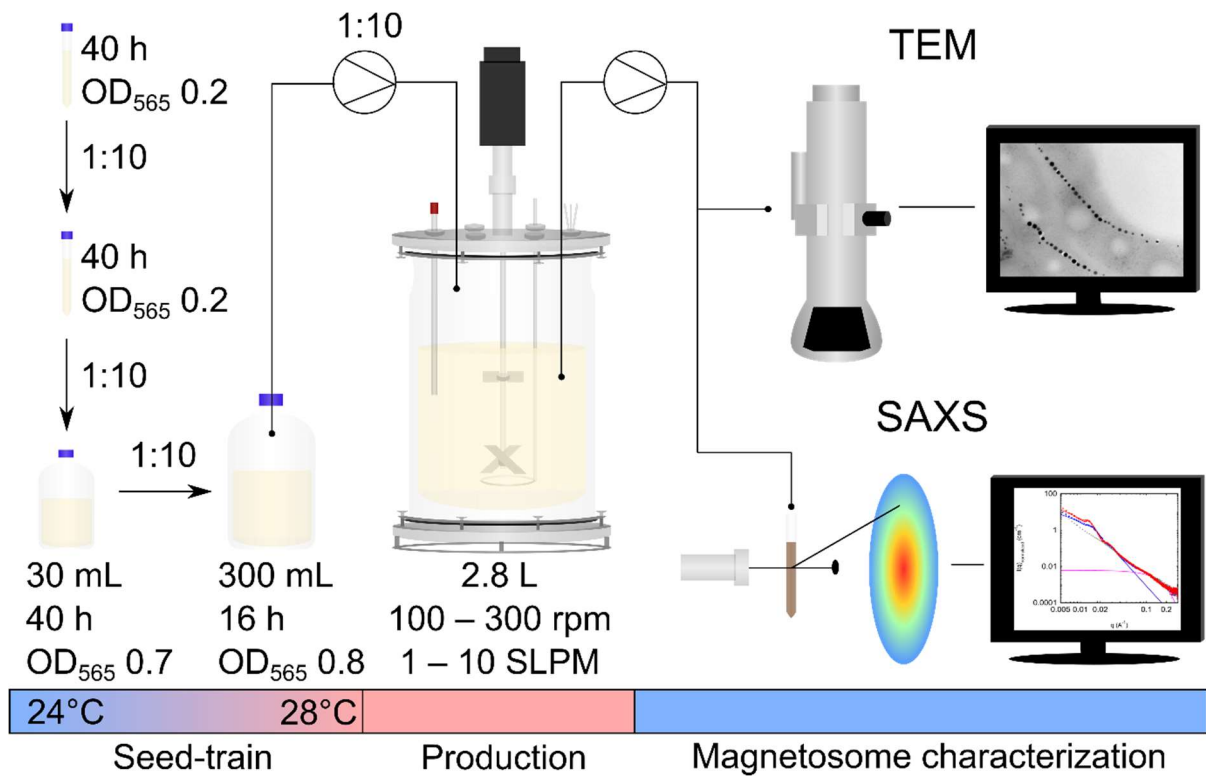


Figure 4: Overview of the oxystat fermentation regime beginning with the standardized seed-train. During the production phase dO_2 concentration was adjusted by stirrer speed (rounds per minute = rpm) and airflow rate (standard liter per minute = SLPM). Subsequently, the produced magnetosomes were characterized by transmission electron microscopy (TEM) and small-angle X-ray scattering (SAXS). Adapted from Manuscript 1 (Article 1).

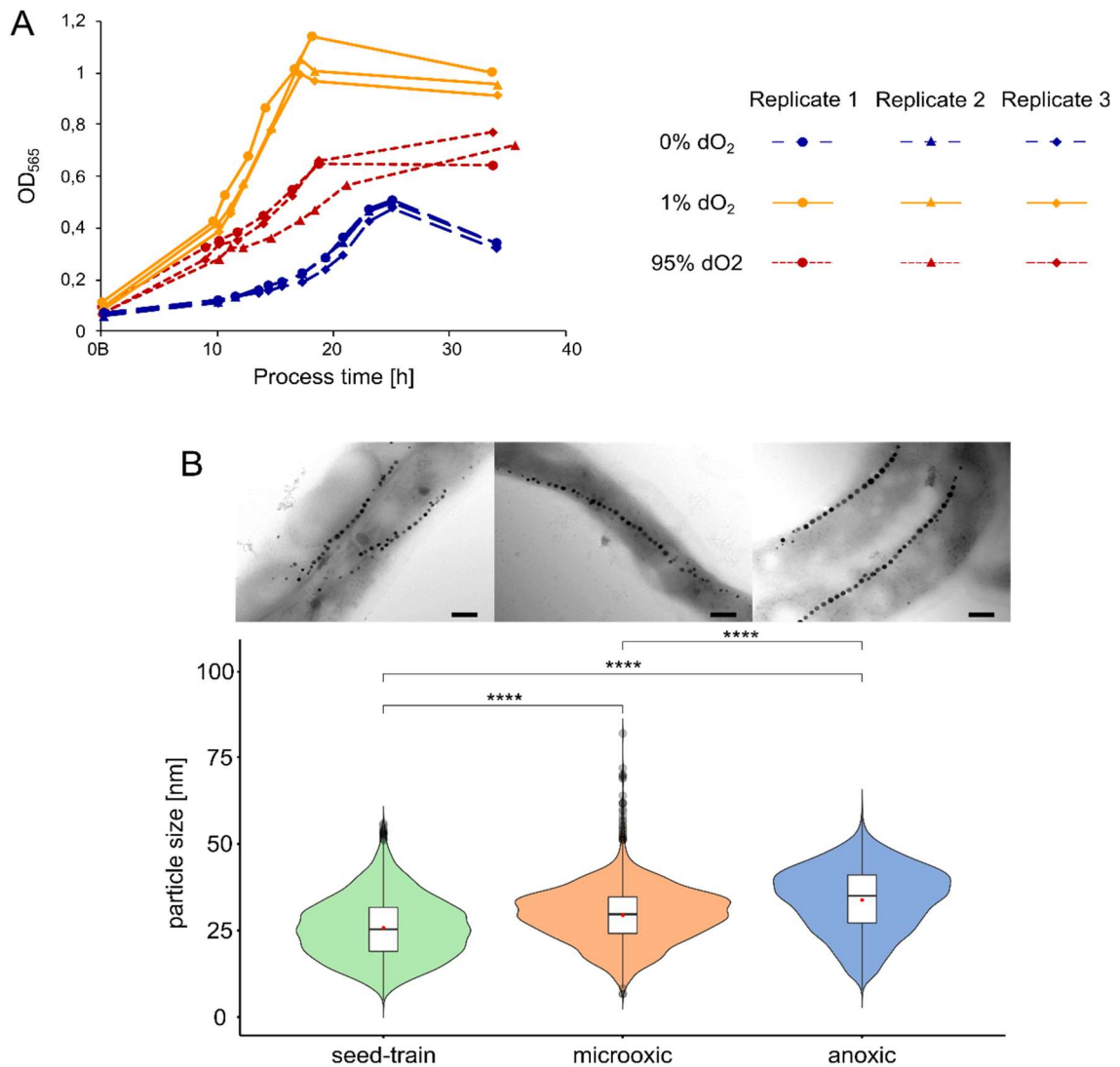


Figure 5: A) Growth triplicates at dO₂ concentrations of 95% (red), 1% (orange) and 0% (blue). Adapted from Riese *et al* 2020 (Article 1) and modified. B) Transmission electron micrographs and magnetosome particle sizes at process end among seed-train (n=2925), microoxic (1% dO₂) (n=3180) and anoxic (0% dO₂) conditions (n=3025) with representative TEM micrographs of cells under the respective conditions (scale bar 200 nm). In box plots, the box indicates the interquartile range, the bar indicates the median, and the red dot represents the mean. Grey dots represent data points above or below the 95th and 5th percentile. The violin plots show the magnetosome particle size distribution of measured particle sizes. For statistical comparison of particle sizes, Wilcoxon rank sum test was performed (****, p < 0.0001). Adapted from Manuscript 1 (Article 1).

2.2 Chapter 2: The complex transcriptional landscape of magnetosome gene clusters in *Magnetospirillum gryphiswaldense*

Magnetosomes have emerged as a model system to study prokaryotic organelles. Understanding the mechanisms underlying control over magnetosome formation has several important practical implications. Transcriptionally engineering of the MagOPs by synthetic biology approaches for enhanced and controlled magnetosome production

would further improve magnetosome biosynthesis in homologous and heterologous host organisms. However, the transcriptional organization of the magnetosome gene clusters has remained poorly understood. Hence, the second article (Article 2) addresses the architecture of *mamABop*, *mamGFDCop*, *mms6op*, *mamXYop* and *feoAB1op*, which were previously considered to follow the simple operon model proposed by Jacob and Monod⁸⁰ with transcription driven by a single primary promoter upstream of the first gene in the operon^{17,20,34}. By applying Cappable-sequencing⁴⁵ and whole-transcriptome shotgun sequencing, we show that *mamGFDCop* and *feoAB1op* are transcribed as single transcriptional units, whereas multiple transcription start sites (TSS) are present in *mms6op*, *mamXYop*, and the long *mamABop* (>16 kb).

The *mms6op* comprises two transcriptional units, *mms6-mmsF* and *mms36-mms48*, which are separated by a terminator, and each driven by a separate promoter (Figure 6). Interestingly, in all known magnetotactic *Magnetospirillum* species, *mms36* and *mms48* are always preceded by *mms6-mmsF*, suggesting that this coupled organization might be preserved by natural selection. The *mamXYop* comprises also two transcriptional units, *mamY* and *mamX-mamZ-ftsZm*, where a very active promoter was identified in the intergenic region of *mamY* and *mamX* (Figure 6). Using a bioluminescence reporter assay and promoter knockouts, we demonstrated that most of the identified TSS originate from biologically meaningful promoters. Intriguingly, the identified promoter within the large intergenic region of *mamXYop* showed no reporter expression with the natural ribosome binding site (RBS), whereas strong light emission became detectable after insertion of an optimized Shine-Dalgarno sequence. This strongly argues against translation of the produced transcript in the native context, including potential leaderless translation⁸¹ and likely suggests transcription of a noncoding RNA.

One further key finding of this study is the discovery of multiple promoters residing within the coding sequences of *mamABop*. For instance, P(*mamH*), which is located in the coding sequence of *mamH*, was identified among the most crucial internal promoters as the downstream genes (*mamI* and *mamE*) are essential for magnetosome formation. The reporter assay demonstrated that P(*mamH*) is one of the most active promoters among the ones measured in the current study and the strongest in *mamABop*, with the activity exceeding that of the primary promoter P*mamH*. To our knowledge, this is the first demonstration that intragenic promoters can exceed primary

promoters in activity and potentially play a major role in driving expression of large operons.

In conclusion, our study has unveiled how a genetically complex pathway is orchestrated at the transcriptional level to ensure the proper assembly of one of the most intricate prokaryotic organelles. In this study, we provide a previously unappreciated transcriptional landscape of the magnetosome operons, which will enable synthetic biology approaches to rationally reengineer the magnetosome operons for enhanced and controlled magnetosome production. Moreover, our study provides a catalog of well-characterized promoters with different strengths for constructing expression cassettes in magnetospirilla and other *Alphaproteobacteria*.

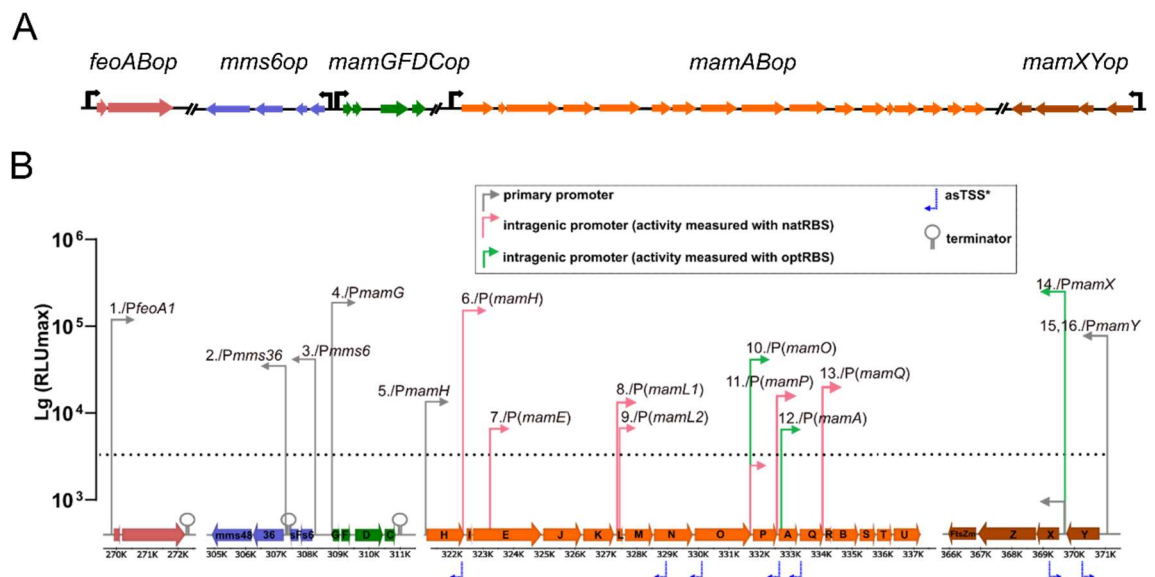


Figure 6: Comparison between A) the previously known MagOP architecture and B) the architecture based on the present study. B) Position of the promoters, whose activities were confirmed by the bioluminescence assay, terminators, and asTSS in the MagOPs. Arrow height indicates the promoter strength measured by luminescence. A slash separates a TSS number designation and the corresponding promoter. Adapted from Manuscript 2 (Article 2).

2.3 Chapter 3: The transcriptome of *Magnetospirillum gryphiswaldense* during magnetosome biomineralization

To form an organelle as intricate as the magnetosome, the transcription of the >30 magnetosome specific genes clustered within the MAI has to be coordinated with the expression of an as-yet unknown number of auxiliary genes encoding several generic metabolic functions. While reverse and forward genetic analysis has implicated

many genes and pathways with essential and auxiliary functions in magnetosome biosynthesis, their global regulation in response to varying growth conditions is much less understood. In addition, global regulatory features, such as promoter and operon structures have remained poorly characterized in *M. gryphiswaldense*. Therefore, this study compares transcriptional profiles of anaerobically (0% dO₂) grown magnetosome forming cells with those in which magnetosome biosynthesis has been inhibited by aerobic (95% dO₂) conditions (Article 3).

Here, we found that from the >4300 genes comprised in the genome, transcription of about 300 genes was significantly increased under anaerobic conditions. Among these genes, 41 were found particularly highly upregulated, most of which have functions in denitrification and cytochrome c maturation. These cellular processes were already indirectly linked to magnetite biomineralization by poisoning proper redox conditions by oxidation of ferrous iron within the cell^{11,22,42}. Additionally, several hemerythrin-like proteins encoded outside of the MAI were upregulated under 0% dO₂. Hemerythrins were previously implicated in magnetosome biosynthesis because of their conspicuous high number in the MAI of *M. gryphiswaldense* and their known function in oxygen sensing as well as iron transport in other bacteria^{82,83}. However, the exact role in metabolism and possibly magnetosome biosynthesis, needs to be further investigated. Furthermore, several highly upregulated genes with so far unknown function, such as MSR1_19280, MSR1_19290 and MSR1_04470 represent novel candidates that might be involved in magnetosome biosynthesis.

By Cappable-sequencing, we found that the predominant promoter structures active under all tested conditions were highly similar to sigma factor σ^{70} dependent promoters in other *Alphaproteobacteria* such as *Gluconobacter oxydans*⁸⁴. Furthermore, with decreasing oxygen concentrations, the transcriptional complexity is reduced with respect to intragenic TSS, and with that sub-operon number as well as 5'-untranslated region (5'-UTR) length. Although new elements with a clear regulatory function, such as a glycine-riboswitch or so far unknown function were detected, they only represent a relatively small fraction compared to the high number of long 5'-UTRs, suggesting that most regulators remain unidentified. It seems that expression regulation under the tested conditions in *M. gryphiswaldense* is based to a significant degree on cis-regulatory elements, as suggested by the 5'-UTR length.

Specific *mam* and *mms*-genes directly controlling magnetosome biosynthesis were found among the most highly transcribed genes in the cell at comparable to, or even exceeding highly expressed housekeeping genes, but their regulation was very poor independent of the growth condition. This high constitutive expression level indicates that magnetosome biosynthesis is among the key cellular functions even under conditions inhibiting magnetosome formation. Furthermore, more TSS within the MagOPs were identified under oxic conditions (Figure 7). Taken together, the absence of magnetite crystals in oxic cells, cannot be explained by downregulation or incomplete transcription of the MagOPs. Additionally, during the investigation of magnetosome biosynthesis by cryo-electron tomography in a previous study, MagOP expression was observed by identification of empty magnetosome vesicles under oxic conditions ¹⁵. This shows magnetosome genes are not only transcribed, but also translated leading at least to vesicle formation.

In summary, the transcriptional regulation and architecture was analyzed genome-wide as well as for the MagOPs by application of high-resolution RNA-sequencing techniques, e.g. Cappable-seq, on samples cultivated under highly controlled oxygen conditions. We showed that the transcriptional complexity of the MagOPs depended on the applied oxygen conditions. Our transcriptome-wide analysis revealed that magnetite biomineralization relies on a complex interplay between generic metabolic processes such as aerobic and anaerobic respiration, cellular redox control, and the biosynthesis of specific magnetosome structures.

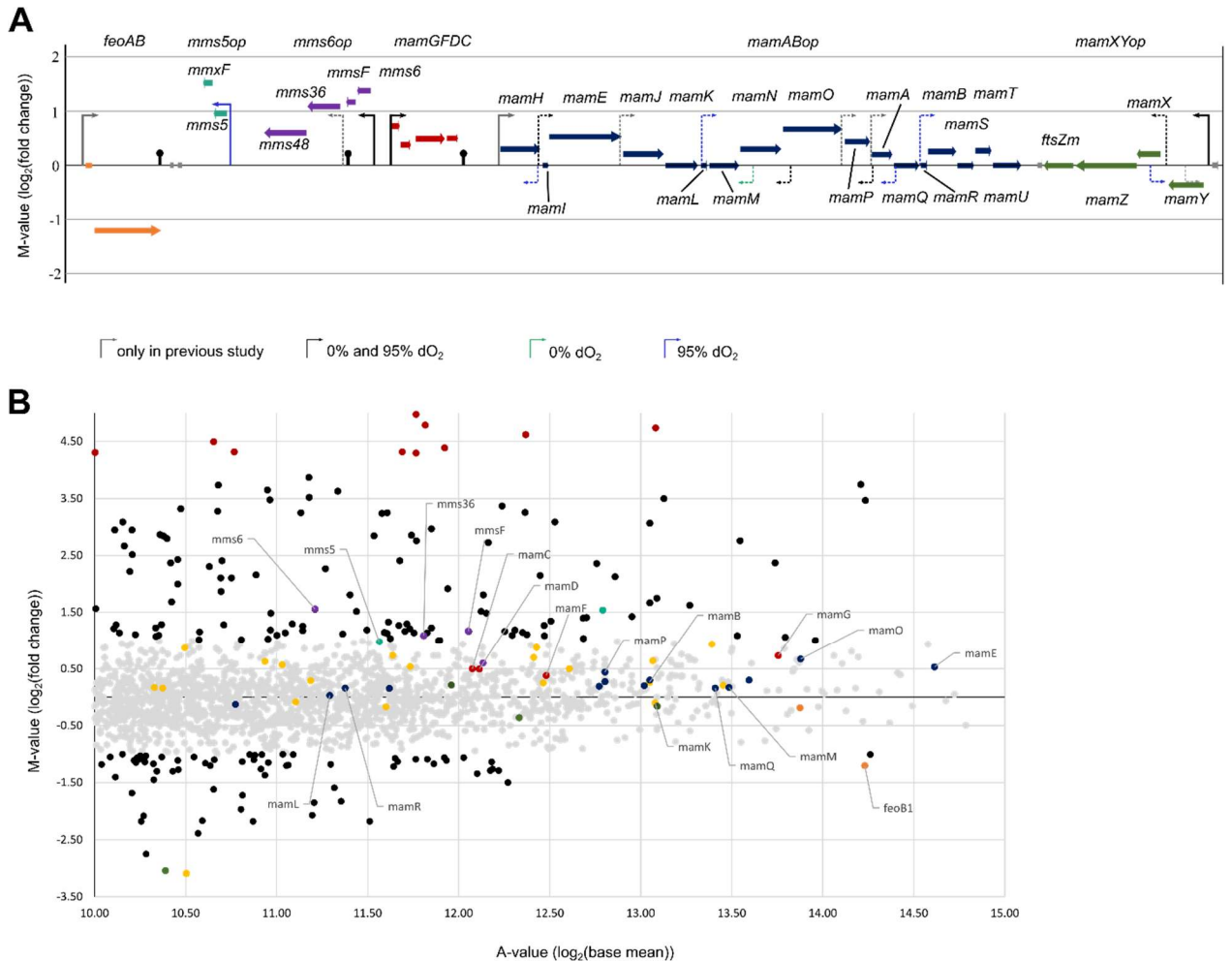


Figure 7: Overview over the MagOPs with previously identified TSS (Article 2). B) Differential expression of genes under anoxic (0% dO₂) vs. oxic (95% dO₂) conditions with upregulated and downregulated ($M\text{-value} \leq -1$, $M\text{-value} \geq 1$, black dots) as well as top highly upregulated ($M\text{-value} \geq 4$, red dots) and highly downregulated ($M\text{-value} \leq -3$, green dots) genes. Grey dots indicate insignificant differential expression ($M\text{-value} \leq 1$, $M\text{-value} \geq -1$). MAI genes are highlighted in yellow. Adapted from Manuscript 3 (Article 3).

2.4 Chapter 4: Establishment of a T7-based expression system

For metabolic engineering of magnetosome biosynthesis genes through overexpression or rational design of synthetic versions of MagOPs, a robust gene expression toolbox is essential. So far in *M. gryphiswaldense* the tetracycline- and lactate- induced promoters are the only two inducible expression systems, which were successfully established^{85,86}. These two promoters are routinely used for expression of single genes, however induced expression of complex operons such as the *mamABop* is limited. To this end, the bacteriophage T7-based expression system was explored because of its high effectivity as well as processivity and its independence of the host's transcription machinery (i.e. orthogonal)⁸⁷.

The T7-RNA polymerase was placed under the regulation of the lactose-promoter (P_{lac}), which is tightly repressed in *M. gryphiswaldense*, and the tetracycline promoter (P_{tet}). Expression of the T7-RNA polymerase was investigated by quantitative Western blotting, which show high expression of the T7-RNA polymerase after induction, even exceeding the expression level in the expression strain *E. coli* BL21. Furthermore, the P_{lac} was used for all further experiments since high levels of T7-RNA polymerase were detected in uninduced cells and only minimal increase after induction, when controlled by P_{tet} .

Next, a codon optimized version of *gfp* (*oegfp*) was applied as reporter for estimating the expression efficiency by both fluorescence microscopy and Western blotting (Figure 8). A subtle increase in fluorescence was observed after induction suggesting a low expression level. Western blot experiments as more sensitive technique showed low levels of oeGFP in cell lysate, thereby supporting the previous observation.

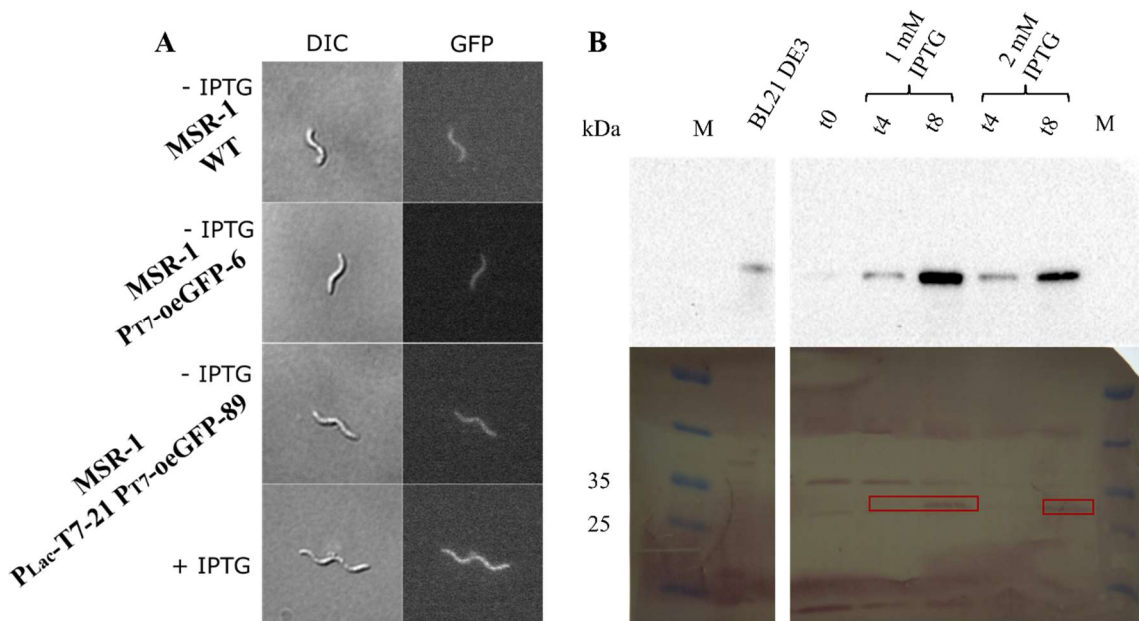


Figure 8: A) Fluorescence microscopy of *M. gryphiswaldense* wildtype (WT) and strains containing the T7 Polymerase under control of the lactose induced Promoter from *E. coli* (P_{lac} -T7) as well as a codon optimized version of *egfp* under the control of the T7-promoter (PT7-*oegfp*). Expression was induced by addition of IPTG and pictures were taken after 8 h of induction. B) Western blot of *M. gryphiswaldense* WT and P_{lac} -T7-PT7-*oegfp*. T7 expression was induced by addition of IPTG and samples were taken after 0 h, 4 h and 8h after induction and enriched to an OD_{565} of 10. Detection was performed using an anti-T7-polymerase-antibody (upper half) and anti-GFP-antibody (lower half). T7-polymerase concentration was highest after 8 h. GFP signal was detected after 8 h (red rectangle).

However, only low amounts of oeGFP were detected in fluorescence and Western blot experiments. This might be due to the copy number of the reporter. The T7-expression system in *E. coli* is also based on a chromosomal copy of the T7-polymerase but the gene of interest is coded on a high copy plasmid⁸⁷, thereby providing multiple targets for the T7-polymerase. Hence, the use of a multicopy plasmid in *M. gryphiswaldense* with the gene of interest would possibly enable to overcome this limitation.

In summary, a T7-expression system for *M. gryphiswaldense* was constructed and successfully applied for *oegfp* expression. Although more experiments are needed for estimation of the activity as well as efficiency, this system shows great potential for future induced expression of large DNA cassettes such as the magnetosome biosynthesis gene clusters.

2.5 Conclusion and Outlook

The first part of (Chapter 1) the thesis focused on the development of a streamlined seed-train and an automated oxystat fermentation regime, which will be of great value for future studies by providing a characterized fermentation regime for reproducible magnetosome biosynthesis. Despite this, cell yields of the batch process were significantly lower compared to the previous described fed-batch processes reaching OD₅₆₅ up to 42⁷⁴. However, future application of feeds based on the calculated substrate consumption rates in this study, optimization of impeller arrangement and application of air and nitrogen gas mixtures would overcome growth limitations leading to higher magnetosome yields. These developments may pave the way for scale-up to industrial production for wide-spread application in various fields.

The second part (Chapters 2 & 3) shed light on the previously unappreciated transcriptional organization of magnetosome gene clusters and the global regulation in response to anoxic conditions most favorable for magnetite biomineralization. This thesis provides a high-resolution image of the transcriptional landscape of the magnetosome operons including a list of well characterized promoters for future applications in the rational reengineering of magnetic bacteria for improved bioproduction of tunable magnetic nanoparticles. This could be achieved, e.g., through replacing the native promoters of individual transcriptional units by stronger and

tunable promoters such as the lactose induced expression system⁸⁵. Furthermore, the T7-based expression system⁸⁷ would enable targeted orthogonal expression of several transcriptional units without the need for multiple inducers.

By comparing global transcriptional profiles of anaerobically grown magnetosome forming cells with those in which magnetosome biosynthesis has been suppressed by aerobic condition, a relaxed transcriptional regulation under oxic conditions was observed. This may originate from the natural habitat of *M. gryphiswaldense*, the oxic-anoxic transition zone. This habitat is influenced by many external parameters such as day-night cycle, metabolic activities of the complete microbial community as well as mechanical disturbances of the sediment itself. In combination with the necessity for magnetosomes as important organelles for targeted motility along substrate gradients, fast changes of the protein composition within the magnetosome membrane may be required to maintain the correct redox potential for magnetosome biosynthesis. Furthermore, the data shows an increasing transcriptional complexity with respect to TSS number and 5'-UTR length increasing oxygen concentrations. A possible explanation might lie in the more frequently occurring fluctuations in oxygen concentration characteristic in these habitats, which might lead to a higher need of regulation to ensure proper expression of the MagOPs. The observed tendency for longer 5'-UTRs under oxic conditions implicating an increase in transcripts with cis-regulatory elements that potentially influence translation, faster responses on changing environmental conditions are facilitated to putatively stabilize the redox potential within the cells. Our analysis predicted new riboswitches in addition to the previously annotated ones in the most recent version of the *M. gryphiswaldense* genome¹⁶. Although some new cis-regulatory elements were found, they only represent a relatively small fraction, which suggests that regulation under the tested conditions in *M. gryphiswaldense* is based to a significant degree on cis-regulatory elements like riboswitches as sensors for environmental cues. Future studies may focus on the regulation elements influencing magnetosome formation to better understand how the proper assembly of one of the most intricate prokaryotic organelles is orchestrated at the transcriptional level, which in turn enables rational design of synthetic magnetosome operons for targeted magnetosome production in homologous and heterologous hosts. Future biomedical applications would greatly benefit from enhancement of biocompatibility by for example depletion of lipopolysaccharide production in *M.*

gryphiswaldense or high yield magnetosome production of correctly sized particles in naturally biocompatible host organisms.

3 References

1. Bellini, S. Ulteriori Studi Sui “Batteri Magnetosensibili.” (Pavia, 1963)
2. Blakemore R. Magnetostactic bacteria. *Science*. 1975; **190**:377–379.
3. Lefèvre CT, Bazylinski DA. Ecology, diversity, and evolution of magnetotactic *Bacteria*. *Microbiol Mol Biol Rev*. 2013; **77**:497–526.
4. Lin W, Zhang W, Paterson GA, Zhu Q, Zhao X, Knight R, Bazylinski DA, Roberts AP Pan Y. Expanding magnetic organelle biogenesis in the domain Bacteria. *Microbiome*. 2020; **8**:152.
5. Matsunaga T, Sakaguchi T, Tadakoro F. Magnetite formation by a magnetic bacterium capable of growing aerobically. *Appl Microbiol Biotechnol*. 1991; **35**:651–655.
6. Blakemore RP, Maratea D, Wolfe RS. Isolation and pure culture of a freshwater magnetic spirillum in chemically defined medium. *J. Bacteriol*. 1979; **140**:720–729.
7. Schüler D, Köhler M. The isolation of a new magnetic spirillum. *Zentralbl Mikrobiol*. 1992; **147**:150–151.
8. Uebe R, Schüler D. Magnetosome biogenesis in magnetotactic bacteria. *Nat Rev Microbiol*. 2016; **14**:621–637.
9. Schleifer KH, Schüler D, Spring S, Weizenegger M, Amann R, Ludwig W, Köhler M. The genus *Magnetospirillum* gen. nov. description of *Magnetospirillum gryphiswaldense* sp. nov. and transfer of *Aquaspirillum magnetotacticum* to *Magnetospirillum magnteotacticum* comb. nov. *Syst Appl Microbiol*. 1991; **14**:379–385.

10. Heyen U, Schüler D. Growth and magnetosome formation by microaerophilic *Magnetospirillum* strains in an oxygen-controlled fermentor. *Appl Microbiol Biotechnol.* 2003; **61**:536–544.
11. Li Y, Katzmann E, Borg S, Schüler D. The periplasmic nitrate reductase Nap is required for anaerobic growth and involved in redox control of magnetite biomineralization in *Magnetospirillum gryphiswaldense*. *J Bacteriol.* 2012; **194**:4847–4856.
12. Toro-Nahuelpan, M, Giacomelli G, Raschdorf O, Borg S, Plitzko JM, Bramkamp M, Schüler D, and Müller FD. 2019. MamY is a membrane-bound protein that aligns magnetosomes and the motility axis of helical magnetotactic bacteria. *Nat Microbiol.* 4:1978–1989.
13. Lohße A, Borg S, Raschdorf O, Kolinko I, Tompa É, Pósfai M, Faivre D, Baumgartner J, Schüler D. Genetic dissection of the *mamAB* and *mms6* operons reveals a gene set essential for magnetosome biogenesis in *Magnetospirillum gryphiswaldense*. *J Bacteriol.* 2014; **196**:2658–2669.
14. Barber-Zucker S, Keren-Khadmy N, Zarivach R. From invagination to navigation: The story of magnetosome-associated proteins in magnetotactic bacteria. *Protein Sci.* 2015; **25**:338–351.
15. Raschdorf O, Forstner Y, Kolinko I, Uebe R, Plitzko JM, Schüler D. Genetic and ultrastructural analysis reveals the key players and initial steps of bacterial magnetosome membrane biogenesis. *PLOS Genetics.* 2016; **12**:e1006101.
16. Uebe R, Schüler D, Jogler C, Wiegand S. Reevaluation of the Complete Genome Sequence of *Magnetospirillum gryphiswaldense* MSR-1 with Single-Molecule Real-Time Sequencing Data. *Genome Announc.* 2018; **6**:e00309-18.

17. Rong C, Huang Y, Zhang w, Jiang W, Li Y, Li J. Ferrous iron transport protein B gene (*feoB1*) plays an accessory role in magnetosome formation in *Magnetospirillum gryphiswaldense* strain MSR-1. Res Microbiol. 2008; **159**:530–536.
18. Rong C, Zhang C, Zhang Y, Qi L, Yang J, Guan G, Li Y, Li J. FeoB2 functions in magnetosome formation and oxidative stress protection in *Magnetospirillum gryphiswaldense* strain MSR-1. J Bacteriol. 2012; **194**:3972–3976.
19. Uebe R, Junge K, Henn V, Poxleitner G, Katzmann E, Plitzko JM, Zarivach R, Kasama T, Wanner G, Pósfai M, Böttger L, Matzanke B, and Schüler D. The cation diffusion facilitator proteins MamB and MamM of *Magnetospirillum gryphiswaldense* have distinct and complex functions, and are involved in magnetite biomineralization and magnetosome membrane assembly. Mol. Microbiol. 2011; **82**:818–835.
20. Raschdorf O, Müller FD, Pósfai M, Plitzko JM, and Schüler D. The magnetosome proteins MamX, MamZ, and MamH are involved in redox control of magnetite biomineralization in *Magnetospirillum gryphiswaldense*. Mol. Microbiol. 2013; **89**:872–886.
21. Murat D, Quinlan A, Vali H, Komeili A. Comprehensive genetic dissection of the magnetosome gene island reveals the step-wise assembly of a prokaryotic organelle. PNAS. 2010; **107**:5593–5598.
22. Jones SR, Wilson TD, Brown ME, Chang MCY. Genetic and biochemical investigations of the role of MamP in redox control of iron biomineralization in *Magnetospirillum magneticum*. PNAS. 2015; **112**:3904–3909.
23. Li Y, Bali S, Borg S, Katzmann E, Ferguson SJ, Schüler D. Cytochrome cd1 nitrite reductase NirS is involved in anaerobic magnetite biomineralisation in

- Magnetospirillum gryphiswaldense* and requires NirN for proper d1 heme assembly. J. Bacteriol. 2013; **195**:4297-4309.
24. Li Y, Sabaty M, Borg S, Silva KT, Pignol D, Schüler D. The oxygen sensor MgFnr controls magnetite biomineralization by regulation of denitrification in *Magnetospirillum gryphiswaldense*. BMC Microbiol. 2014; **14**:153.
25. Uden G, Becker S, Bongaerts J, Holighaus G, Schirawski J, Six S. O₂-sensing and O₂-dependent gene regulation in facultatively anaerobic bacteria. Arch Microbiol. 1995; **164**:81–90.
26. Bueno E, Mesa S, Bedmar EJ, Richardson DJ, Delgado MJ. Bacterial Adaptation of respiration from oxic to microoxic and anoxic conditions: Redox control. Antioxid Redox Signal. 2012 **16**:819–852.
27. Li Y, Raschdorf O, Silva KT, Schüler D. The terminal oxydase cbb3 functions in redox control of magnetite biomineralization in *Magnetospirillum gryphiswaldense*. J Bacteriol. 2014; **196**:2552–2562.
28. Yang W, Li R, Peng T, Zhang Y, Jiang W, Ying L, Li J. mamO and mamE genes are essential for magnetosomes crystal biomineralization in *Magnetospirillum gryphiswaldense* MSR-1. Res Microbiol. 2010; **161**:701–705.
29. Scheffel A, Gärdes A, Grünberg K, Wanner G, and Schüler D. The major magnetosome proteins MamGFDC are not essential for magnetite biomineralization in *Magnetospirillum gryphiswaldense*, but regulate the size of magnetosome crystals. J Bacteriol. 2008; **190**:377–386.
30. Mickoleit F and Schüler D. Generation of nanomagnetic biocomposites by genetic engineering of bacterial magnetosomes. Bioinspired, Biomimetic and Nanobiomaterials. 2018; **8**:86–98.

31. Komeili A, Vali H, Beveridge TJ, Newman DK. Magnetosome vesicles are present before magnetite formation, and MamA is required for their activation. PNAS. 2004; **101**:3839–3844.
32. Tanaka M, Mazuyama E, Arakaki A, Matsunaga T. MMS6 protein regulates crystal morphology during nano-sized magnetite biomineralization *in vivo*. J Biol Chem. 2011; **286**:6386–6392.
33. Toro-Nahuelpan, M, Müller FD, Klumpp S, Plitzko, Bramkamp JM, and Schüler D. Segregation of prokaryotic magnetosome organelles is driven by treadmilling of a dynamic actin-like MamK filament. BMC Biology. 2016;**14**:88.
34. Schübbe S, Würdemann C, Heyen U, Wawer C, Peplies J, Glöckner FO, Schüler D. Transcriptional organization and regulation of magnetosome operons in *Magnetospirillum gryphiswaldense*. Appl. Environ. Microbiol. 2006; **72**:757-765.
35. Ullrich S, Kube M, Schübbe S, Reinhardt R, Schüler D. A hypervariable 130 kb genomic region of *Magnetospirillum gryphiswaldense* comprises a magnetosome island, which undergoes frequent rearrangements during stationary growth. J. Bacteriol. 2005; **187**:7176-7184.
36. Raschdorf O, Schüler D, and Uebe R. Preparation of Bacterial Magnetosomes for Proteome Analysis. Methods Mol. Biol. 2018; **1841**:45-57.
37. Kolinko I, Lohße A, Borg S, Raschdorf O, Jogler C, Tu Q, Pósfai M, Tompa É, Plitzko JM, Brachmann A, Wanner G, Müller R, Zhang Y, Schüler D. Biosynthesis of magnetic nanostructures in a foreign organism by transfer of bacterial magnetosome gene clusters. Nat. Nanotech. 2014; **9**:193–197.

38. Dziuba MV, Zwiener T, Uebe R, Schüler D. Single-step transfer of biosynthetic operons endows a non-magnetotactic *Magnetospirillum* strain from wetland with magnetosome biosynthesis. *Environmental Microbiology*. 2020; **22**:1603–1618.
39. Arakaki A., Webbs J, Matsunaga T. A novel protein tightly bound to bacterial magnetite particles in *Magnetospirillum magnetotacticum* strain AMB-1. *J Biol Chem*. 2003; **278**:8745–8750.
40. Arakaki A, Yamagishi A, Fukuyo A, Tanaka M, Matsunaga T. Co-ordinated functions of Mms proteins define the surface structure of cubo-octahedral magnetite crystals in magnetotactic bacteria. *Mol Microbiol*. 2014; **93**:554–567.
41. Rawlings AE, Bramble JP, Walker R, Bain J, Galloway JM, Staniland SS. Self-assembled MmsF proteinosomes control magnetite nanoparticle formation in vitro. *Proc. Natl Acad. Sci. USA* 111. 2014; 16094–16099.
42. Silva KT, Schüler M, Mickoleit F, Zwiener T, Müller FD, Awal RP, Weig A, Brachmann A, Uebe R, Schüler D. Genome-wide identification of essential and auxiliary gene sets for magnetosome biosynthesis in *Magnetospirillum gryphiswaldense*. *mSystems*. 2020; **5**:1–20.
43. Würdemann C, Peplies J, Schübbe S, Ellrott A, Schüler D, Glöckner FO. Evaluation of gene expression analysis using RNA-targeted partial genome arrays. *System. Appl. Microbiol*. 2006; **29**:349–357.
44. Wang X, Wang Q, Zhang Y, Wang Y, Zhou Y, Zhang W, Wen T, Li L, Zuo M, Zhang Z, Tian J, Jiang W, Li Y, Wang L, Li J. Transcriptome analysis reveals physiological characteristics required for magnetosome formation in *Magnetospirillum gryphiswaldense* MSR-1. *Environ Microbiol Rep*. 2016; **8**:371–381.

-
45. Ettwiller L, Buswell J, Yigit E, Schildkraut I. 2016. A novel enrichment strategy reveals unprecedented number of novel transcription start sites at single base resolution in a model prokaryote and the gut microbiome. *BMC Genomics*. 2016; **17**:1–14.
 46. Staniland SS, Ward B, Harrison A, van der Laan G, Telling N. Rapid magnetosome formation shown by real-time X-ray magnetic circular dichroism. *Proc Natl Acad Sci U S A*. 2007; **104**:19524–19528.
 47. Staniland SS, Rawlings AE. Crystallizing the function of the magnetosome membrane mineralization protein Mms6. *Biochem Soc Trans*. 2016; **44**:883–890.
 48. Nan X, Teng Y, Hu Z, Fang Q. A comprehensive assessment of the biocompatibility of *Magnetospirillum gryphiswaldense* MSR-1 bacterial magnetosomes *in vitro* and *in vivo*. *Toxicology*. 2021; **462**:152949.
 49. Mickoleit F, Jörke C, Geimer S, Maier DS, Müller JP, Demut J, Gräfe C, Schüler D, and Clement JH. Biocompatibility, uptake and subcellular localization of bacterial magnetosomes in mammalian cells. *Nanoscale Advances*. 2021; **3**:3799–3815.
 50. Hergt R, Hiergeist R, Zeisberger M, Schüler D, Heyen U, Hilger I, Kaiser WA. Magnetic properties of bacterial magnetosomes as diagnostic and therapeutic tools. *J Magn Magn Matter*. 2005; **293**:80–86.
 51. Alphantéry E, Guyot F, Chebbi I. Preparation of chains of magnetosomes, isolated from *Magnetospirillum magneticum* strain AMB-1 magnetotactic bacteria, yielding efficient treatment of tumors using magnetic hyperthermia. *Int J Pharm*. 2012; **434**:444–452.

-
52. Sangnier AP, Preveral S, Curcio A, Silva AKA, Lefèvre C, Pignol D, Lalatonne Y, Wilhelm C. Targeted thermal therapy with genetically engineered magnetic magnetosomes@RGD: Photothermia is far more efficient than magnetic hyperthermia. *J Control Release*. 2018; **279**:271–281.
53. Hafsi M, Preveral S, Hoog C, Hérault J, Perrier GA, Lefèvre CT, Michel H, Pignol D, Doyen J, Pourcher T, Humbert O, Thariat J, Cambien B. RGD-functionalized magnetosomes are efficient tumor radioenhancers for X-rays and protons. *Nanomedicine: NBM*. 2020; **23**:102084.
54. Heinke D, Kraupner A, Eberbeck D, Schmidt D, Radon P, Uebe R, Schüler D, Briel A. MPS and MRI efficacy of magnetosomes from wild-type and mutant bacterial strains. *Int J Magn Part Imaging*. 2017; **3**:1706004.
55. Kraupner A, Eberbeck D, Heinke D, Uebe R, Schüler D, Briel A. Bacterial magnetosomes—nature’s powerful contribution to MPI tracer research. *Nanoscale*. 2017; **9**:5788–5793.
56. Mériaux S, Boucher M, Marty B, Lalatonne Y, Prévéral S, Motte L, Lefèvre CT, Geffroy, Lethimonnier F, Péan M, Garcia D, Adryanczyk-Perrier G, Pignol D, Ginet N. Magnetosomes, biogenic magnetic nanomaterials for brain molecular imaging with 17.2 T MRI scanner. *Adv Healthc Mater*. 2015; **4**:1076–1083.
57. Tanaka T, Takeda H, Ueki F, Obata K, Tajima H, Takeyama H, Goda Y, Fujimoto S, Matsunaga T. Rapid and sensitive detection of 17 β -estradiol in environmental water using automated immunoassay system with bacterial magnetic particles. *J Biotechnol*. 2004; **108**:153–159.
58. Vargas G, Cypriano J, Correa T, Leão P, Bazylinski DA, Abreu F. Applications of magnetotactic bacteria, magnetosomes and magnetosome crystals in biotechnology and nanotechnology: Mini-Review. *Molecules*. 2018; **23**:2438.

-
59. Matsunaga T, Kamiya S. Use of magnetic particles isolated from magnetotactic bacteria for enzyme immobilization. *Appl Microbiol biotechnol.* 1987; **26**:328–332.
60. Ginet, N., Pardoux, R., Adryanczyk, G., Garcia, D., Brutesco, C., & Pignol, D. Single-step production of a recyclable nanobiocatalyst for organophosphate pesticides biodegradation using functionalized bacterial magnetosomes. *PLoS One*, 2011; **6**:e21442.
61. Mickoleit F, Lanzloth C, Schüler D. A versatile toolkit for controllable and highly selective multifunctionalization of bacterial magnetic nanoparticles. *Small.* 2020; **16**:1906922.
62. Honda T, Yasuda T, Tanaka T, Hagiwara K, Arai T, Yoshino T. Functional expression of full-length TrkA in prokaryotic host *Magnetospirillum magneticum* AMB-1 by using a magnetosome display system. *Appl Environ Microbiol.* 2014; **81**:1472–1476.
63. Xu J, Hu J, Liu L, Li L, Wang X, Zhang H, Jiang W, Tian J, Li Y, Li J. Surface expression of protein A on magnetosomes and capture of pathogenic bacteria by magnetosome/antibody complexes. *Front Microbiol.* 2014; **5**:136.
64. Xu J, Liu L, He J, Ma S, Li S, Wang Z, Xu T, Jiang W, Wen Y, Li Y, Tian J, Li F. J. Engineered magnetosomes fused to functional molecule (protein A) provide a highly effective alternative to commercial immunomagnetic beads. *Nanobiotechnol.* 2019; **17**:37.
65. Wacker R, Ceyhan B, Alhorn P, Schüler D, Lang C, Niemeyer CM. Magneto Immuno-PCR: A novel immunoassay based on biogenic magnetosome nanoparticles. *Biochem Biophys Res Commun.* 2003; **357**:391–396.

-
66. Mickoleit F, Jérôme V, Freitag R, Schüler D. Bacterial magnetosomes as novel platform for the presentation of immunostimulatory, membrane-bound ligands in cellular biotechnology. *Adv Biosys.* 2020; **4**:1900231.
 67. Borg S, Rothenstein D, Bill J, Schüler D. Generation of multi-shell magnetic hybrid nanoparticles by encapsulation of genetically engineered and fluorescent bacterial magnetosomes with ZnO and SiO₂. *Small.* 2015; **11**:4209–4217.
 68. Mickoleit F, Borkner CB, Toro-Nahuelpan M, Herold HM, Maier DS, Pitzko JM, Scheibel T, Schüler D. *In vivo* coating of bacterial magnetic nanoparticles by magnetosome expression of spider silk-inspired peptides. *Biomacromolecules.* 2018; **19**:962–972.
 69. De Vincentiis S, Falconieri A, Mickoleit F, Cappello V, Schüler D, and Raffa V. Induction of axonal outgrowth in mouse hippocampal neurons via bacterial magnetosomes. *Int J Mol Sci.* 2021; **22**:4126.
 70. Schüler D, Bäuerlein E. Dynamics of iron uptake and Fe₃O₄ biomineralization during aerobic and microaerobic growth of *Magnetospirillum gryphiswaldense*. *J Bacteriol.* 1998; **180**:159–162.
 71. Zhuang S, Anyaogu DC, Kasama T, Workman M, Mortensen UH, Hobley TJ. Effects of dissolved oxygen concentration and iron addition on immediate-early gene expression of *Magnetospirillum gryphiswaldense* MSR-1. *FEMS Microbiol Lett.* 2017; **364**:fnx079.
 72. Sun JB, Zhao F, Tang T, Jiang W, Tian JS, Li Y, Li JL. High-yield growth and magnetosome formation by *Magnetospirillum gryphiswaldense* MSR-1 in an oxygen-controlled fermentor supplied solely with air. *Appl Microbiol Biotechnol.* 2008; **79**:389–397.

-
73. Liu Y, Li GR, Guo FF, Jiang W, Li Y, Li LJ. Large-scale production of magnetosomes by chemostat culture of *Magnetospirillum gryphiswaldense* at high cell density. *Microb Cell Fact*. 2010; **9**:99.
74. Zhang Y, Zhang X, Jiang W, Li Y, Li J. Semicontinuous culture of *Magnetospirillum gryphiswaldense* MSR-q cells in an autofermentor by nutrient-balanced and isosmotic feeding strategy. *Appl Environ Microbiol*. 2011; **77**:5851–5856.
75. Fernandez-Castané A, Li H, Thomas ORT, Overton TW. Development of a simple intensified fermentation strategy for growth of *Magnetospirillum gryphiswaldense* MSR-1: Physiological responses to changing environmental conditions. *New Biotechnol*. 2018; **46**:22–30.
76. Berny C, Le Fèvre R, Guyot F, Blondeau K, Guizonne C, Rousseau E, Bayan N, Alphanbéry E. A method for producing highly pure magnetosomes in large quantity for medical applications using *Magnetospirillum gryphiswaldense* MSR-1 magnetotactic bacteria amplified in minimal growth media. *Front Bioeng Biotechnol*. 2020; **8**:16.
77. Fernandez-Castané A, Li H, Thomas OR, Overton TW. Flow cytometry as a rapid analytical tool to determine physiological responses to changing O₂ and iron concentration by *Magnetospirillum gryphiswaldense* strain MSR-1. *Sci Rep*. 2017; **7**:13118.
78. Schüler D, Uhl R, Bäuerlein E. A simple light scattering method to assay magnetism in *Magnetospirillum gryphiswaldense*. *FEMS Microbiol Lett*. 1995; **132**:139–145.

-
79. Dar, D, Shamir, M, Mellin, JR, Koutero, M, Stern-Ginossar, N, Cossart, P and Sorek, R. Term-seq reveals abundant ribo-regulation of antibiotics resistance in bacteria. *Science*, 2016; **352**:aad9822.
80. Pardee AB, Jacob F, Monod J. The genetic control and cytoplasmic expression of “Inducibility” in the synthesis of β -galactosidase by *E. coli*. *J Mol Biol.* 1961; **1**:165–178.
81. Cortes T, Schubert OT, Rose G, Arnvig KB, Comas I, Aebersold R, Young D. Genome-wide mapping of transcription start sites defines an extensive leaderless transcriptome in *Mycobacterium tuberculosis*. *Cell Rep.* 2013; **5**:1121–1131.
82. French CE, Bell JML, Ward FB. Diversity and distribution of hemerythrin-like proteins in prokaryotes. *FEMS Microbiol Lett.* 2007; **279**:131–145.
83. Frankel RB, Bazylnski DA. Magnetosomes and magneto-aerotaxis. *Contrib Microbiol.* 2009; **16**:182–193.
84. Kranz A, Busche T, Vogel A, Usadel B, Kalinowski J, Bott M, Polen T. RNAseq analysis of α -proteobacterium *Gluconobacter oxydans* 621H. *BMC Genomics.* 2018; **19**:24.
85. Lang C, Pollithy A, and Schüler D. Identification of promoters for efficient gene expression in *Magnetospirillum gryphiswaldense*. *Appl. Environ. Microbiol.* 2009; **75**:4206–4210.
86. Borg S, Hofmann J, Pollithy A, Lang C, Schüler D. New vectors for chromosomal integration enable high-level constitutive or inducible magnetosome expression of fusion proteins in *Magnetospirillum gryphiswaldense*. *Appl. Environ. Microbiol.* 2014; **80**:2609-2616.
87. Studier FW, Moffatt BA. Use of bacteriophage T7 RNA polymerase to direct selective high-level expression of cloned genes. *J Mol Biol.* 1986; **189**:113–130.

4 Publications and manuscripts

Article 1

Manuscript 1

An automated oxystat fermentation regime for microoxic cultivation of
Magnetospirillum gryphiswaldense

Cornelius N. Riese, René Uebe, Sabine Rosenfeldt, Anna S. Schenk, Valérie Jérôme,
Ruth Freitag and Dirk Schüler.

Microbial Cell Factories (2020) 19:206

doi: 10.1186/s12934-020-01469-z

RESEARCH

Open Access



An automated oxystat fermentation regime for microoxic cultivation of *Magnetospirillum gryphiswaldense*

Cornelius N. Riese¹ , René Uebe¹, Sabine Rosenfeldt^{2,3}, Anna S. Schenk^{3,4}, Valérie Jérôme⁵, Ruth Freitag^{5*} and Dirk Schüler^{1*}

Abstract

Background: Magnetosomes produced by magnetotactic bacteria represent magnetic nanoparticles with unprecedented characteristics. However, their use in many biotechnological applications has so far been hampered by their challenging bioproduction at larger scales.

Results: Here, we developed an oxystat batch fermentation regime for microoxic cultivation of *Magnetospirillum gryphiswaldense* in a 3 L bioreactor. An automated cascade regulation enabled highly reproducible growth over a wide range of precisely controlled oxygen concentrations (1–95% of air saturation). In addition, consumption of lactate as the carbon source and nitrate as alternative electron acceptor were monitored during cultivation. While nitrate became growth limiting during anaerobic growth, lactate was the growth limiting factor during microoxic cultivation. Analysis of microoxic magnetosome biomineralization by cellular iron content, magnetic response, transmission electron microscopy and small-angle X-ray scattering revealed magnetosomal magnetite crystals were highly uniform in size and shape.

Conclusion: The fermentation regime established in this study facilitates stable oxygen control during culturing of *Magnetospirillum gryphiswaldense*. Further scale-up seems feasible by combining the stable oxygen control with feeding strategies employed in previous studies. Results of this study will facilitate the highly reproducible laboratory-scale bioproduction of magnetosomes for a diverse range of future applications in the fields of biotechnology and biomedicine.

Keywords: Magnetosomes, *Magnetospirillum gryphiswaldense*, Oxystat fermentation, Magnetosome biomineralization

Background

Magnetosomes are membrane-enveloped magnetite (Fe_3O_4) or greigite (Fe_3S_4) crystals produced by magnetotactic bacteria for orientation along the Earth's magnetic

field [1]. Magnetosome biosynthesis is a complex, stepwise process involving the formation of a dedicated magnetosome vesicle, which serves as a nanoreactor for the subsequent uptake of iron and the biomineralization of magnetic crystals [2, 3].

In the widely studied alphaproteobacterium *Magnetospirillum gryphiswaldense* each step is highly regulated by a set of more than 30 genes leading to the formation of single crystalline magnetite particles with defined size, shape and magnetic properties, which are so far unmatched by magnetic nanoparticles produced by

*Correspondence: Ruth.Freitag@uni-bayreuth.de; Dirk.Schueler@uni-bayreuth.de

¹ Department of Microbiology, University of Bayreuth, Universitätsstraße 30, 95447 Bayreuth, Germany

⁵ Chair for Process Biotechnology, University of Bayreuth, Universitätsstraße 30, Bayreuth 95447, Germany

Full list of author information is available at the end of the article



© The Author(s) 2020. This article is licensed under a Creative Commons Attribution 4.0 International License, which permits use, sharing, adaptation, distribution and reproduction in any medium or format, as long as you give appropriate credit to the original author(s) and the source, provide a link to the Creative Commons licence, and indicate if changes were made. The images or other third party material in this article are included in the article's Creative Commons licence, unless indicated otherwise in a credit line to the material. If material is not included in the article's Creative Commons licence and your intended use is not permitted by statutory regulation or exceeds the permitted use, you will need to obtain permission directly from the copyright holder. To view a copy of this licence, visit <http://creativecommons.org/licenses/by/4.0/>. The Creative Commons Public Domain Dedication waiver (<http://creativecommons.org/publicdomain/zero/1.0/>) applies to the data made available in this article, unless otherwise stated in a credit line to the data.

chemical synthesis [4–7]. Hence, magnetosomes are of great potential in the biomedical and biotechnological field, and isolated magnetosomes were already successfully applied for cancer treatment, such as magnetic hyperthermia [8–10], phototherapy [11] and radiosensitization [12], as contrast agent for magnetic imaging [13–16] and as a tool in immune assays [17]. Furthermore, the proteinaceous membrane of magnetosomes from *M. gryphiswaldense* and related organisms can be functionalized by genetic or chemical coupling of additional functional moieties, such as enzymes for immobilization of enzymatic cascades [18–21], fluorophores, antibodies for diagnostic purposes e.g. Immuno-PCR [20, 22–24], immunostimulatory ligands [25], or various inorganic and organic coating materials for enhancement of biocompatibility [26, 27].

Practical applications of magnetosomes have so far been limited by their poor availability, which is due to the lack of precise techniques for highly controlled large-scale production with defined process parameters. Mass cultivation of the available magnetobacterial strains is challenging due to their fastidious microaerophilic to anoxic lifestyle, and the dependence of magnetosome biosynthesis on suboxic conditions, which results in slow growth and low biomass as well as magnetosome yields in routine batch cultivation [1]. The most robust and widely used strain for magnetosome engineering and bio-production is *M. gryphiswaldense*, which produces up to 60 cuboctahedral magnetite crystals with 20–50 nm in diameter [28, 29].

As for other magnetotactic bacteria, magnetite biomineralization in *M. gryphiswaldense* is strongly affected by growth conditions [30, 31]. While fastest growth occurs at moderately low oxygen partial pressures (pO_2) of 0.25–2 mbar (equivalent to a dissolved oxygen (dO_2) concentration of 0.1–1% of air saturation), magnetite biomineralization is increasingly stimulated by a decrease in oxygen concentration [30, 32]. Highest quantity and largest magnetite crystals are formed under denitrifying conditions in the entire absence of oxygen with nitrate (NO_3^-) as the only electron acceptor for respiration [30, 32–35]. However, anoxic flask cultivation to yields higher than about 0.3 OD_{565} is difficult due to the resulting toxic effects of denitrification intermediates such as nitrite (NO_2^-), which accumulate at NO_3^- concentrations higher than 10 mM [33, 34]. This tradeoff can be alleviated by microaerobic cultivation, where oxygen and nitrate respiration overlap [32–35]. Nonetheless, the controlled microoxic conditions below 10% dO_2 , needed for optimal magnetosome production, are difficult to maintain and often require specific adaptations for the stable regulation, such as the programming of a reliable automated control cascade, and the bioreactor setup has to be

characterized and optimized to enable homogenous mixing as well as precise and stable dO_2 adjustment.

In the first systematic study, Heyen and Schüller [32] investigated growth and magnetosome biosynthesis of *M. gryphiswaldense*, *M. magnetotacticum* and *M. magneticum* in a 4 L bioreactor at various pO_2 tensions from 0.25 mbar to 212 mbar (dO_2 of 0.1% to 100% of air saturation) using an automated oxygen regulation with a specialized pO_2 measurement and gas supply setup. They showed a clear correlation between pO_2 and magnetosome biosynthesis in all three magnetospirilla and a maximum magnetosome yield of 7.9 mg L^{-1} was reached with *M. gryphiswaldense* at 0.25 mbar pO_2 with a biomass yield of 0.4 g dry weight per liter ($g_{dw} L^{-1}$) (OD_{565} 1.4) [32].

Sun et al. [36] applied a microoxic fed-batch oxystat strategy, where oxygen intake into the medium was regulated solely by agitation with a fixed airflow rate. Highest biomass and magnetosome yields of 2.17 $g_{dw} L^{-1}$ (OD_{565} 7.24) and 41.7 mg L^{-1} , respectively, were reached in a 42 L bioreactor, where stirrer speed was increased manually in increments of 40 rpm whenever the growth rate decreased markedly. Furthermore, dO_2 was permanently kept below the dO_2 -probe's sensitivity. In follow-up studies by Liu et al. [37] and Zhang et al. [38], the feeding strategy was further improved, resulting in biomass and magnetosome yields of OD_{565} 12.2 and 82.23 ± 5.36 mg L^{-1} up to 9.16 $g_{dw} L^{-1}$ (OD_{565} 42) and 356.52 mg L^{-1} , respectively. Again, in these studies, the stirrer speed was increased in pre-set time intervals independent of measured dO_2 . A different approach was applied by Fernandez-Castané et al. [39] in a 5 L bioreactor, where dO_2 was controlled by manual adjustment of airflow between 0 and 0.1 standard liter per minute (SLPM) and agitation between 100 and 500 rpm, thereby keeping the dO_2 permanently below the dO_2 -probe's sensitivity (dO_2 below 1% of air saturation). This resulted in biomass and magnetosome yields of OD_{565} 16.6 and 54.3 ± 0.4 mg L^{-1} , respectively [39]. Moreover, cell morphology and viability were further investigated by flow cytometry, thereby showing viable cells throughout the fermentation process [40].

The most recent study conducted by Berny et al. [41] employed a manual regulation regime to cultivate *M. gryphiswaldense* in a minimal medium avoiding complex, non-defined constituents such as peptone and yeast extract. Maximal biomass and magnetosome yields were 2.4 $g_{dw} L^{-1}$ (OD_{565} 8) and 10 mg L^{-1} , respectively [41].

During an investigation of oxygen and iron impact on gene expression, an automated oxystat regime in a 1 L bioreactor based on dynamic gas blending of nitrogen and air was applied, whereas agitation and maximal gas flow remained constant at 120 rpm and

1 SLPM, respectively [42]. In this study, set dO_2 values of 0.5% and 5% were kept stable over the fermentation, however this regime led to a steady decrease of oxygen concentration during growth at set dO_2 values above 15% [42].

Despite the impressive improvements in *M. gryphiswaldense* fermentation, which resulted in ODs as high as 16–42 and magnetosome yields > 35 mg magnetite L^{-1} [38, 39], respectively, application has been hampered by the discontinuous dO_2 control throughout cultivation. This in turn makes scale-up and transfer of protocols to other fermenter systems difficult, due to the highly specific, empirically determined parameters optimized for the particular type of bioreactor used in these studies. By contrast, an automated oxygen regulation regime would allow to overcome these limitations and thereby enhances reproducibility and handling through standardization of the process. Moreover, while it is well known that dissolved oxygen concentrations also greatly affect the size, shape and crystallinity of magnetite particles, previous studies mostly focused on the analysis and optimization of growth parameters rather than magnetosome characteristics. Typically, the C_{mag} (i.e. a light-scattering parameter for the semiquantitative estimation of average magnetic alignment of cells [29]) and the intracellular iron content were used as proxies to quantify magnetosome bioproduction, even though these techniques do not provide precise information on the number, size and shape of magnetite particles. Finally, another important, but so far neglected aspect of process reproducibility is the preparation and treatment of precultures from stock to inoculation (i.e. the 'seed-train').

The aim of this study was the establishment and characterization of an oxystat fermentation regime for cultivation of *M. gryphiswaldense* employing an automatic cascade regulation for precise control of dO_2 , which was successfully applied for 95%, 10% and 1% dO_2 values. Additionally, magnetosome biosynthesis was monitored throughout cultivation employing a combination of complementary analytical techniques including atomic absorption spectroscopy (AAS), quantitative transmission electron microscopy (TEM) and small-angle X-ray scattering (SAXS) [43] to study the composition and structure of the forming nanoparticles. To the best of our knowledge, the unique combination of complementary analytical techniques employed in this study provides the first truly quantitative assessment of magnetosome bioproduction at well-defined oxygen concentrations, thus enhancing the understanding of oxygen impact in magnetite biomineralization.

Results

Establishment of an automated oxystat fermentation regime

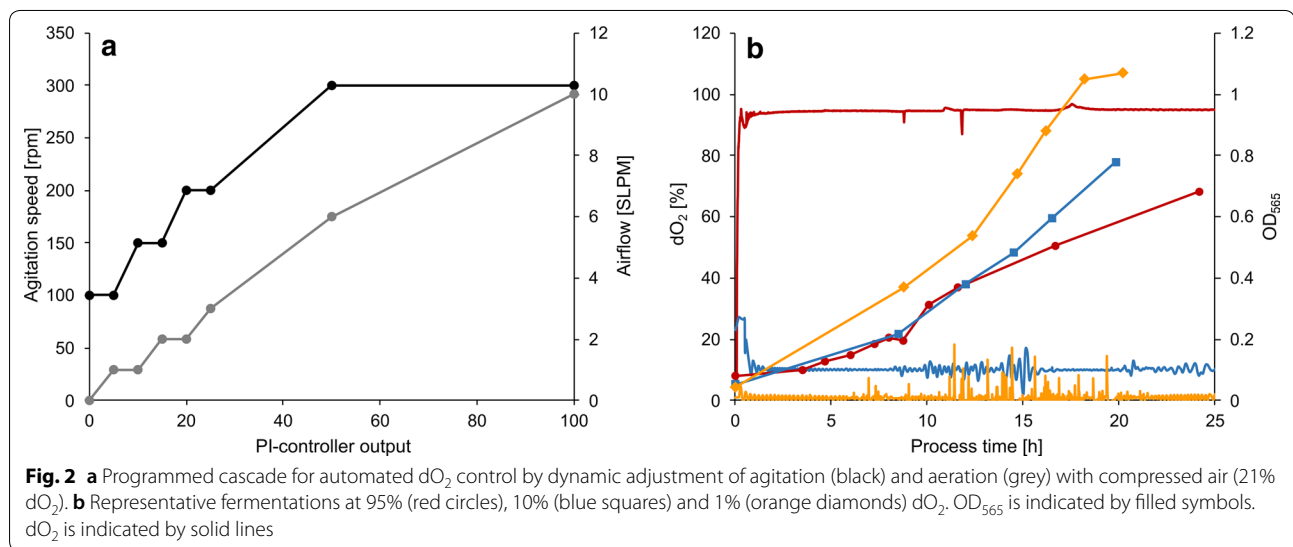
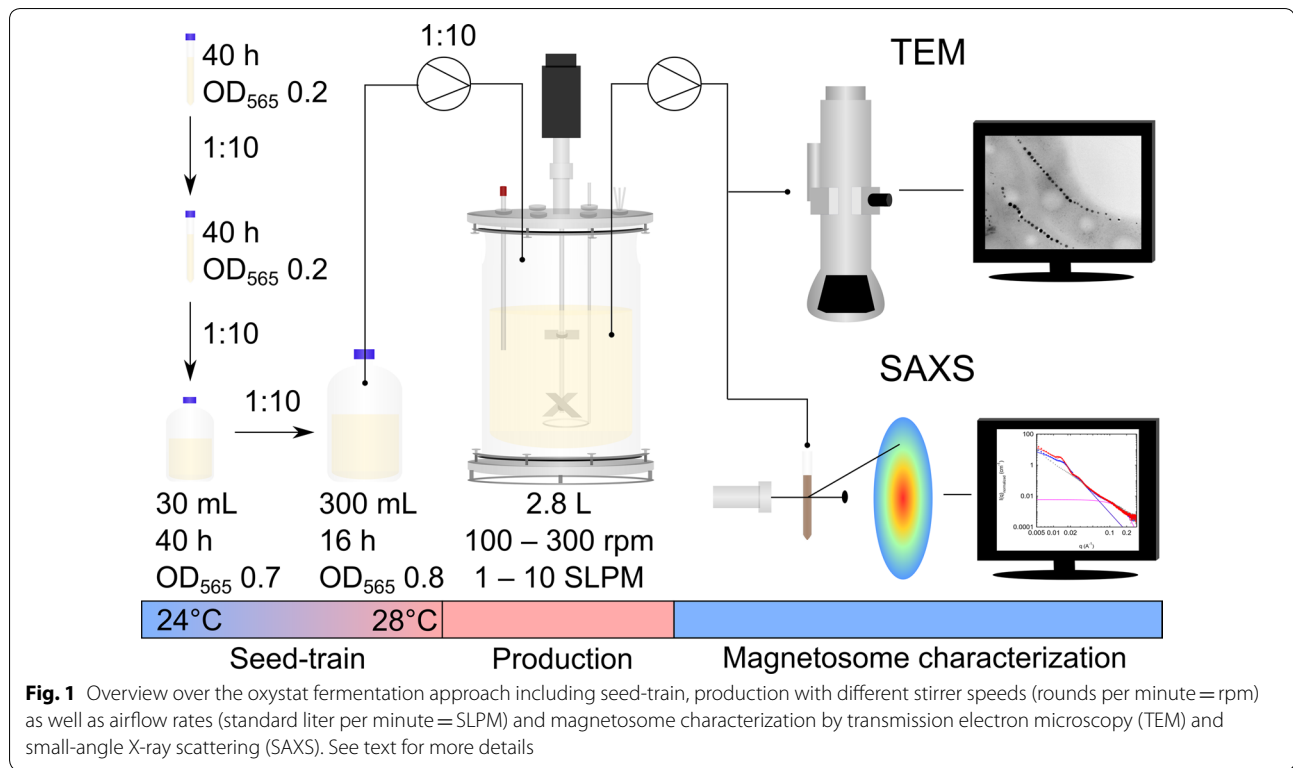
The seed-train used in this study encompassed two passages for initial subcultures incubated in 10 mL at room temperature (24 °C) for 40 h. Further subcultivation was performed by step-wise scale-up in screw-capped bottles of different sizes to reach the final inoculum of 300 mL at an OD_{565} of 0.8 (equivalent to about 1.8×10^8 cells mL^{-1}) after 16 h with magnetic ($C_{mag} = 1.20$), highly viable cells (as judged by their motility), encompassing ~ 15 generations from stock to final inoculum. This seed-train (as summarized in Fig. 1) was used in all subsequent fermentation experiments.

To ensure optimal and reproducible oxygen input and dispersion, we first characterized and optimized the setup of the 3 L bioreactor. Mixing and oxygen transfer could be greatly improved by combining a radial (Rushton) and axial mixing (pitched blade) impeller type [44].

Next, we aimed to establish a controlled oxystat fermentation regime for a wide range of oxygen concentrations. To ensure constant dO_2 throughout growth, we used a *Proportional Integral* (PI) controller mediated cascade for automated regulation by combining control of airflow and stirrer speed. The cascade was programmed to match the requirements that both stirrer speed and airflow have to be precisely maintained at low levels in the beginning, but need to be sufficiently high to sustain increasing cell densities throughout cultivation. Accordingly, stirring as well as airflow were increased in a step-wise manner independently from each other, exclusively regulated by the PI-controller output (Fig. 2a). To test the precision of the optimized dO_2 regulation, fermentations were performed at oxic (dO_2 95%) and microoxic (dO_2 10% and 1%) conditions.

With a set value of 95% (200 mbar), dO_2 was maintained precisely over the entire cultivation, with only minor fluctuations (median of 94.9%) (Fig. 2b). The final OD_{565} of 0.76 was reached after 30 h, but as expected only a weak C_{mag} of 0.1 was detectable, due to known inhibition of magnetite biomineralization by dO_2 above 5% (10 mbar) [32].

At 10% (20 mbar) set dO_2 value, monitored oxygen was consistently stable with a median of 10% dO_2 . Larger fluctuations at 10% dO_2 were observed during main growth phase between 10–16 h of incubation, where the control cascade has to cope with increasing oxygen requirements of the culture (Fig. 2b). Although growth was greatly enhanced (maximal OD_{565} of 1.2 after 35 h) compared to oxic conditions (95% dO_2), magnetosome biomineralization was still inhibited as indicated by a low C_{mag} value of 0.1 at the end of process, similar as previously described [32].



At 1% (2 mbar) set dO_2 value, the median of measured dO_2 was 0.9%. Here, most of the sporadically occurring fluctuations in dO_2 were also observed during main growth phase between 11–20 h of incubation. These fluctuations result most likely by a combination of both probe sensitivity, visible by higher background fluctuations at 1% dO_2 in comparison to higher set dO_2

values and cascade reactivity, indicated by a higher fluctuation frequency during the main growth phase. Despite of the sporadic dO_2 fluctuations (Fig. 2b), growth and magnetosome formation (C_{mag}) were consistent in duplicate experiments with maximal OD_{565} of 1.1 after 18 h and highest C_{mag} of 0.7 (Additional file 1: Figure S2). Since at dO_2 concentrations below 1%, the frequency of these sporadic fluctuations would

increase, thereby disrupting stable oxygen control, 1% dO₂ was investigated as lowest oxygen condition in the following experiments.

Effect of the oxygen concentration on growth, substrate consumption and biomineralization

In order to estimate the effect of different dO₂ tensions on growth and magnetosome biomineralization, we performed batch fermentations in biological triplicates and with independent seed-trains at oxic (95% dO₂) and microoxic (1% dO₂) conditions. For comparison, anoxic (0% dO₂) fermentations were performed, which were expected to sustain optimal magnetosome biosynthesis. For anoxic (denitrifying) growth, the concentration of nitrate as electron acceptor was increased to 10 mM to enable higher cell yields, while 4 mM nitrate was supplemented at microoxic and oxic growth conditions.

Under all tested conditions, growth was highly consistent among replicates as shown in Fig. 3d. As observed before, growth was lowest at 95% dO₂ with a growth rate of $0.07 \pm 0.009 \text{ h}^{-1}$ (doubling time of $9.61 \pm 1.3 \text{ h}$). The maximal OD₅₆₅ under this condition of 0.71 ± 0.05 was reached after 35 h. Maximal growth among all tested conditions was observed at 1% dO₂ with a growth rate of $0.15 \pm 0.007 \text{ h}^{-1}$ (doubling time of $4.76 \pm 0.23 \text{ h}$) and a maximal OD₅₆₅ of 1.06 ± 0.06 after ca. 18 h. In the absence of O₂ (0% dO₂), the growth rate was reduced to $0.13 \pm 0.005 \text{ h}^{-1}$ (doubling time of $5.24 \pm 0.21 \text{ h}$) with a maximal OD₅₆₅ of 0.49 ± 0.01 after 25 h. In all three cases, cells were highly motile (i.e. viable) and showed apparently identical sizes and helical cell shapes at the end of growth (average cell length of $3.4 \pm 0.9 \mu\text{m}$) (Fig. 3a–c).

Consistent with the observed growth rates, lactate as the main carbon source and nitrate as the main nitrogen source as well as the main electron acceptor under anoxic and oxygen-limited conditions were depleted from the medium with different rates during the main growth phase (Fig. 3e, f). Both oxic (95% dO₂) and anoxic (0% dO₂) cultures showed low lactate consumption rates with 2.67 ± 1.17 and $3.12 \pm 1.17 \text{ mM h}^{-1} \text{ OD}_{565}^{-1}$, respectively. The highest lactate consumption was observed under microoxic (1% dO₂) conditions with $4.76 \pm 0.23 \text{ mM h}^{-1} \text{ OD}_{565}^{-1}$, whereas biomass yields in mg dry-weight per mmol substrate ($Y_{x/s}$) did not significantly differ between oxygen conditions (Table 1).

The lowest NO₃[−] consumption was observed during aerobic growth ($0.71 \pm 0.28 \text{ mM h}^{-1} \text{ OD}_{565}^{-1}$), because here nitrate serves only as nitrogen source, due to repression of respiratory nitrate reduction by O₂ as electron acceptor (Fig. 3f) [33, 34].

At low (1%) dO₂ tensions, nitrate as well as oxygen were both simultaneously used as electron acceptors for respiration [34, 35], which is consistent with an increased

NO₃[−] consumption of $1.09 \pm 0.15 \text{ mM h}^{-1} \text{ OD}_{565}^{-1}$ (Table 1).

Highest nitrate consumption was observed during anaerobic growth. After 25 h, nitrate initially present at 10 mM was completely consumed ($6.13 \pm 0.83 \text{ mM h}^{-1} \text{ OD}_{565}^{-1}$), resulting in limited growth under these conditions as indicated by the early onset of the stationary phase marked by the slight decrease of OD₅₆₅ as typically observed for *M. gryphiswaldense* (Fig. 3d, f). Although a clear correlation between growth and nitrate concentration was observed, the use of a higher initial amount of nitrate is prohibited by the accumulation of toxic intermediates during denitrification [33, 34]. Alternatively, addition of nitrate upon depletion could theoretically prolong the main growth phase, since substrates such as lactate and iron are still sufficiently present in the fermentation medium.

For evaluation of the oxygen impact on magnetite biomineralization, we characterized magnetosome quality at 95%, 1% and 0% dO₂ by the *at line* techniques C_{mag} and AAS (Fig. 3g, h) as well as the quantitative techniques TEM and SAXS (Additional file 2: Figure S3). Different oxygen conditions had a clear effect on biomineralization: A C_{mag} value of 0.99 ± 0.01 was measured under anoxic conditions, indicating optimal magnetosome production of the culture, which was also confirmed by TEM (Fig. 4a, TEM). Here, largest magnetosome particles were observed with average diameters of $33.8 \pm 9.4 \text{ nm}$ at the end of the process after 34 h. At the start of growth, magnetosome particle sizes originating from the microoxic inoculum were at $25.8 \pm 8.9 \text{ nm}$ with a wide distribution including both smaller and larger particles (Fig. 4a, seed-train). Already after 15 h in mid-growth phase, particle sizes steadily increased to $32.0 \pm 9.5 \text{ nm}$ with fewer smaller particles (Fig. 4a, mid-growth). At the end of growth after 20 h, a further increase to $33.5 \pm 9.1 \text{ nm}$ was observed (Table 2), whereas longer incubation did not lead to a significant increase in magnetosome size, thus marking the maximum of magnetosome particle sizes in the batch fermentation experiment (Fig. 4a, end of growth). To further estimate O₂ effects on biomineralization during cell elongation, the determined average magnetosome number per cell was normalized to cell length. Throughout cultivation numbers of magnetosomes remained constant at around 25 with approximately 8 magnetosomes (MS) per μm cell length (=MS μm^{-1}). Only in mid-growth phase, a slight increase of around $0.7 \text{ MS } \mu\text{m}^{-1}$ was observed, most likely caused by smaller cells during faster division in this growth phase (Table 2). Additionally, particle morphology was much more homogeneous at the end of the process in comparison to the start (Fig. 4a, TEMs). Overall magnetite crystals appeared more evenly shaped under

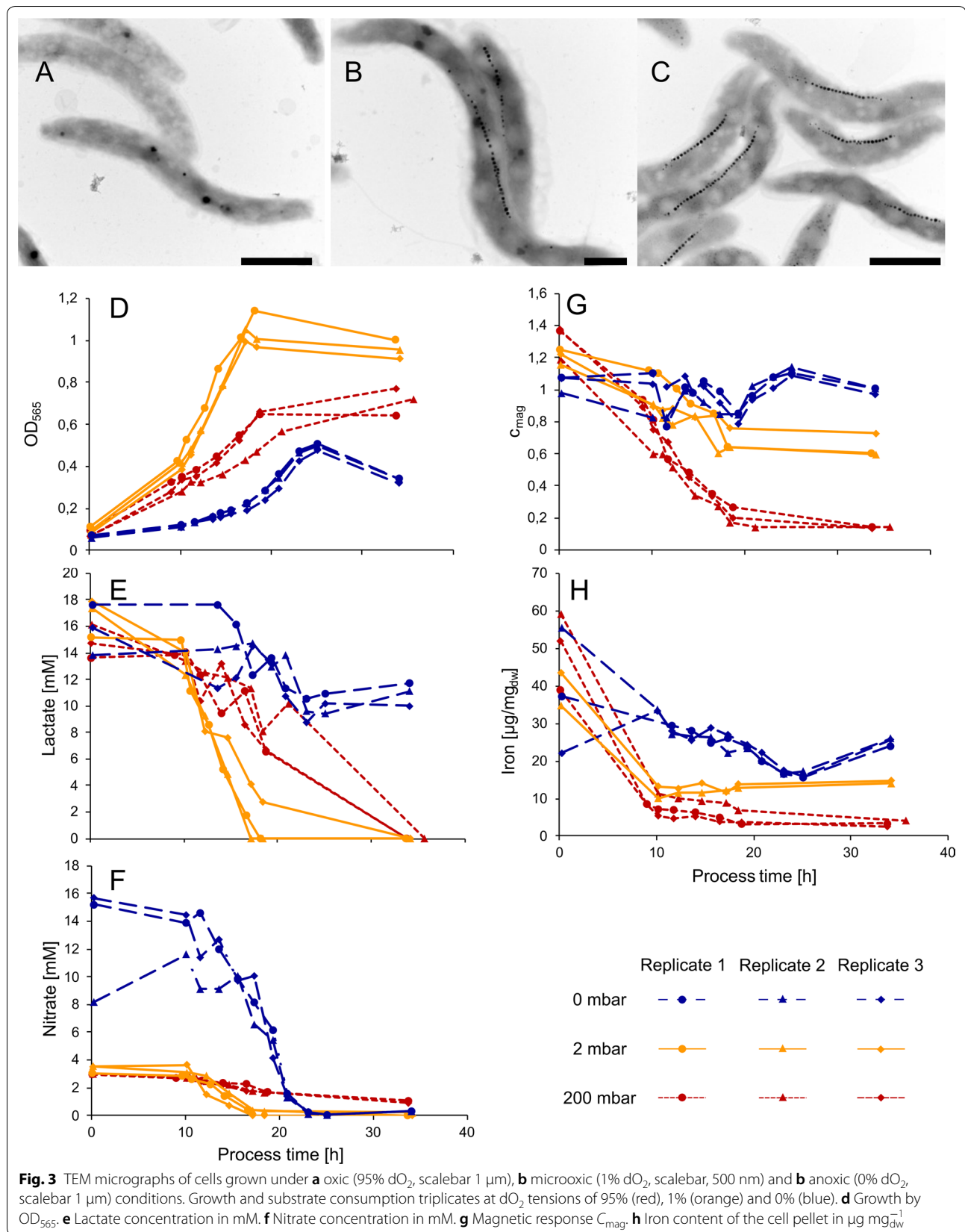


Table 1 Growth and substrate consumption rates of cells during main growth phase at 95% (12–18 h), 1% (10–17 h) and 0% (17–23 h) dO₂

| | 95% dO ₂ | 1% dO ₂ | 0% dO ₂ |
|--|---------------------|--------------------|--------------------|
| Growth rate μ [h ⁻¹] | 0.07 ± 0.009 | 0.15 ± 0.007 | 0.13 ± 0.005 |
| Doubling time [h] | 9.61 ± 1.3 | 4.76 ± 0.23 | 5.24 ± 0.21 |
| Maximal OD ₅₆₅ | 0.71 ± 0.05 | 1.06 ± 0.06 | 0.49 ± 0.01 |
| Lactate consumption rate [mM h ⁻¹ OD ₅₆₅ ⁻¹] | 2.67 ± 1.17 | 4.63 ± 1.02 | 3.12 ± 1.17 |
| Y _{x/s} [mg _{dw} mmo _{lactate} ⁻¹] | 4.59 ± 0.88 | 4.08 ± 0.43 | 5.40 ± 1.04 |
| Nitrate consumption rate [mM h ⁻¹ OD ₅₆₅ ⁻¹] | 0.71 ± 0.28 | 1.09 ± 0.15 | 6.13 ± 0.83 |
| Y _{x/s} [mg _{dw} mmo _{nitrate} ⁻¹] | 26.5 ± 4.6 | 21.1 ± 4.2 | 2.5 ± 0.9 |
| Cellular iron content [mg g _{dw} ⁻¹] | 3.3 ± 0.7 | 14.4 ± 0.4 | 25.3 ± 0.9 |

Rates were measured in biological triplicates. Iron content of the biomass was measured after the end of cultivation at 35 h. Biomass productivity per mol substrate for lactate and nitrate (Y_{x/s}) was calculated for the end of growth, where OD₅₆₅ reached the maximum

anoxic conditions. Consistently, throughout growth also the intracellular iron content increased steadily, reaching up to 25.3 ± 0.9 mg g_{dw}⁻¹ (Fig. 3h).

At 1% dO₂ a medium C_{mag} of 0.74 ± 0.007 was measured. Accordingly, microoxic conditions led to intermediate-sized magnetosome particles of 29.3 ± 7.9 nm in comparison to anoxic and oxic conditions (Table 2). Here, particle sizes increased throughout the fermentation process. Seed-train cultures under uncontrolled dO₂ conditions showed particle sizes of 26.7 ± 8.5 nm (Fig. 4b, seed-train). In mid-growth phase after 14 h of incubation, average particle diameter was 26.7 ± 8.4 nm (Fig. 4b, mid-growth), but reached a maximum of 29.3 ± 7.9 nm after 18 h incubation. Due to the fact that no further increase in magnetosome size was observed under anoxic conditions as optimal magnetosome forming conditions between mid-growth and stationary phase, final magnetosome sizes were investigated at the end of the main growth phase. Cells contained ca. 28 magnetosome particles per cell with ca. 8 MS μm⁻¹. Furthermore, particle and chain morphology became more regular throughout the process (Fig. 4b, TEMs). The intracellular iron content steadily increased up to 14.4 ± 0.4 mg g_{dw}⁻¹ (Fig. 3h).

Oxic (95% dO₂) conditions entirely abolished magnetosome bioproduction, as indicated by a steady decrease of C_{mag} down to nearly 0 (Table 3). Additionally, in TEM analyses only 10% of the cells showed up to three magnetosomes per cell likely originating from the microoxic

inoculum. Further a steady decrease of iron content in the biomass was detected to 3.3 ± 0.7 mg g_{dw}⁻¹ (Fig. 3h).

To further verify average magnetosome sizes determined by TEM image analysis, we applied SAXS as a volume-sensitive non-destructive bulk technique for the quantitative assessment of nanostructural parameters. Most importantly, SAXS analysis enables us to extract the radii of both, the magnetosome core (R_{core}) and the surrounding magnetosome membrane (R_{membrane}), while avoiding possible artifacts caused by sample preparation.

Average magnetosome radii (R, R = R_{core} + R_{membrane}) analyzed by SAXS were derived from the first form factor minimum at q ≈ 0.03 Å⁻¹ resulting in overall magnetosome diameters of 2R = 39 ± 7 nm for 0% dO₂ and 2R = 34 ± 7 nm for 1% dO₂ (both Gaussian size distribution, Additional file 2: Figure S3 A solid blue and yellow line). The contribution of surrounding vesicles to the magnetosome radius R was estimated by modeling the Guinier law representative of small spherical objects to the SAXS profile of aerobically cultivated samples, which do contain little or no magnetite within the empty vesicle. In this model, the proteinaceous vesicle membrane is regarded as an envelope composed of spherical protein structures with radii smaller than the magnetite core (Additional file 2: Figure S3 B, solid green line). Since the sharp phase boundary in the excess electron density distribution between magnetite crystal and its surrounding membrane blurs in polydisperse multi-particle systems,

(See figure on next page.)

Fig. 4 a Transmission electron micrographs of representative cells (scale bar 200 nm) and magnetosome particle sizes under anoxic (0% dO₂) conditions at different timepoints of the process. Seed-train = 0 h (n = 2925), mid-growth = 15 h (n = 3069) and end of growth = 20 h (n = 3058).

b Transmission electron micrographs (scale bar 1 μm (left micrograph) and 200 nm) and magnetosome particle sizes under microoxic (1% dO₂) conditions at different timepoints of the process. Seed-train = 0 h (n = 3421), mid-growth = 14 h (n = 2267) and end of growth = 18 h (n = 3180).

In box plots, the box indicates the interquartile range, the bar indicates the median, and the red dot represents the mean. Grey dots represent data points above or below the 95th and 5th percentile. The violin plots show the magnetosome particle size distribution of measured particle sizes. For statistical comparison of particle sizes, Wilcoxon rank sum test was performed (****, p < 0.0001; ns, not significant)

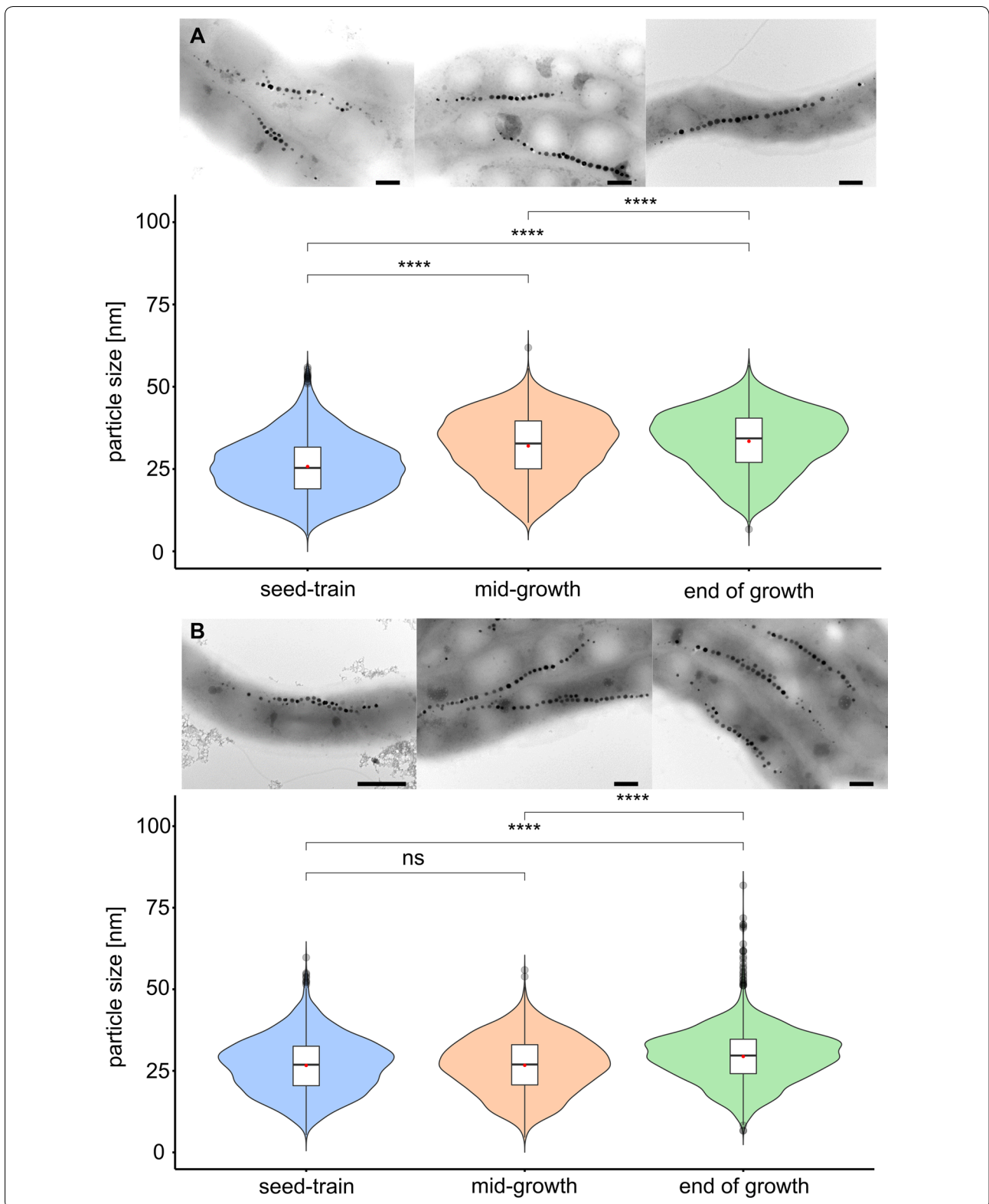


Table 2 Characteristics of magnetosomes produced under anoxic and microoxic conditions

| Process time | MS diameter [nm] | Cell length [μm] | MS/Cell | MS/cell length [μm^{-1}] |
|--------------|------------------|-------------------------------|----------------|---------------------------------------|
| Anoxic | | | | |
| 0 h | 25.8 \pm 8.9 | 3.0 \pm 0.7 | 24.4 \pm 2.3 | 8.1 \pm 0.5 |
| 15 h | 32.0 \pm 9.5 | 2.9 \pm 0.6 | 25.6 \pm 0.6 | 8.8 \pm 0.8 |
| 20 h | 33.5 \pm 9.1 | 3.0 \pm 0.8 | 25.5 \pm 2.1 | 8.4 \pm 0.2 |
| 34 h | 33.8 \pm 9.4 | 3.1 \pm 0.7 | 25.3 \pm 0.6 | 8.1 \pm 0.2 |
| Microoxic | | | | |
| 0 h | 26.7 \pm 8.5 | 3.3 \pm 0.8 | 29.2 \pm 2.7 | 8.8 \pm 0.1 |
| 14 h | 26.7 \pm 8.4 | 3.1 \pm 0.8 | 27.9 \pm 0.9 | 8.9 \pm 1.1 |
| 18 h | 29.3 \pm 7.9 | 3.4 \pm 0.9 | 28.4 \pm 2.8 | 7.7 \pm 0.6 |

Magnetosome diameter was measured with approximately 1000 particles per triplicate. Cell length was determined for 100 cells

the membrane thickness of $R_{\text{membrane}} = 1.7$ nm estimated from the radius of gyration ($R_g = 1.3$ nm), has to be subtracted prior to comparison with TEM data, which are predominantly sensitive to the high contrast magnetite core. Taking the thickness of the biomembrane into account, the dimensions extracted from SAXS measurements are in very good agreement with the TEM results (Table 3).

Discussion

Since optimum growth and magnetosome biosynthesis only occur within a narrow range of oxygen concentration, reproducibility of both greatly suffers from unstable O_2 control. In this study we established a well characterized, automated oxystat fermentation regime, which enables both reproducible cultivation of *M. gryphiswaldense* over several oxygen conditions (0%, 1% and 95% dO_2) as well as highly uniform magnetosome production. The regime was designed to solve three major limitations: First, a standardized microoxic seed-train procedure was developed to enhance process stability by inoculation of the bioreactor with highly viable cells resulting in highly reproducible growth behavior among biological

Table 3 C_{mag} and magnetite particle sizes measured by quantitative TEM and SAXS under the three tested dO_2 conditions at the end of cultivation after 34 h (95% dO_2), 18 h (1% dO_2) and 34 h (0% dO_2)

| | C_{mag} | TEM | | SAXS [nm] |
|-------------------------------|------------------|-------------|-----------------------|--------------|
| | | Median [nm] | Average diameter [nm] | |
| Oxic (95% dO_2) | 0.13 \pm 0.005 | – | – | – |
| Microoxic (1% dO_2) | 0.74 \pm 0.07 | 29.7 | 29.3 \pm 7.9 | 30.6 \pm 7 |
| Anoxic (0% dO_2) | 0.99 \pm 0.01 | 35.0 | 33.8 \pm 9.4 | 35.6 \pm 7 |

triplicates (Fig. 3a). Second, a cultivation process with an automated oxygen control cascade was designed and successfully applied for stable regulation of oxic and microoxic dO_2 concentrations. Even at 1% as lowest dO_2 condition tested, cultures showed highly consistent growth behavior (Additional file 1: Figure S2). Third, a comprehensive analytical workflow for magnetosome particle characterization combining a variety of different techniques was established for evaluation of magnetosome quality. Additionally, magnetosome production was assessed by theoretically calculated productivities of pure magnetite based on intracellular iron measurements.

Our automated cultivation regime thus enabled higher reproducibility and more precise regulation of cultivation conditions in comparison to manually controlled fermentation regimes [36–39, 41]. This was achieved by a dynamic response to changing oxygen requirements of the culture using an up-to-date fermentation system with standard oxygen electrodes and thermal mass flow controllers for gas inlet instead of specialized custom bioreactor modifications [32].

As already observed in previous studies [30, 32] differences in growth and magnetosome biosynthesis between O_2 conditions were confirmed. Maximal growth rates during the main growth phase were reached at 1% dO_2 . Growth became limited by the depletion of lactate, whereas the depletion of nitrate could be compensated by oxygen as electron acceptor and other nitrogen sources.

With increasing oxygen concentration, growth became impaired by oxidative stress, as indicated by a decrease in growth rate at 95% dO_2 . Again, growth was inhibited by lactate depletion, whereas nitrate consumption was much lower because of repression of denitrification by high oxygen access regulated by a homologue of the oxygen-sensing transcription factor Fnr called MgFnr [34]. In *M. gryphiswaldense* nitrate reduction is the only pathway for energy production instead of oxygen respiration in anoxia resulting in rapid nitrate depletion [33]. Accordingly, anoxic growth was limited by nitrate depletion in the growth medium. Additionally, weakest growth was observed under anoxic conditions, caused by consumption of nitrate as the sole electron acceptor [33]. Since the results show rapid nitrate depletion and increasing the initial nitrate concentration is limited due to the accumulation of toxic intermediates in batch processes, a way to increase biomass yield would be a dynamic nitrate feeding strategy in future studies. While ammonium seems to be the preferred nitrogen source for several bacteria like *Escherichia coli* [45, 46], nitrate enabled highest growth and magnetite yields in magnetospirilla under microoxic conditions [33, 47].

The main scope of our study was the automation of the process and characterization of magnetosome

parameters, rather optimization of high cell yields. Indeed, despite of the high reproducibility of our method, yields of biomass were still substantially lower (1 OD₅₆₅) compared to previous fed-batch processes (14–42 OD₅₆₅) [38, 39]. However, by employing feeding strategies based on the substrate consumption rates determined in our study, and an improved understanding of the metabolic mechanisms affecting cell growth and magnetosome formation, e.g. by metabolomic studies of *M. gryphiswaldense* [48], also biomass production can likely be substantially increased in future efforts using our oxystat regime.

Oxically grown cells (95% dO₂) were essentially devoid of magnetosomes and displayed a C_{mag} of nearly 0 and a cellular iron content of 3.3 mg g_{dw}⁻¹. Decreasing the dO₂ led to initiation of magnetosome biomineralization with an iron content of 14.4 mg_{iron} g_{dw}⁻¹ at 1% dO₂ and 25.3 mg_{iron} g_{dw}⁻¹ at 0% dO₂ marking maximal magnetosome production. The size of magnetite particles increased during anoxic and microoxic fermenter growth, as well as the uniformity of both size and morphology, whereas uncontrolled oxygen conditions, such as in shaking flasks, led to a much wider distribution in magnetite particle diameter (Fig. 4).

Taken together, if we assume, that as much as 99% of the intracellular iron content is bound in magnetite [49], the highest overall magnetite productivity of the complete process was obtained at a dO₂ of 1% of 0.109 mg L⁻¹ h⁻¹ resulting from the highest maximal cell densities measured in this study (OD₅₆₅ of 1). In contrast optimal magnetosome biosynthesis was reached anaerobically, yielding 0.048 mg L⁻¹ h⁻¹. Highest proportion (66.4%) of magnetosomes larger than 30 nm in diameter was obtained at 0% dO₂, compared to 48.0% at 1% dO₂ (Fig. 5). Furthermore, smaller magnetosomes (<30 nm) are lost during magnetosome isolation and purification [50].

Small-angle X-ray scattering (SAXS) intensities I(q) of magnetite producing cells (0% and 1% dO₂, Additional file 2: Figure S3 A symbols) exhibited pronounced oscillations at low and intermediate q, which are not visible in the scattering pattern of magnetosome deficient cells (95% dO₂, Additional file 2: Figure S3 B solid lines). In contrast to these magnetosome-deficient samples, the scattering intensities of different batches of magnetosome-rich bacteria produced at identical dO₂ conditions was remarkably reproducible concerning the size and polydispersity of the magnetosomes, which underlines the precise biological control of magnetite biomineralization (Additional file 2: Figure S3 B symbols, 3 batches, 0% dO₂).

Although nearly no magnetosomes were detected in aerobically grown cells, differences between oxic samples (Additional file 2: Fig S3 B solid lines) in the q range of 0.01–0.15 Å⁻¹ hint towards the presence of flake-like particles with a radius of about R=10 nm and a thickness

of about 3.5 nm, which may point to precursor particles of hematite resulting from the disturbed magnetite biomineralization.

Conclusion

The streamlined seed-train and automated oxystat regime presented in this study provides well characterized and stable culturing environments for reproducible magnetosome production. By further expanding this regime with an optimized feeding strategy, future approaches can overcome growth limitations caused by substrate depletion. This would lead to higher yields with improved and reproducible magnetosome characteristics. In addition, variable oxygen control may be used to adjust the size of magnetite particles with distinct magnetic characteristics ‘tailored’ for the desired application. The future development of high-yield fermentation protocols combined with high process reproducibility and magnetosome characteristics, will pave the way for industrial production for wide-spread application in various fields.

Materials and methods

Bacterial strains

Magnetospirillum gryphiswaldense strain MSR-1 (DSM 6361; [28, 51]) was used in all experiments.

Determination of storage influence on cell viability

For investigation of effects on cell viability after prolonged storage at 4 °C, the number of passages, which are needed for minimal lag-phase length, was determined. Therefore, cells were inoculated from 4 °C stock cultures in 30 mL FSM in 50 mL conical centrifuge tubes incubated shaking at 120 rpm and 28 °C for 24 h. After each passage (maximal 4 passages), cell growth was monitored with an initial OD₅₆₅ of 0.01 using an Infinite 200pro microplate reader (Tecan, Männedorf, Switzerland) in 24-well microtiter plates with 1 mL FSM and incubated shaking at 28 °C. In case of first passage, growth experiments were inoculated directly from 4 °C stock cultures.

Seed-train standardization

We first sought to establish a robust seed-train under microoxic conditions by optimizing scale up, incubation conditions, aeration (by variation of agitation, headspace to volume ratio, and closed lids vs. free exchange with air) and media composition (peptone and iron concentrations). Microoxic conditions were chosen for practical reasons, since they are known to provide a reasonable trade-off between growth and magnetosome biomineralization, whereas anoxic and oxic conditions cause limited or impaired growth, respectively [32].

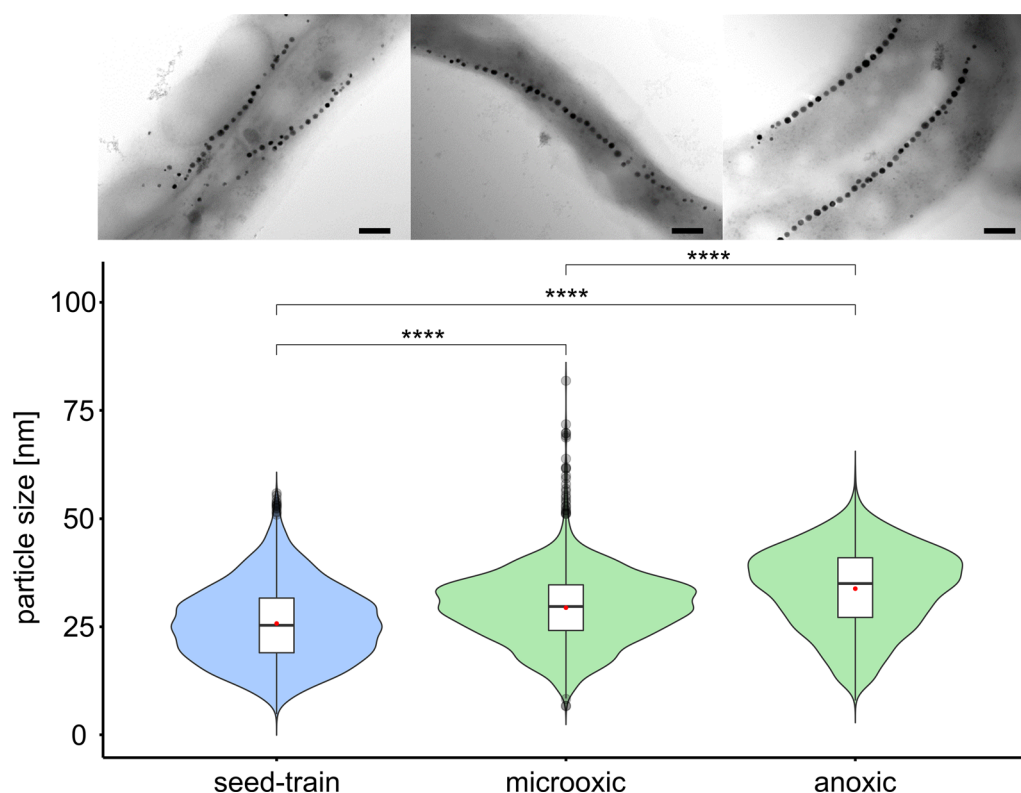


Fig. 5 Transmission electron micrographs and magnetosome particle sizes at process end among seed-train ($n = 2925$), microoxic (1% dO_2) ($n = 3180$) and anoxic (0% dO_2) conditions ($n = 3025$) with representative TEM micrographs of cells under the respective conditions (scale bar 200 nm). In box plots, the box indicates the interquartile range, the bar indicates the median, and the red dot represents the mean. Grey dots represent data points above or below the 95th and 5th percentile. The violin plots show the magnetosome particle size distribution of measured particle sizes. For statistical comparison of particle sizes, Wilcoxon rank sum test was performed (****, $p < 0.0001$)

As first step of the seed-train, *M. gryphiswaldense* cells were incubated at 24 °C in 15 mL conical centrifuge tubes with 10 mL flask standard medium (FSM) comprising: 10 mM 2-[4-(2-hydroxyethyl)piperazin-1-yl]ethanesulfonic acid (HEPES) (pH 7.0), 15 mM potassium lactate, 4 mM $NaNO_3$, 0.74 mM KH_2PO_4 , 0.6 mM $MgSO_4 \times 7H_2O$, 50 μM iron citrate, 3 g L^{-1} soy peptone and 0.1 g L^{-1} yeast extract [32]. For cultivation in screw-cap bottles, preculture medium was used comprising of 10 mM HEPES (pH 7.0), 15 mM potassium lactate, 4 mM $NaNO_3$, 0.74 mM KH_2PO_4 , 0.6 mM $MgSO_4 \times 7H_2O$, 150 μM iron citrate, 1 g L^{-1} soy peptone and 0.1 g L^{-1} yeast extract.

For standardization of the flask cultivation, growth and C_{mag} were tested of cultures cultivated in 50 mL and 100 mL firmly closed screw-capped bottles with 30 mL medium incubated at 24 °C for 24, 40 and 48 h. Cultures were inoculated 1:10 with cells cultured in 15 mL tubes as described before. Samples were taken at the end of incubation to not disturb growth conditions by the sampling procedure. The same experimental setup was used for cultivation in 500 mL and 1000 mL slightly opened

screw-capped bottles with 300 mL medium incubated at 28 °C for 16 or 20 h.

For routine cultivation, liquid stock cultures of 10 mL are usually stored at 4 °C, which however gradually decreases viability after prolonged storage (4–9 weeks) as observed in growth experiments (Additional file 3: Figure S1). We found that incubation of two successive passages at 28 °C for 24 h with slight agitation exposed to air resulted in efficient reactivation and robust outgrowth. Accordingly, the two passages were adapted for initial subcultures incubated in 10 mL at room temperature (24 °C) for 40 h, followed by one step in a 100 mL screw-capped bottle with 30 mL medium at 24 °C for 40 h and one step in a 500 mL slightly opened screw-capped bottle with 300 mL at 28 °C for 16 h. All culturing steps described in this section were inoculated with a culture to medium ratio of 1/10 and incubated at 120 rpm in an orbital shaking incubator.

Oxystat cultivation

A stirred-tank 3 L jacketed bioreactor was employed in this study (Bioflo™ 320, Eppendorf Bioprocess, Jülich,

Germany) equipped with four baffles and a stirrer with one pitched-blade impeller at the end of the agitator shaft and one Rushton impeller 4 cm above the pitched-blade impeller. Two cable ties were installed at the headspace part of the stirrer shaft leading to adequate, mechanical foam dispersion in fermentation experiments. The control units of the fermenter system were equipped with thermal mass flow controllers for gas inlet.

During the process, pH was monitored online with an InPro3253i (Mettler-Toledo, Columbus, USA) pH probe and was controlled at $\text{pH}=7\pm 0.1$ by automated addition of 1 M H_2SO_4 to compensate for the basification during main growth or 1 M KOH in stationary phase. Oxygen concentration was measured online with an InPro6850i (Mettler-Toledo, Columbus, USA) O_2 sensor with a lower limit of 6 parts per billion (ppb) an accuracy of $\pm 1\%$. After sterilization and cooling of the fermenter vessel to process temperature (28 °C), the medium was sparged first with nitrogen (dO_2 0%) until measured raw current values were stable prior to zero calibration, followed by sparging with air to saturation (dO_2 100%) for O_2 probe calibration.

Cultivation in bioreactors was carried out in 2.8 L of large-scale medium (LSM) comprising 15 mM potassium lactate, 4 mM NaNO_3 , 0.74 mM KH_2PO_4 , 0.6 mM $\text{MgSO}_4 \times 7\text{H}_2\text{O}$, 150 μM iron citrate, 3 g L^{-1} soy peptone and 0.1 g L^{-1} yeast extract. For anaerobic fermentation processes, additional sodium nitrate was supplemented to 10 mM to prolong the main growth phase due to the increased nitrate requirement. Prior to inoculation of anoxic and microoxic processes, oxygen was gassed out with nitrogen. During anaerobic processes, the medium was continuously sparged with 0.2 SLPM nitrogen to prevent oxygen diffusion into the system. Agitation was kept constant at 100 rpm. For processes under controlled oxygen conditions (dO_2 set point 1% and 95%), a programmed cascade controlled dO_2 by automated adjustment of agitation (100–300 rpm) and airflow (0–10 SLPM) with compressed air (see results for cascade specifications).

Cell growth and magnetic response

Cell growth and magnetic response was monitored turbidimetrically by measuring the optical density at 565 nm (OD_{565}) with an Ultraspec2000 pro spectrophotometer. Magnetic response of the culture was measured as described in Schöler et al. [29]. Briefly, cells were magnetically aligned perpendicular and vertical to the light beam of a photometer resulting in a change of the OD_{565} . The ratio of maximal and minimal scattering intensities subtracted by 1 (C_{mag}) represents the magnetic response of the cells as estimation for magnetosome biomineralization.

Substrate monitoring

The lactate concentration was measured with the handheld device DiaSpect Tm (EKF Diagnostics, Germany) according manufacturer's instructions.

The nitrate concentration was measured using the Szechrome NAS reagent (Polysciences inc., Warrington, USA) according to manufacturer's instructions. Briefly, the working solution was prepared by mixing 85–86% phosphoric acid and 95–97% sulfuric acid in equimolar amounts. Afterwards 5 g L^{-1} reagent were added and mixed until the reagent was completely dissolved. Samples were diluted with ddH_2O to the expected sensitivity ratio (1–20 mg L^{-1}) of the reagent, followed by mixing of 100 μL of diluted sample with 1000 μL of the working solution in a cuvette. After 5 min of incubation, the absorption at 570 nm was measured using an Ultraspec2000 pro spectrophotometer.

Nitrite concentration was determined by using the Griess reagent kit (Sigma-Aldrich, St. Louis, USA) according to manufacturer's instructions. Briefly, 1 g of Griess reagent was mixed with 25 mL ddH_2O . Afterwards, 500 μL of the working solution were mixed with 500 μL of the sample and after 5 min of incubation, measured photometrically at 540 nm.

Determination of iron content

To follow iron enrichment within cell pellets of *M. gryphiswaldense*, iron content was determined by atomic absorption spectroscopy (AAS) throughout the cultivation. 10 mL of fermentation broth from the bioreactor were pelleted at 3700 g for 10 min at room temperature using an Allegra® X-15R centrifuge (Beckman Coulter, Brea, USA). The pellet was resuspended in 5 mL 0.5 M HEPES pH 7.0 and was subsequently analyzed using an Analytik Jena contraAA300 high-resolution atomic absorption spectrometer (Analytik Jena, Jena, Germany) equipped with a 300 W xenon short-arc lamp (XBO 301, GLE, Berlin, Germany) as continuum radiation source. Detection was carried out with a compact high-resolution double monochromator and a charge-coupled device (CCD) array detector with a resolution of 2 pm per pixel in the far ultraviolet range. The wavelength for detection was set to 248.3 nm using an oxidizing air/acetylene flame. The measured values are given in mean values representing averaged values from three experiments measured in technical quintuplicates.

Transmission electron microscopy (TEM)

Transmission electron microscopy of whole cells was performed with specimens directly deposited onto carbon-coated copper grids (Science Services, Munich,

Germany). For TEM imaging a Jeol Jem 1400 + (Freising, Germany) was operated at an acceleration voltage of 80 kV. Image acquisition was performed with a Gatan Erlangshen ES500W CCD camera. Average particle sizes were measured by data processing with ImageJ software package v1.52i. For quantitative assessment of magnetite particle biomineralization at different timepoints, specifically at the process start, in the mid-exponential growth phase and at end of growth 1000 magnetosome particles per triplicate were counted and combined for evaluation.

Small-angle X-ray scattering (SAXS)

Nanostructural investigation of magnetosomes was performed as described in Rosenfeldt et al. [43]. Briefly, harvested cells were centrifuged at 8300 g for 10 min using a Sorvall RC-5B Plus centrifuge (Thermo Fisher Scientific, Waltham, USA), resuspended in 50 mM HEPES buffer pH 7.0 and filled into glass capillaries ($\varnothing = 1$ mm, Hilgenberg, Germany). Samples were measured using a Double Ganesha AIR system (SAXSLAB, Skovlunder, Denmark). A rotating anode (Cu, MicroMax 007HF, Rigaku Corporation, Japan) served as source for monochromatic radiation with a wavelength of $\lambda = 1.54$ Å. Two dimensional scattering patterns were recorded with a position-sensitive detector (PILATUS 300 K, Dectris) and converted into 1-dimensional intensity profiles of $I(q)$ vs q by radial averaging. The obtained 1D-SAXS data were normalized to accumulation time, sample thickness and transmission before subtraction of the scattering contributions of the solvent. A glass capillary filled with HEPES buffer was used for background correction. The scattering curves were analyzed based on a model of monodispersed, non-interacting spheres arranged in a chain using the software SasView 4.2.

Statistical analyses

Group data are reported as mean \pm standard deviation. For determination of statistical significance, Wilcoxon rank sum test was performed using R-software.

Supplementary information

Supplementary information accompanies this paper at <https://doi.org/10.1186/s12934-020-01469-z>.

Additional file 1: Figure S1. Influence of storage duration in weeks on cell viability.

Additional file 2: Figure S2. Oxystat fermentations at 1% dO₂.

Additional file 3: Figure S3. Representative small-angle X-ray scattering curves of *M. gryphiswaldense* cells.

Acknowledgements

We thank Matthias Völkl and Sophia Tessaro for contributing some of the produced data as part of their Master's theses at the Department of Microbiology and the Chair for Process Biotechnology (University of Bayreuth). The authors are grateful to the Bavarian Polymer Institute (BPI) for providing access to small-angle X-ray scattering facilities as part of the Keylab Mesoscale Characterization: Scattering Techniques. This work also benefited from the use of the SasView application, originally developed under NSF award DMR-0520547. SasView contains code developed with funding from the European Union's Horizon 2020 research innovation program under the SINE2020 project, grant agreement 654000.

Authors' contributions

CNR, RU, VJ, RF and DS conceived and designed research. CNR, RU and SR performed experiments. CNR and RU performed seed-train standardization, oxystat fermentations and analyzed the data. SR performed SAXS measurements and CNR together with SR and ASS analyzed the data. CNR and DS analyzed the whole dataset and wrote the paper. All authors provided critical feedback and helped to shape the research, analysis and manuscript. All authors read and approved the final manuscript.

Funding

Open Access funding enabled and organized by Projekt DEAL. We gratefully acknowledge financial support from the Deutsche Forschungsgemeinschaft (INST 91/374-1 LAGG to D.S.), the European Research Council (ERC) under the European Union's Horizon 2020 research and innovation program (Grant No. 692637 to D.S.) and the Federal Ministry of Education and Research (BMBF) (Grant MagBioFab to R.U. and D.S.). A.S.S. acknowledges financial support from the Bavarian Academy of Sciences and Humanities (BAW).

Availability of data and materials

Not applicable.

Ethics approval and consent to participate

Not applicable.

Consent for publication

Not applicable.

Competing interests

The authors declare that they have no competing interests.

Author details

¹ Department of Microbiology, University of Bayreuth, Universitätsstraße 30, 95447 Bayreuth, Germany. ² Physical Chemistry I, University of Bayreuth, Universitätsstraße 30, Bayreuth 95447, Germany. ³ Bavarian Polymer Institute (BPI), University of Bayreuth, Universitätsstraße 30, Bayreuth 95447, Germany. ⁴ Physical Chemistry - Colloidal Systems, University of Bayreuth, Universitätsstraße 30, Bayreuth 95447, Germany. ⁵ Chair for Process Biotechnology, University of Bayreuth, Universitätsstraße 30, Bayreuth 95447, Germany.

Received: 10 August 2020 Accepted: 29 October 2020

Published online: 10 November 2020

References

- Lefèvre CT, Bazylinski DA. Ecology, diversity, and evolution of magnetotactic bacteria. *Microbiol Mol Biol Rev.* 2013;77:497–526.
- Uebe R, Schüler D. Magnetosome biogenesis in magnetotactic bacteria. *Nat Rev Microbiol.* 2016;14:621–37.
- Barber-Zucker S, Keren-Khadmy N, Zarivach R. From invagination to navigation: the story of magnetosome-associated proteins in magnetotactic bacteria. *Protein Sci.* 2015;25:338–51.
- Lohße A, Ullrich S, Katzmann E, Borg S, Wanner G, Richter M, Voigt B, Schweder T, Schüler D. Functional analysis of the magnetosome island in *Magnetospirillum gryphiswaldense*: the *mamAB* operon is sufficient for magnetite biomineralization. *PLoS ONE.* 2011;6:e25561.

5. Lohße A, Borg S, Raschdorf O, Kolinko I, Tompa É, Pósfai M, Favre D, Baumgartner J, Schüler D. Genetic dissection of the *mamAB* and *mms6* operons reveals a gene set essential for magnetosome biogenesis in *Magnetospirillum gryphiswaldense*. *J Bacteriol*. 2014;196:2658–69.
6. Staniland SS, Ward B, Harrison A, van der Laan G, Telling N. Rapid magnetosome formation shown by real-time X-ray magnetic circular dichroism. *Proc Natl Acad Sci USA*. 2007;104:19524–8.
7. Staniland SS, Rawlings AE. Crystallizing the function of the magnetosome membrane mineralization protein Mms6. *Biochem Soc Trans*. 2016;44:883–90.
8. Hergt R, Hiergeist R, Zeisberger M, Schüler D, Heyen U, Hilger I, Kaiser WA. Magnetic properties of bacterial magnetosomes as diagnostic and therapeutic tools. *J Magn Magn Mater*. 2005;293:80–6.
9. Alphandéry E, Guyot F, Chebbi I. Preparation of chains of magnetosomes, isolated from *Magnetospirillum magneticum* strain AMB-1 magnetotactic bacteria, yielding efficient treatment of tumors using magnetic hyperthermia. *Int J Pharm*. 2012;434:444–52.
10. Gandia D, Gandarias L, Rodrigo I, Robles-García, Das R, Garaio E, García JA, Phan MH, Srikanth H, Orue I, Alonso J, Muela A, Fdez-Gubieda. Unlocking the potential of magnetotactic bacteria as magnetic hyperthermia agents. *Small*. 2019;15:1902626.
11. Sangnier AP, Preveral S, Curcio A, Silva AKA, Lefèvre C, Pignol D, Lalatonne Y, Wilhelm C. Targeted thermal therapy with genetically engineered magnetic magnetosomes@RGD: photothermia is far more efficient than magnetic hyperthermia. *J Control Release*. 2018;279:271–81.
12. Hafsi M, Preveral S, Hoog C, Héroult J, Perrier GA, Lefèvre CT, Michel H, Pignol D, Doyen J, Pourcher T, Humbert O, Thariat J, Cambien B. RGD-functionalized magnetosomes are efficient tumor radioenhancers for X-rays and protons. *Nanomedicine NBM*. 2020;23:102084.
13. Mériaux S, Boucher M, Marty B, Lalatonne Y, Prévéral S, Motte L, Lefèvre CT, Geffroy, Lethimonnier F, Péan M, Garcia D, Adryanczyk-Perrier G, Pignol D, Ginet N. Magnetosomes, biogenic magnetic nanomaterials for brain molecular imaging with 17.2 T MRI scanner. *Adv Healthc Mater*. 2015;4:1076–83.
14. Orlando T, Mannucci S, Fantechi E, Conti G, Tambalo S, Busato A, Innocenti C, Ghin L, Bassi R, Arosio P, Orsini F, Sangregorio C, Corti M, Casula MF, Marzola P, Lascialfari A, Sbarbati A. Characterization of magnetic nanoparticles from *Magnetospirillum gryphiswaldense* as potential theranostics tools. *Contrast Media Mol Imaging*. 2016;11:139–45.
15. Heinke D, Kraupner A, Eberbeck D, Schmidt D, Radon P, Uebe R, Schüler D, Briel A. MPS and MRI efficacy of magnetosomes from wild-type and mutant bacterial strains. *Int J Magn Part Imaging*. 2017;3:1706004.
16. Kraupner A, Eberbeck D, Heinke D, Uebe R, Schüler D, Briel A. Bacterial magnetosomes—nature's powerful contribution to MPI tracer research. *Nanoscale*. 2017;9:5788–93.
17. Tanaka T, Takeda H, Ueki F, Obata K, Tajima H, Takeyama H, Goda Y, Fujimoto S, Matsunaga T. Rapid and sensitive detection of 17 β -estradiol in environmental water using automated immunoassay system with bacterial magnetic particles. *J Biotechnol*. 2004;108:153–9.
18. Matsunaga T, Kamiya S. Use of magnetic particles isolated from magnetotactic bacteria for enzyme immobilization. *Appl Microbiol Biotechnol*. 1987;26:328–32.
19. Ginet N, Pardoux R, Adryanczyk G, Garcia D, Brutescio C, Pignol D. Single-step production of a recyclable nanobiocatalyst for organophosphate pesticides biodegradation using functionalized bacterial magnetosomes. *PLoS ONE*. 2011;6:e21442.
20. Mickoleit F, Lanzloth C, Schüler D. A versatile toolkit for controllable and highly selective multifunctionalization of bacterial magnetic nanoparticles. *Small*. 2020;16:1906922.
21. Honda T, Yasuda T, Tanaka T, Hagiwara K, Arai T, Yoshino T. Functional expression of full-length TrkA in prokaryotic host *Magnetospirillum magneticum* AMB-1 by using a magnetosome display system. *Appl Environ Microbiol*. 2014;81:1472–6.
22. Xu J, Hu J, Liu L, Li L, Wang X, Zhang H, Jiang W, Tian J, Li Y, Li J. Surface expression of protein A on magnetosomes and capture of pathogenic bacteria by magnetosome/antibody complexes. *Front Microbiol*. 2014;5:136.
23. Xu J, Liu L, He J, Ma S, Li S, Wang Z, Xu T, Jiang W, Wen Y, Li Y, Tian J, Li FJ. Engineered magnetosomes fused to functional molecule (protein A) provide a highly effective alternative to commercial immunomagnetic beads. *Nanobiotechnol*. 2019;17:37.
24. Wacker R, Ceyhan B, Alhorn P, Schüler D, Lang C, Niemeyer CM. Magneto-Immuno-PCR: a novel immunoassay based on biogenic magnetosome nanoparticles. *Biochem Biophys Res Commun*. 2003;357:391–6.
25. Mickoleit F, Jérôme V, Freitag R, Schüler D. Bacterial magnetosomes as novel platform for the presentation of immunostimulatory, membrane-bound ligands in cellular biotechnology. *Adv Biosyst*. 2020;4:1900231.
26. Borg S, Rothenstein D, Bill J, Schüler D. Generation of multi-shell magnetic hybrid nanoparticles by encapsulation of genetically engineered and fluorescent bacterial magnetosomes with ZnO and SiO₂. *Small*. 2015;11:4209–17.
27. Mickoleit F, Borkner CB, Toro-Nahuelpan M, Herold HM, Maier DS, Pitzko JM, Scheibel T, Schüler D. In vivo coating of bacterial magnetic nanoparticles by magnetosome expression of spider silk-inspired peptides. *Biomacromol*. 2018;19:962–72.
28. Schleifer KH, Schüler D, Spring S, Weizenegger M, Amann R, Ludwig W, Köhler M. The genus *Magnetospirillum* gen. nov. description of *Magnetospirillum gryphiswaldense* sp. nov. and transfer of *Aquaspirillum magnetotacticum* to *Magnetospirillum magnetotacticum* comb. nov. *Syst Appl Microbiol*. 1991;14:379–85.
29. Schüler D, Uhl R, Bäuerlein E. A simple light scattering method to assay magnetism in *Magnetospirillum gryphiswaldense*. *FEMS Microbiol Lett*. 1995;132:139–45.
30. Schüler D, Bäuerlein E. Dynamics of iron uptake and Fe₃O₄ biomineralization during aerobic and microaerobic growth of *Magnetospirillum gryphiswaldense*. *J Bacteriol*. 1998;180:159–62.
31. Katzmann E, Eibauer M, Lin W, Pan Y, Pitzko JM, Schüler D. Analysis of magnetosome chains in magnetotactic bacteria by magnetic measurements and automated image analysis of electron micrographs. *Appl Environ Microbiol*. 2013;79:7755–62.
32. Heyen U, Schüler D. Growth and magnetosome formation by microaerophilic *Magnetospirillum* strains in an oxygen-controlled fermentor. *Appl Microbiol Biotechnol*. 2003;61:536–44.
33. Li Y, Katzmann E, Borg S, Schüler D. The periplasmic nitrate reductase Nap is required for anaerobic growth and involved in redox control of magnetite biomineralization in *Magnetospirillum gryphiswaldense*. *J Bacteriol*. 2012;194:4847–56.
34. Li Y, Sabaty M, Borg S, Silva KT, Pignol D, Schüler D. The oxygen sensor MgFnr controls magnetite biomineralization by regulation of denitrification in *Magnetospirillum gryphiswaldense*. *BMC Microbiol*. 2014;14:153.
35. Li Y, Raschdorf O, Silva KT, Schüler D. The terminal oxidase cbb3 functions in redox control of magnetite biomineralization in *Magnetospirillum gryphiswaldense*. *J Bacteriol*. 2014;196:2552–62.
36. Sun JB, Zhao F, Tang T, Jiang W, Tian JS, Li Y, Li JL. High-yield growth and magnetosome formation by *Magnetospirillum gryphiswaldense* MSR-1 in an oxygen-controlled fermentor supplied solely with air. *Appl Microbiol Biotechnol*. 2008;79:389–97.
37. Liu Y, Li GR, Guo FF, Jiang W, Li Y, Li LJ. Large-scale production of magnetosomes by chemostat culture of *Magnetospirillum gryphiswaldense* at high cell density. *Microb Cell Fact*. 2010;9:99.
38. Zhang Y, Zhang X, Jiang W, Li Y, Li J. Semicontinuous culture of *Magnetospirillum gryphiswaldense* MSR-1 cells in an autofermentor by nutrient-balanced and isosmotic feeding strategy. *Appl Environ Microbiol*. 2011;77:5851–6.
39. Fernández-Castané A, Li H, Thomas ORT, Overton TW. Development of a simple intensified fermentation strategy for growth of *Magnetospirillum gryphiswaldense* MSR-1: physiological responses to changing environmental conditions. *New Biotechnol*. 2018;46:22–30.
40. Fernández-Castané A, Li H, Thomas OR, Overton TW. Flow cytometry as a rapid analytical tool to determine physiological responses to changing O₂ and iron concentration by *Magnetospirillum gryphiswaldense* strain MSR-1. *Sci Rep*. 2017;7:13118.
41. Berny C, Le Fèvre R, Guyot F, Blondeau K, Guizonne C, Rousseau E, Bayan N, Alphandéry E. A method for producing highly pure magnetosomes in large quantity for medical applications using *Magnetospirillum gryphiswaldense* MSR-1 magnetotactic bacteria amplified in minimal growth media. *Front Bioeng Biotechnol*. 2020;8:16.
42. Zhuang S, Anyaogu DC, Kasama T, Workman M, Mortensen UH, Hobbey TJ. Effects of dissolved oxygen concentration and iron addition on immediate-early gene expression of *Magnetospirillum gryphiswaldense* MSR-1. *FEMS Microbiol Lett*. 2017;364:fx079.

43. Rosenfeldt S, Riese CN, Mickoleit F, Schüler D, Schenk AS. Probing the nanostructure of bacterial magnetosomes by small-angle X-ray scattering. *Appl Environ Microbiol.* 2019;85:e01513–9.
44. Gogate PR, Beenackers AACM, Pandit AB. Multiple-impeller systems with a special emphasis on bioreactors: a critical review. *Biochem Eng J.* 2000;6:109–44.
45. Reitzer L. Nitrogen assimilation and global regulation in *Escherichia coli*. *Annu Rev Microbiol.* 2003;57:155–76.
46. Chubukov V, Gerosa L, Kochanowski K, Sauer U. Coordination of microbial metabolism. *Nat Rev Microbiol.* 2014;12:327–40.
47. Blakemore RP, Short KA, Bazylnski DA, Rosenblatt C, Frankel RB. Micro-aerobic conditions are required for magnetite formation within *Aquaspirillum magnetotacticum*. *Geomicrobiol J.* 1985;4:53–71.
48. Abdelrazig S, Safo L, Rance GA, Fay MW, Theodosiou E, Topham PD, Kim DH, Fernández-Castané A. Metabolic characterisation of *Magnetospirillum gryphiswaldense* MSR-1 using LC-MS-based metabolite profiling. *RSC Adv.* 2020;10:32548–60.
49. Grünberg K, Müller EC, Otto A, Reszka R, Linder D, Kube M, Reinhardt R, Schüler D. Biochemical and proteomic analysis of the magnetosome membrane in *Magnetospirillum gryphiswaldense*. *Appl Environ Microbiol.* 2004;70:1040–50.
50. Rosenfeldt S, Mickoleit F, Jörke C, Clement JH, Markert S, Jérôme V, Schwarzingler S, Freitag R, Schüler D, Uebe R, Schenk AS. Towards standardized purification of bacterial magnetic nanoparticles for future in vivo applications. *Acta Biomater.* 2020. <https://doi.org/10.1016/j.actbio.2020.07.042>.
51. Schüler D, Köhler M. The isolation of a new magnetic spirillum. *Zentralbl Mikrobiol.* 1992;147:150–1.

Publisher's Note

Springer Nature remains neutral with regard to jurisdictional claims in published maps and institutional affiliations.

Ready to submit your research? Choose BMC and benefit from:

- fast, convenient online submission
- thorough peer review by experienced researchers in your field
- rapid publication on acceptance
- support for research data, including large and complex data types
- gold Open Access which fosters wider collaboration and increased citations
- maximum visibility for your research: over 100M website views per year

At BMC, research is always in progress.

Learn more biomedcentral.com/submissions



Article 2

Manuscript 2

The complex transcriptional landscape of magnetosome gene clusters in
Magnetospirillum gryphiswaldense

Marina Dziuba*, Cornelius N. Riese*, Lion Borgert, Manuel Wittchen, Tobias Busche,
Jörn Kalinowski, René Uebe and Dirk Schüler.

mSystems (2021) 6:e0089321

doi: [org/10.1128/mSystems.00893-21](https://doi.org/10.1128/mSystems.00893-21)

*These authors contributed equally



The Complex Transcriptional Landscape of Magnetosome Gene Clusters in *Magnetospirillum gryphiswaldense*

 Marina Dziuba,^{a,b}
 Cornelius N. Riese,^a
 Lion Borgert,^{a*}
 Manuel Wittchen,^{c,d}
 Tobias Busche,^d
 Jörn Kalinowski,^d
 René Uebe,^a
 Dirk Schüler^a

^aDepartment of Microbiology, University of Bayreuth, Bayreuth, Germany

^bInstitute of Bioengineering, Research Center of Biotechnology of the Russian Academy of Sciences, Moscow, Russia

^cGerman Network for Bioinformatics Infrastructure, Bielefeld, Germany

^dCenter for Biotechnology, University of Bielefeld, Bielefeld, Germany

Marina Dziuba and Cornelius N. Riese contributed equally to this work. Author order was determined alphabetically.

ABSTRACT Magnetosomes are complex membrane organelles synthesized by magnetotactic bacteria (MTB) for navigation in the Earth's magnetic field. In the alphaproteobacterium *Magnetospirillum gryphiswaldense*, all steps of magnetosome formation are tightly controlled by >30 specific genes arranged in several gene clusters. However, the transcriptional organization of the magnetosome gene clusters has remained poorly understood. Here, by applying Cappable-seq and whole-transcriptome shotgun RNA sequencing, we show that *mamGFDCop* and *feoAB1op* are transcribed as single transcriptional units, whereas multiple transcription start sites (TSS) are present in *mms6op*, *mamXYop*, and the long (>16 kb) *mamABop*. Using a bioluminescence reporter assay and promoter knockouts, we demonstrate that most of the identified TSS originate from biologically meaningful promoters which mediate production of multiple transcripts and are functionally relevant for proper magnetosome biosynthesis. In addition, we identified a strong promoter in a large intergenic region within *mamXYop*, which likely drives transcription of a noncoding RNA important for gene expression in this operon. In summary, our data suggest a more complex transcriptional architecture of the magnetosome operons than previously recognized, which is largely conserved in other magnetotactic *Magnetospirillum* species and, thus, is likely fundamental for magnetosome biosynthesis in these organisms.

IMPORTANCE Magnetosomes have emerged as a model system to study prokaryotic organelles and a source of biocompatible magnetic nanoparticles for various biomedical applications. However, the lack of knowledge about the transcriptional organization of magnetosome gene clusters has severely impeded the engineering, manipulation, and transfer of this highly complex biosynthetic pathway into other organisms. Here, we provide a high-resolution image of the previously unappreciated transcriptional landscape of the magnetosome operons. Our findings are important for further unraveling the complex genetic framework of magnetosome biosynthesis. In addition, they will facilitate the rational reengineering of magnetic bacteria for improved bioproduction of tunable magnetic nanoparticles, as well as transplantation of magnetosome biosynthesis into foreign hosts by synthetic biology approaches. Overall, our study exemplifies how a genetically complex pathway is orchestrated at the transcriptional level to ensure the balanced expression of the numerous constituents required for the proper assembly of one of the most intricate prokaryotic organelles.

KEYWORDS MTB, *Magnetospirillum*, magnetosomes, operons, promoters, transcription, transcriptome

Citation Dziuba M, Riese CN, Borgert L, Wittchen M, Busche T, Kalinowski J, Uebe R, Schüler D. 2021. The complex transcriptional landscape of magnetosome gene clusters in *Magnetospirillum gryphiswaldense*. *mSystems* 6:e00893-21. <https://doi.org/10.1128/mSystems.00893-21>.

Editor Caroline M. Ajo-Franklin, Rice University

Copyright © 2021 Dziuba et al. This is an open-access article distributed under the terms of the [Creative Commons Attribution 4.0 International license](https://creativecommons.org/licenses/by/4.0/).

Address correspondence to Dirk Schüler, dirks.schueler@uni-bayreuth.de.

* Present address: Lion Borgert, Department of Biochemistry and Molecular Biology, University Hospital of Bonn, Bonn, Germany.

 The research reveals a previously unappreciated complexity of transcriptional architecture of biosynthetic operons controlling the assembly of magnetosomes, one of the most intricate prokaryotic organelles.

Received 14 July 2021

Accepted 11 August 2021

Published 14 September 2021

One of the most complex organelles found in prokaryotic cells is the magnetosome, which serves in magnetotactic bacteria (MTB) as a sensor for navigation in the Earth's magnetic field (1). In the long-standing model organism *Magnetospirillum gryphiswaldense* strain MSR-1 (referred to here as MSR-1) and related MTB, magnetosomes consist of a monocrystalline core of magnetite (Fe_3O_4) enclosed within a membrane. The unprecedented crystalline and magnetic properties of bacterial magnetosomes make them highly attractive in several biotechnical and biomedical settings, such as magnetic imaging and hyperthermia, as well as magnetic separation and drug targeting (2). Their application potential can be further enhanced by genetic or chemical coupling of functional moieties to the magnetosome membrane (3). Furthermore, it has been suggested to build magnetic nanostructures within eukaryotic cells for local heat generation or as reporters for magnetic imaging by borrowing genetic parts from bacterial magnetosome biosynthesis in the field of "magnetogenetics" (4, 5).

In MSR-1, biosynthesis of magnetosomes proceeds in several steps, including (i) invagination of the cytoplasmic membrane to form a magnetosome membrane (MM) vesicle; (ii) sorting and dense packing of specific magnetosome proteins (MAP) into the MM; (iii) uptake of iron and biomineralization of well-ordered magnetite crystals; and (iv) the assembly and positioning of nascent magnetosomes into linear chains (6–8). Besides some functions contributed by generic metabolic pathways (9), all these processes are governed by more than 30 proteins designated as Mam (magnetosome membrane), Mms (magnetosome particle membrane-specific), and Feo (magnetosome-specific Fe^{2+} transport system), which together constitute a sophisticated machinery exerting strict control over each step of magnetosome biosynthesis. In MSR-1, all MAPs are encoded within five major polycistronic operons (MagOPs, Fig. 1A) as follows: *mamABop* (16.4 kb), *mamGFDCop* (2.1 kb), *mms6op* (3.6 kb), *mamXYop* (5 kb), and *feoAB1op* (2.4 kb) (10–13). The MagOPs are clustered within an ~110-kb chromosomal region termed the genomic magnetosome island (MAI), where they are interspersed with genes irrelevant for magnetosome biosynthesis (14–17). The long *mamABop* comprises 17 genes and encodes all the essential factors for magnetosome biosynthesis, whereas the other four operons play important but accessory roles in magnetite biomineralization, chain assembly, and its intracellular positioning (10, 17, 18). Transfer and expression of all five MagOPs from MSR-1 caused magnetosome biosynthesis in two different nonmagnetic bacteria, further substantiating the key roles of this gene set in the process (19, 20). However, several further attempts to transplant magnetosome biosynthesis to other bacteria have so far failed, partly owing to the poor and imbalanced transcription from the as-yet-uncharacterized native promoters (Dziuba and Schüler, unpublished).

In order to build such an intricate organelle, the MAPs have to be properly expressed and targeted to the MM in defined and highly balanced stoichiometries that range, for example, from 2 (e.g., MamX and MamZ) to 120 copies (Mms6) per magnetosome particle (21), which requires a precise control over expression. One fundamental layer of regulation is expected to act at the level of gene transcription, which has been addressed by only few studies so far. Schübbe et al. demonstrated by reverse transcription-PCR (RT-PCR) that genes from the three magnetosome gene clusters known at the time, *mamABop*, *mms6op*, and *mamGFDCop*, are cotranscribed and thus represent genuine operons in MSR-1 (11). Additionally, the study also identified a single transcription start site (TSS) for each transcript by primer extension analysis, which suggested that each operon is transcribed as a single unit (TU) driven by a primary promoter residing upstream of the first gene of each operon. (11). Although no additional promoters could be identified within the operons in that study, the presence of internal promoters, especially in *mamABop* (16.4 kb), could not be ruled out based on the data available at that time (11). Later, the activity of a primary promoter (*PmamY*) upstream of the newly discovered *mamXYop* was demonstrated by a green fluorescent protein (GFP) reporter, whereas no additional promoters were identified (12). In *feoAB1op*, a primary promoter (*PfeoA1*) was revealed by a LacZ reporter gene fusion in MSR-1 (13). Despite that magnetosomes are synthesized only within a narrow range of growth conditions, i.e., microoxic to anaerobic and in the presence of sufficient iron (22, 23),

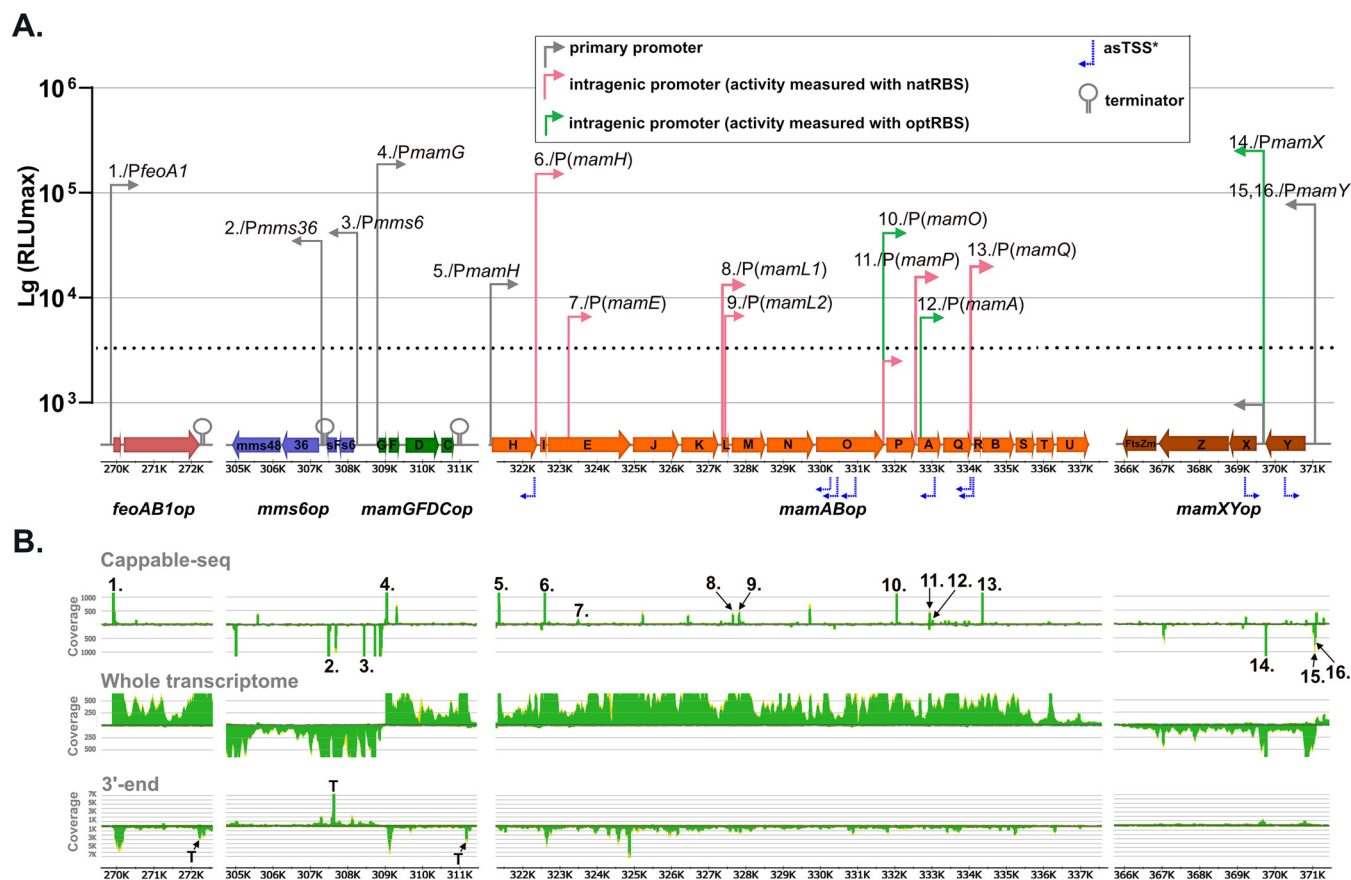


FIG 1 Molecular organization and transcriptional architecture of the MagOPs revealed in this study. (A) Position of the promoters, whose activities were confirmed by the bioluminescence assay, terminators, and asTSS in the MagOPs. Arrow height indicates the promoter strength measured by luminescence (see the text for details). A slash separates a TSS number designation and the corresponding promoter (as in Table S2 in the supplemental material). (B) Localization of TSS and TTS predicted by the transcriptome data sets. Numbers indicate TSS as in Table S2. "T" in the 3'-end panel indicate TTS.

magnetosome genes have been found to be mostly constitutively expressed, where growth conditions only weakly affected the abundance of magnetosome proteins, as demonstrated by quantitative reverse transcription-PCR (qRT-PCR), Western blotting (11), and transcriptome analysis (Riese et al., in preparation).

While these previous studies seemed to indicate a rather simple transcriptional organization of magnetosome genes, a growing amount of data suggest that a large fraction of operons in other prokaryotes are complex, i.e., contain more than one internal promoter, terminator, or both, and hence are transcribed as mutually overlapping TUs (24–27). For instance, studies on the 14-kb photosynthetic gene cluster in purple nonsulfur *Proteobacteria* and the 27-kb *fla/che* cluster in *Bacillus subtilis* (28, 29), suggested that an intricate landscape of transcriptional regulatory elements may be common to such long polycistronic operons. Understanding of the transcriptional organization of MagOPs in comparable detail is not only essential for unraveling the magnetosome biosynthesis regulation, but also for its future reconstitution, engineering, and tuning by synthetic biology approaches in homologous and heterologous hosts. All of this prompted us to reassess the architecture of the major magnetosome operons in MSR-1 by a comprehensive approach that included various RNA sequencing techniques, bioluminescence reporter assays, and promoter knockouts. By this, we confirmed the activity of the primary promoters suggested before and revealed multiple novel promoters within the MagOPs. We further show that these internal promoters can drive expression of downstream genes in the absence of primary promoters. Taken together, our data suggest a much more complex transcriptional organization of the MagOPs than deemed before and thus contribute to unveiling the fundamentals of magnetosome biosynthesis.

RESULTS

Identification of putative TSS and TTS in magnetosome operons by RNA sequencing.

Transcription start sites (TSS) were determined across the genome by the Cappable-seq technique and whole transcriptome shotgun sequencing (WTSS). Cappable-seq is a method of enriching for the 5' end of primary transcripts by enzymatically tagging the triphosphorylated 5' end of RNA, which enables the determination of TSS at single-base resolution (30). In addition, transcription termination sites (TTS) were determined using 3' end sequencing, by unambiguous peaks in combination with a read coverage decrease in the WTSS data set (31). The identified TSS were classified into four groups using an automated script: (i) primary TSS (pTSS, i.e., positioned in front of the coding sequence), (ii) intragenic TSS in sense (iTSS) or (iii) antisense orientation (asTSS), and (iv) other TSS (oTSS) (Fig. S1 in the supplemental material). From a total of 9,639 TSS identified in the entire transcriptome, 319 were found in the MAI (position bp 269182 to 371200 in the genome), and 77 within the MagOPs (Summarized in Table S2 and Fig. 1B). Similar to the previously reported prevalence of intragenic TSS in bacterial and archaeal transcriptomes (25, 30), the majority (69.3%/6,674 TSS) of the TSS defined across the genome of MSR-1 occur within coding sequences, with 3,273 TSS (34.0%) in sense orientation (iTSS), 3,401 TSS (35.3%) in antisense orientation (asTSS), and 319 (3.3%) classified as others (oTSS) (Fig. S1). Only 2,646 (27.4%) represented primary TSS (pTSS). The distribution of TSS within the MAI and the MagOPs was largely similar (Fig. S1), with a total of 23 pTSS (25.0%), 39 iTSS (42.4%), and 27 asTSS (29.3%) identified within the MagOPs. For enhancement of the TSS detection specificity, we increased the enrichment score threshold to 1.4 and compared the putative TSS to the other RNA-seq data sets (see Materials and Methods), resulting in 8 pTSS (32%), 7 iTSS (28%), 9 asTSS (36%), and 1 oTSS (4%) within the MagOPs (positions and number designations are shown in Table S2 and Fig. 1B).

Among the MagOPs, *feoAB1op* and *mamGFDCop* appear to have a canonical structure, with only a single pTSS located immediately upstream of the first gene of each operon (TSS 1 and TSS 4), but no internal TSS were found. Transcriptional terminations within the last 180 bp of *feoB* (*feoAB1op*) and 10 bp downstream of *mamC* (*mamGFDCop*) were detected in the 3' end data set.

In *mms6op*, a single pTSS (TSS 3) was detected 346 nucleotides (nt) upstream of *mms6*. In addition, another unambiguous pTSS (TSS 2) is present within the intergenic 175-bp region between *mmsF* and *mms36*. Furthermore, a putative TTS immediately downstream of *mmsF* was found, whereas no TTS was determined after *mms48* in the 3' end sequencing data set. These observations indicate that *mms6op* might be transcribed as two separate TUs, *mms6-mmsF* and *mms36-mms48*, each driven by its own TSS and separated by a terminator.

In *mamXYop*, two pTSS were located upstream of *mamY* (TSS 15 and TSS 16). An additional pTSS (TSS 14) was found 102 bp upstream of *mamX*. The presence of a promoter in this region was hypothesized previously, but could not be confirmed by a GFP reporter assay (12). Besides, two asTSS were identified at positions 369,133 bp and 370,214 bp within *mamXYop*. The read coverage in the WTSS data set showed steady transcription throughout the complete operon, gradually declining at the end of *ftsZm*, but with no unambiguous TTS suggested by the 3' end sequencing (Fig. 1B).

Although the single pTSS (TSS 5), which was found 17 bp upstream of *mamH*, the first gene in *mamABop*, did not exceed the thresholds applied for TSS identification, it was added since its position is associated with the promoter "P*mamAB*" (referred to as *PmamH* in this study) determined in the previous studies (11, 32). Furthermore, eight iTSS were detected within the coding sequences of *mamH* (TSS 6), *mamE* (TSS 7), *mamL* (TSS 8), *mamO* (TSS 10), *mamP* (TSS 11), *mamA* (TSS 12), and *mamQ* (TSS 13). Additionally, a second putative iTSS (TSS 9) in *mamL*, which was identified by a conspicuous rise in read coverage in the WTSS data set, was further investigated. In addition, seven asTSS with significant read coverage in the Cappable-seq as well as the WTSS data set were detected within *mamH*, *mamO*, *mamA*, and *mamQ*. The asTSS at the position 330,492 bp was assigned due to the overlapping read coverage to the neighboring asTSS (330,355 bp), despite being below the applied threshold of 1.4.

Sequencing of 3' ends revealed no distinct TTS within or at the end of the operon. Although a conspicuous increase in the 3' end sequencing read coverage was observed within *mamE*, this was not accompanied by a decrease of read coverage in the downstream genes in the WTSS data. The continuous read coverage of the *mamABop* in WTSS argues for its uninterrupted transcription and the possible generation of at least one single long transcript, as suggested by Schübbe et al. (11). However, the presence of multiple additional TSS within *mamABop* implies the existence of several overlapping TUs along with this potential long transcript.

Evaluation of predicted TSS by luminescence reporter assay. Next, we wanted to experimentally verify the predicted sense TSS and estimate the activities of the potential corresponding promoters. Bacterial luminescence was chosen as a reporter because of its extremely high sensitivity in comparison to fluorescence and chromogenic reporters previously used in magnetospirilla (33–35). The maximal value of normalized light units (RLU_{max}) was used to compare the relative strength of the tested promoters (Fig. 1A, Table S3). By precise chromosomal integration of all cassettes into the *attTn7* site by Tn7 transposition (R. Uebe, manuscript in preparation), we aimed to eliminate potential positional effects (Fig. 2A). Two terminator sequences, tr2 of phage lambda and *rnnB* T1 from *Escherichia coli*, were inserted immediately upstream of the promoter of interest (POI) to insulate it. However, preliminary tests of promoterless (P-less) control cassettes revealed a weak ($3,213.64 \pm 496.32 RLU_{max}$) but detectable light signal (Fig. 2Bi). This was likely caused by transcriptional activity of the neighboring promoter(s) and indicated that the efficiency of termination by tr2 and T1 in MSR-1 was much lower than in *E. coli*, in which it can approach 100% (36). Nonetheless, tests of several clones containing the control cassette demonstrated that this activity remained roughly identical in at least three independent experiments. Therefore, these signals were treated as background that would be predictably reproduced in all measured promoters, and only those POI that exceeded the RLU_{max} of the P-less control were assumed to be active promoters (Fig. 2Bi to 2Bvii).

Reporter fusions exhibited significant transcriptional activity for all tested TSS, confirming that they are generated by genuine promoters. Thus, the activities of *PfeoA1* and *PmamG* ranged from 100,592.9 to 143,000.8 RLU_{max} and 131,925.3 to 325,856.8 RLU_{max} , respectively (Table S3). This result was consistent with previous observations of high activities estimated by a GFP reporter for *PmamG* and *lacZ* for *PfeoA1* (13, 34). In *mms6op*, both putative promoters associated with TSS 2 and TSS 3 (*Pmms6* and *Pmms36*, respectively) exhibited significant activities: 29,347.87 to 36,089.24 RLU_{max} for *Pmms36* and 35,956.18 to 66,616.58 RLU_{max} for *Pmms6*. This substantiates the putative existence of two bicistronic mRNAs, as suggested by RNA sequencing.

In *mamXYop*, the primary promoter *PmamY* generated 69,670.43 to 88,076.17 RLU_{max} . Previously, *PmamY* was estimated to exhibit only 22.5% of *PmamG* activity by GFP and GusA reporters (12). Here, the use of bioluminescence revealed a slightly higher, but still comparable, activity of approximately 35.3% of *PmamG*. Previously, fusion of the intergenic fragment between *mamY* and *mamX* (*PmamX*) to a GFP reporter failed to reveal promoter activity (12). Consistently, we were unable to detect any activity of this region with our bioluminescence reporter, even when up to 20 nt from the 5' end of the *mamX* coding sequence was included in the leader (data not shown). Inspection of this region did not reveal any sequence resembling a canonical ribosome binding site (RBS) (5'-AGGAGA-3') between -5 to -10 nt ahead of the start codon of *mamX* (Table S4). However, when the fusion construct was augmented by insertion of the optimized Shine-Dalgarno sequence (optRBS, see Materials and Methods, [34]), strong light emission became detectable (174,463.3 to 337,600.0 RLU_{max}). This confirmed the high transcriptional activity of this region as predicted by the transcriptomic data but suggested that translation is inefficient due to the absence of a native RBS and, hence, *PmamX* might rather generate an as-yet-unidentified species of noncoding RNA (ncRNA) in its native context.

The predicted primary promoter *PmamH* of the *mamABop* demonstrated relatively weak but significant activity (10,467.7 to 23,270.1 RLU_{max}). The activity of the potential

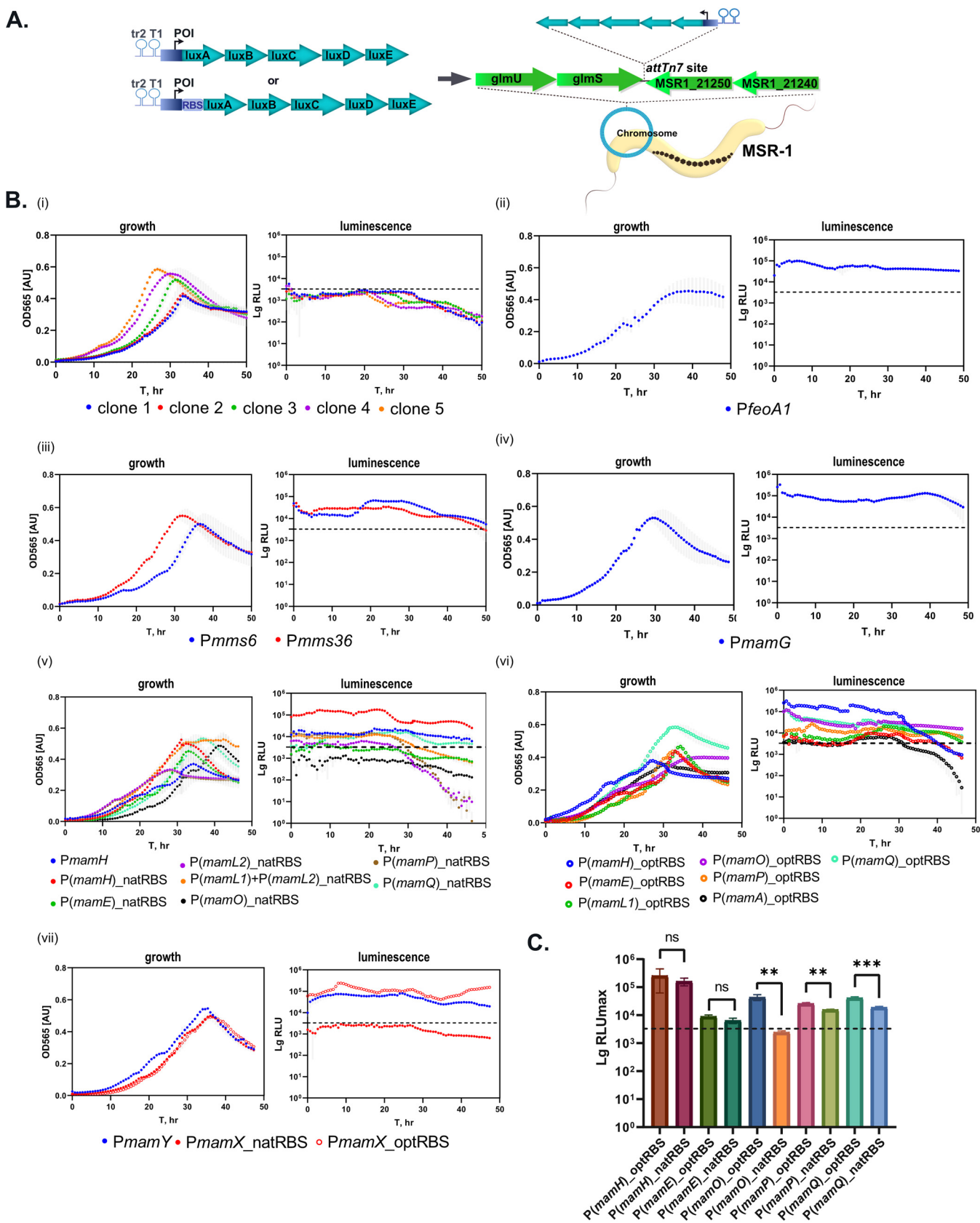


FIG 2 Activity of promoters from the MagOPs evaluated by the bioluminescence assay. (A) Schematic representation of the cloning strategy for the *in vivo* measurement of the promoter activity. Tr2 and T1, terminators; POI, promoter of interest. (B) Growth and luminescence curves of representative clones:

(Continued on next page)

intragenic promoters corresponding to the predicted TSS 6 to 11 and TSS 13 (Table S2), i.e., P(*mamH*), P(*mamE*), P(*mamL1*), P(*mamL2*), P(*mamO*), P(*mamP*), and P(*mamQ*), were first measured with their native leader sequences. Indeed, inspection of the regions directly upstream of the next genes immediately following each intragenic promoter revealed sequences that may function as an RBS for translation of the *mamI*, *mamJ*, *mamM*, and *mamA* products (hereafter referred to as natRBS [native RBS]). However, no natRBS close to the start codons of *mamP*, *mamQ*, or *mamR* could be predicted with confidence (Table S4). Nonetheless, all promoter regions were cloned according to the same procedure, i.e., with the leader sequence spanning to the start codon of the next downstream gene.

Within *mamL*, iTSS 8 and 9 were found separated by 161 nt, suggesting that two different promoters reside within the gene, which, however, have overlapping leader sequences with a shared natRBS upstream of *mamM*. Therefore, a longer sequence comprising both promoters, P(*mamL1*) + P(*mamL2*), and a shorter sequence harboring only the putative second promoter (P*mamL2*), were individually fused to the *luxAE* reporter.

When tested with their potential natRBS, P(*mamH*), P(*mamL1*)+P(*mamL2*), P*mamP*, and P*mamQ* demonstrated significant activity, whereas the signals generated from P(*mamE*) and P(*mamL2*) were very weak, and no activity above the background could be detected for P(*mamO*) (Fig. 1A, Fig. 2Bv). Among these promoters, P(*mamH*) demonstrated the highest RLU_{max} ranging from 117,963.0 to 215,346.9, which is approximately 75% of the P*mamG* activity. The activity of P(*mamA*) with the natRBS was not estimated; however, it exceeded the threshold signal when cloned with the optRBS (see below). In summary, we confirmed transcriptional activity for most of the tested intragenic promoters which was also coupled to translation of the bioluminescence reporter, likely due to the presence of natRBS in the leader sequences of the corresponding transcripts. This also suggests that multiple mRNAs are likely produced within the *mamABop*.

The activity of the predicted intragenic promoters was also evaluated after augmenting the sequences with optRBS. This allowed us to estimate the activity of the promoters independent of the efficiency of naturally occurring RBS. The activity of P(*mamH*) and P(*mamE*) measured with optRBS did not differ significantly from the natRBS, whereas the light emission with optRBS was enhanced approximately 1.5-fold in P(*mamP*), and 2-fold in P(*mamQ*) (Fig. 2C). This was likely caused by different ribosome-binding efficiencies of the natRBS in comparison to the optRBS. Interestingly, P(*mamO*) did not cause any significant bioluminescence when cloned with its native leader, but demonstrated considerable activity with optRBS, ranging from 35,344.6 to 55,643.9 RLU_{max}. As in the case of P*mamX*, this correlates with the absence of a canonical RBS in the putative leader downstream of the iTSS within *mamO* (Table S4) and implies the lack of efficient translation despite the significant transcriptional activity. Similarly, this suggests that an ncRNA might be generated from this promoter. In addition, the use of optRBS allowed us to independently measure the activity of P(*mamL1*), which reached up to 22,164.3 RLU_{max} and the activity of a putative promoter corresponding to TSS 12, P(*mamA*), which demonstrated only weak activity ranging from 5,741.4 to 6,874.2 RLU_{max}.

Exploration of the newly identified promoters *in vivo* by promoter knockout.

Next, we asked whether the promoters revealed within the magnetosome operons can drive transcription of downstream genes independently of the primary promoters located immediately upstream of their operons. In this case, one would expect that inactivation of P*mamH*, P*mms6*, and P*mamY* will not completely abolish transcription of the corresponding operons, resulting in weaker phenotypes resembling the Δ *mamH*, Δ *mms6* Δ *mmsF*, and Δ *mamY* mutants (10, 12, 18). On the contrary, if P*mamH*, P*mms6*, and P*mamY* are the

FIG 2 Legend (Continued)

(i) P-less control. Five clones are shown to demonstrate reproducibility of the maximal background light signal that was used as a threshold for all the subsequent measurements; (ii) *feoAB1op*; (iii) *mms6op*; (iv) *mamGFDCop*; (v) *mamABop*, with native RBS (natRBS); (vi) *mamABop*, with optimized RBS (optRBS); (vii) *mamXYop*. Dotted line indicates the background activity derived from the RLU_{max} of the P-less control. Standard deviations are shadowed in gray. (C) Comparison of the maximal RLU (RLU_{max}) generated by the tested promoters with their native RBS (natRBS) with those augmented with the optimized RBS (optRBS). Statistical significance was estimated using the *t* test. Asterisks indicate the points of significance, **, *P* value < 0.01; ***, *P* value < 0.001.

only or main promoters driving the transcription of the entire operons, their elimination would result in significantly more severe impairments of magnetosome formation, likely phenocopying $\Delta mamABop$, $\Delta mms6op$, and $\Delta mamXYop$ deletions, respectively (10, 17). Likewise, by knockout of *Pmms36* and *PmamX*, the phenotypes of $\Delta mms36\Delta mms48$ and $\Delta mamX\Delta mamZ\Delta ftsZm$, respectively, would be expected (10, 12, 37). To test this hypothesis, promoter knockouts were generated by replacing the promoter-comprising sequences by an artificial promoter-free sequence (PFS) of equal length (except *PmamY*, see Materials and Methods) (Fig. 3A).

Elimination of the primary promoter *PmamH* resulted in a mutant ($\Delta PmamH$) forming smaller (26.9 ± 8.3 nm versus 32.3 ± 10.5 nm in the wild type [WT]) and fewer magnetosomes in comparison to the WT (Fig. 3B and C), but not with complete absence of magnetosomes, as in $\Delta mamABop$ (10). Instead, the phenotype of $\Delta PmamH$ was virtually identical to that previously described for $\Delta mamH$, in which the magnetosome size and number were also significantly reduced (12). This suggests that only *mamH* was silenced by the *PmamH* knockout, whereas transcription of the remaining 16 genes of *mamABop* was still driven by intragenic promoters. Since *mamH* is immediately followed by the essential magnetosome genes *mamI* and *mamE*, whose deletion entirely eliminates magnetosome formation (10), this implies that their expression has to be mediated primarily by *P(mamH)* (TSS 6). Consistently, complementation of the $\Delta PmamH$ with *PmamH-mamH* in *trans* essentially restored the magnetosome diameter and number to WT levels (Fig. 3C, Fig. S2).

In $\Delta Pmms6$, neither the magnetosome number nor magnetic response of cells was affected (Fig. 3B, Fig. S3), whereas magnetosomes appeared to be smaller than in the WT (29.9 ± 9.8 nm versus 32.3 ± 10.5 nm in the WT) (Fig. 3B and 3Ci). This moderate decrease in the size reproduced the phenotype of the $\Delta mms6\Delta mmsF$ mutant, but was unlike the more severe decrease in magnetosome size and number that was described for the mutant lacking the entire *mms6op* (10). Complementation of $\Delta Pmms6$ with *Pmms6-mms6-mmsF* restored the magnetosome size back to the WT level (Fig. 3C, Fig. S2). Furthermore, elimination of *Pmms36* resulted in a significantly reduced magnetosome number in comparison to the WT, which also could be restored by complementation with *Pmms36-mms36-mms48* (Fig. 3B and C, Fig. S2). Taken together, these results suggest that transcription of *mms36* and *mms48* is primarily driven by *Pmms36*. Notably, the phenotypic effect of simultaneous silencing of *mms36* and *mms48* was different from their individual deletions, which had previously demonstrated enlarged magnetosomes with up to a 10 to 30% increase in the average diameter (10).

The $\Delta PmamY$ strain demonstrated the characteristically displaced magnetosome chains of $\Delta mamY$ in 77% of analyzed cells, which also correlated with a reduced cellular magnetic response (C_{mag} 1.01 ± 0.09 , Fig. S3) (18). Under standard conditions, the cells had an inconsistent phenotype, with most cells having regular magnetosomes and a minor proportion containing aberrant flake-like magnetosomes, reminiscent of the mutant with the entire *mamXYop* eliminated (Fig. 3B) (17). It has been demonstrated that the formation of flake-like magnetosomes observed after the individual deletions of *mamX*, *mamZ* and *ftsZm* is more pronounced under nitrate-deprived conditions, likely due to the shared redox control over the biomineralization by their products and the denitrifying enzymes (12, 37). Therefore, to check whether *PmamY* drives transcription of the entire *mamXYop* operon, we grew $\Delta PmamY$ cells under microoxic conditions in a medium in which sodium nitrate was replaced by an equimolar amount of ammonium chloride. As expected, under these conditions, $\Delta PmamY$ mutants showed severely impaired biomineralization and the displaced magnetosome chains (Fig. 4), suggesting that elimination of *PmamY* affects transcription of the entire operon. It also indicates that, unlike the additional promoters in *mms6op* and *mamABop*, the intergenic promoter *PmamX* does not compensate for the absence of *PmamY*. Under standard conditions, cells of $\Delta PmamX$ were virtually indistinguishable from the WT with respect to magnetic response, magnetosome biomineralization, or chain organization (Fig. 3B, Fig. S3). However, cultivation of them with ammonium resulted in flake-like magnetosomes as in $\Delta PmamY$ (Fig. 4). This implies that both *PmamY* and *PmamX* are required for proper expression of *mamX-mamZ-ftsZm* genes.

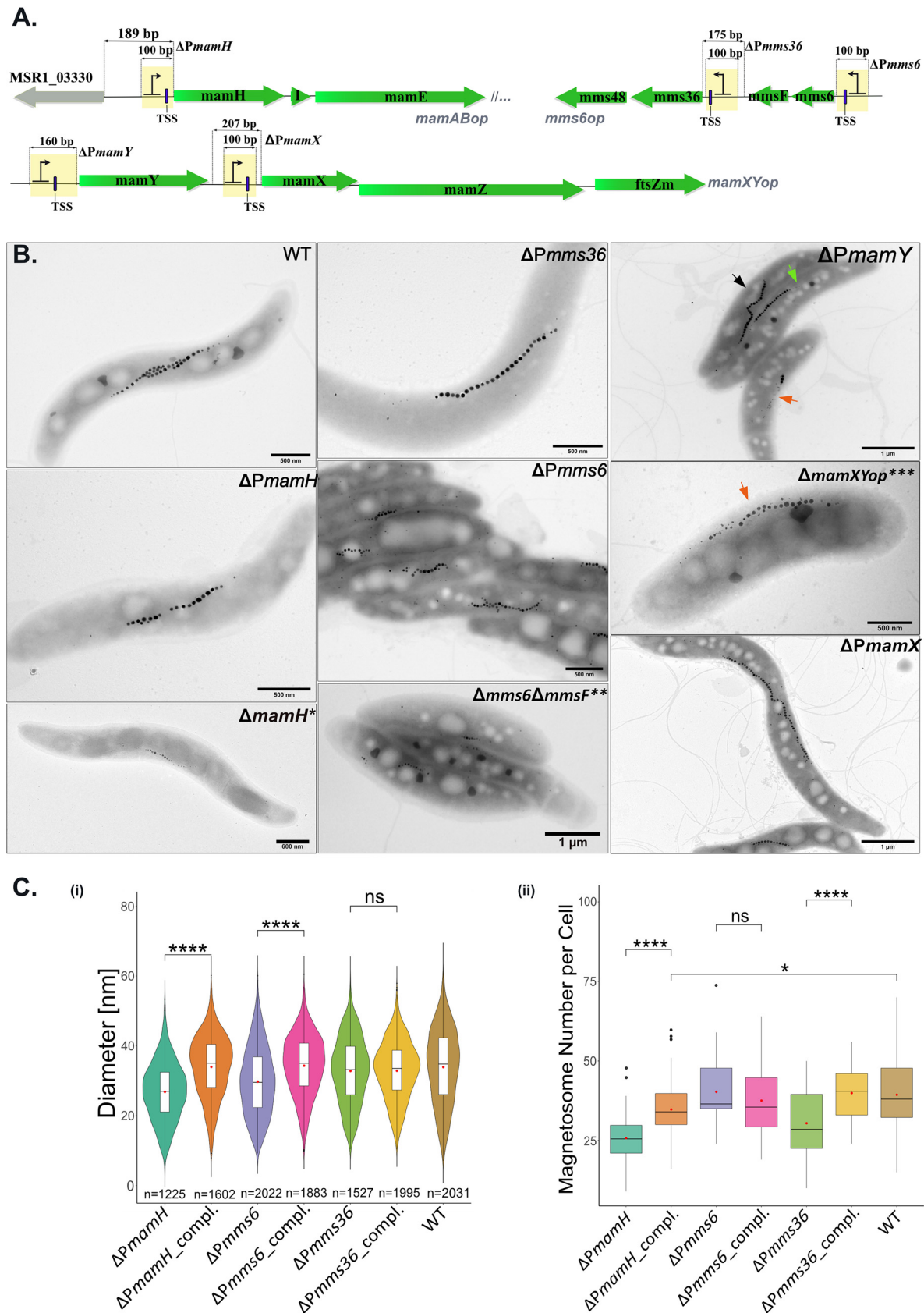


FIG 3 Exploration of the newly identified promoters in vivo by promoter knockout. (A) Schematic representation of the mutagenesis strategy. Yellow bars indicate the regions that were replaced with the promoter-free sequences (PFS). (B) TEM micrographs of the (Continued on next page)

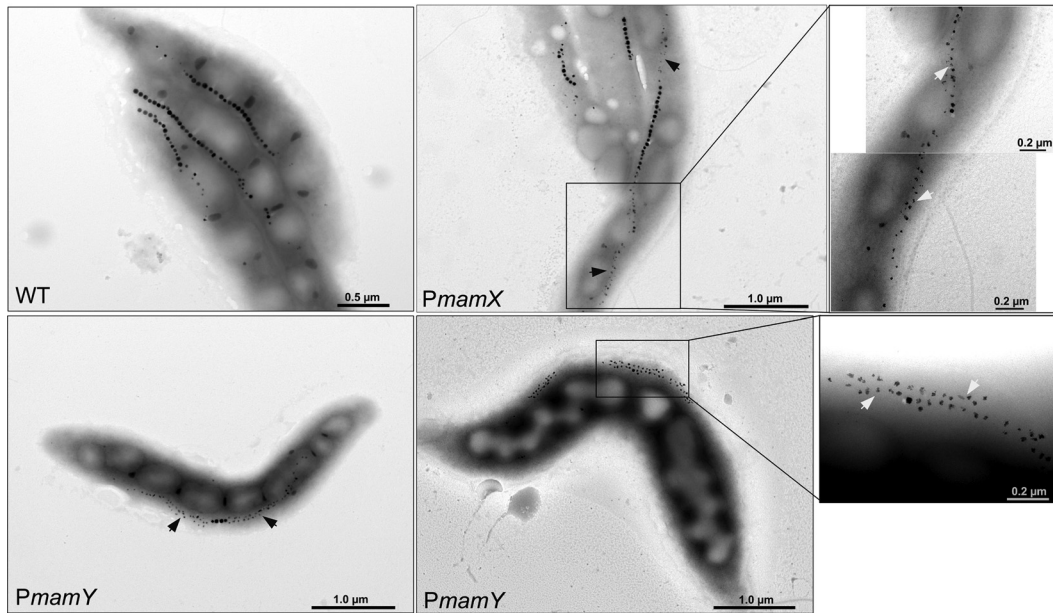


FIG 4 TEM micrographs of the $\Delta PmamY$ and $\Delta PmamX$ mutants grown under nitrate deprivation. Two representative cells of the $\Delta PmamY$ are shown. Arrows indicate flake-like magnetosomes.

The complementation of $\Delta PmamY$ with *PmamY-mamY* restored the regular chain position. However, frequent flake formation was still observed, suggesting a lack or low expression of *mamX*, *mamZ*, and *ftsZm* (Fig. S2). Interestingly, complementation of $\Delta PmamX$ with *PmamX-mamXZftsZm* essentially restored the WT-like appearance of the magnetosomes observed in cells cultivated with ammonium (Fig. S2). Hence, the result reinforces that *PmamX* can modulate the expression of the *mamX-mamZ-ftsZm* genes in addition to *PmamY*, although the exact role of the generated transcript is not clear. Since *mamX*, *mamZ*, and *ftsZm* seem to be especially important for magnetosome biomineralization under nitrate deprivation conditions, we next tested whether the activity of either *PmamY* or *PmamX* is regulated by nitrate. To this end, bioluminescence was measured in clones harboring *PmamY* and *PmamX* fused to *luxABCDE* in the absence or presence of nitrate. However, no significant difference in light emission was detected (Fig. S4), suggesting that the activity of these promoters is not regulated in response to nitrate deprivation.

Promoter sequences within magnetosome operons are conserved across *Magnetospirillum* spp. The complex landscape of transcription initiation in the MagOPs revealed in MSR-1 raised the question of whether such an organization is significant for proper magnetosome formation. If so, it would be expected to be conserved to a certain degree across different species. In other MTB, genes associated with magnetosome biosynthesis are also found in operon-like gene clusters (38–42). Although the gene content and order vary between different taxonomic lineages, some magnetosome genes have higher synteny rates even in distantly related groups (38, 39). Interestingly, in many cases, the first gene in syntenic gene groups is an orthologue of the gene found to comprise a functional promoter

FIG 3 Legend (Continued)

promoter mutants grown in the standard medium. TEM micrographs of the $\Delta mamH$, $\Delta mms6\Delta mmsF$, and $\Delta mamXYop$ published previously are shown for comparison (*, from reference 12 [© John Wiley & Sons Ltd., reproduced with permission]; **, republished from reference 10; ***, republished from *PLoS One* [17]). In $\Delta PmamY$, three typical cell types occurring in the population are indicated by arrows: black, cells with magnetosome chains indistinguishable from the WT; green, a chain mispositioned to the geodetic line within the cells; orange, magnetosome chains with prevailing flake-like magnetosomes. (C) (i) Violin plots displaying magnetosome diameter in the mutants in which the promoters were substituted with PFS and the corresponding complemented mutants. Numbers of the measured particles are indicated at the bottom of each violin plot. (ii) Boxplots demonstrating the magnetosome number per cell in the promoter substitution and complemented mutants. Significance values were calculated by Kruskal-Wallis test; ****, *P* value of less than 0.0001; ns, not significant. Boxplots display the minimum, maximum, and median of each data set. Red points indicate mean. At least 50 cells were measured for each strain.

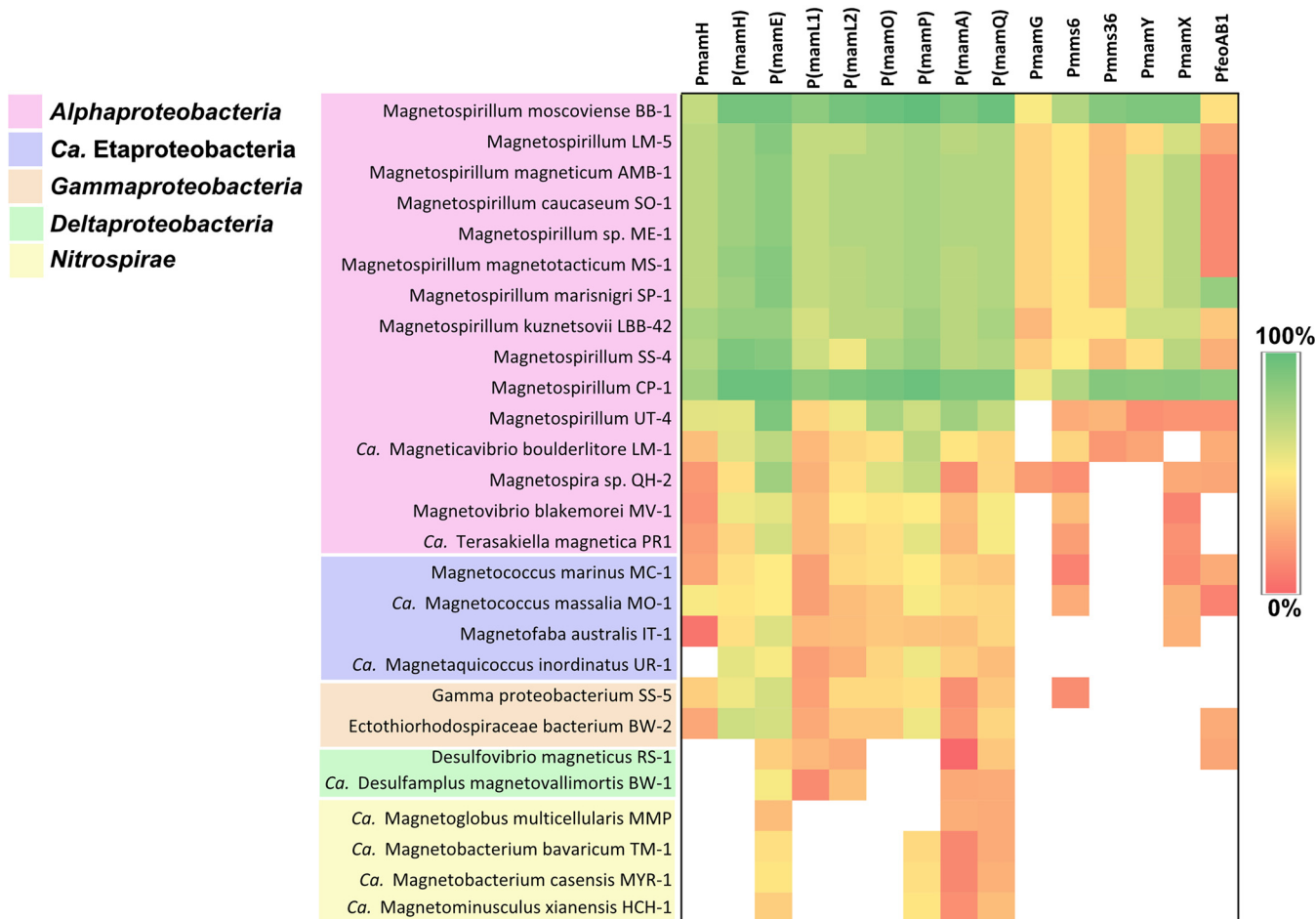


FIG 5 Conservation of the promoter sequences from magnetosome operons as identified in MSR-1 across MTB (see the text for details). White regions indicate that the region is not found in a genome.

in the current research. For instance, *mamL* is followed by *mamM* in many phyla in which these genes are present (except *Nitrospirae* and *Omnitrophica*), and the order *mamQ*-(*mamR*)-*mamB* is preserved in *Nitrospirae*, *Nitrospinae*, and *Proteobacteria*. This prompted us to estimate the sequence conservation of the promoter-containing regions in various phylogenetic groups of MTB (Fig. 5). To this end, sequences positioned -5 to -50 to a confirmed TSS were extracted from promoters tested in MSR-1 and compared to the orthologous sequences in other species.

As expected, sequence conservation was highest across *Magnetospirillum* species, where high similarity was found for *PmamH*, *Pmms6*, *PmamY*, *PmamX*, and all intragenic promoters, whereas *PmamG*, *Pmms36*, and *PfeoAB1* regions were more variable. This implies functional conservation of most of the promoters and, in general, similar organization of transcriptional landscape in MagOPs for different magnetospirilla. A notorious exception is *Magnetospirillum* strain UT-4, in which only several intragenic promoter sequences, *P(mamE)*, *P(mamO)*, *P(mamP)*, *P(mamA)*, *P(mamQ)*, were conserved. This correlates with the distant, ancestral position of the magnetosome genes from this strain to other known *Magnetospirillum* spp. (42). Although relatively high similarity of the sequences orthologous to promoters within *mamE* and *mamP* were found in alphaproteobacterial MTB, in general, the promoters from the MagOPs were not conserved outside of *Magnetospirillum* spp.

DISCUSSION

By combination of various techniques, we were able to map multiple TSS within the magnetosome operons with high precision, evaluate the transcriptional activity of the corresponding promoters, and estimate their function in magnetosome biosynthesis.

The results suggested that *mamGFDCop* and *feoAB1op* are organized as classic polycistronic operons, in which transcription is driven by a single conventional promoter and intercepted by a terminator at the 3' end. The other three operons turned out to have a more complex transcriptional landscape.

One of the key findings of this study is the discovery of multiple promoters residing within the coding sequences of the long *mamABop* operon. Knockout of *PmamH*, the primary promoter of this operon, had only a minor effect on magnetosome formation and silenced only the gene that is located immediately downstream of it, i.e., *mamH*, suggesting that *PmamH* is not essential for transcription of the major part of *mamABop*. At the same time, the transcription of the following genes, including all the essential ones in the operon, were maintained by the intragenic promoters. One of the most crucial internal promoters must be *P(mamH)*, as the downstream genes (*mamI* and *mamE*) are essential for magnetosome formation. Moreover, the reporter assay demonstrated that *P(mamH)* is one of the most active promoters among the ones measured in the current study and the strongest in *mamABop*, with the activity exceeding that of the primary promoter *PmamH* ~10 times. Interestingly, the unintended elimination of *P(mamH)* concurrent with the deletion of *mamH* by Raschdorf et al. did not entirely abolish magnetosome biosynthesis, but only caused the formation of fewer and smaller particles (12). This effect was attributed to the absence of *mamH*, suggesting that the primary promoter *PmamH* can also drive low-level transcription of following genes in the absence of the intragenic *P(mamH)*, thus supporting the existence of a long polycistronic transcript, as previously suggested (11). Nonetheless, complementation with *mamH* in *trans* only partially restored the magnetosome size and number in the Δ *mamH* mutant according to Raschdorf et al. (12), whereas complementation of the *PmamH* knockout mutant in this study restored the magnetosome size to the WT levels (12). Therefore, the weaker activity of *PmamH* putatively compensates the lack of *P(mamH)* only to some extent, which emphasizes the importance of the latter for proper transcription of the essential magnetosome genes in *mamABop* (12). To our knowledge, this is the first demonstration that intragenic promoters can exceed primary promoters in activity and potentially play a major role in driving expression of large operons.

The adaptive role of multiple transcripts generated in the *mamABop* is not yet clear. On the one hand, the multiple promoters residing within the 16-kb *mamABop* operon might compensate the potential instability of the single long mRNA by splitting the operon into several smaller TUs, thus making the transcription of the whole operon more efficient. On the other hand, this might represent one of the mechanisms to ensure a certain stoichiometric ratio of gene products required for the proper assembly of the magnetosome organelle. As we found no obvious correlation between the MAP abundance (21) and the promoter strengths defined either by Cappable-seq scores or RLU_{max} (data not shown), the highly divergent copy numbers of MAPs are likely to be further regulated at the translational level. This has been shown to be largely independent of the growth conditions, suggesting that the promoters within the operons, like the primary promoters of the MagOPs, are unlikely to be subjected to any conditional regulation.

Mms6op comprises two TUs, *mms6-mmsF* and *mms36-mms48*, separated by a terminator and each driven by a separate promoter. The presence of a terminator does not mean *per se* that the TUs are independent, since the transcriptional readthrough due to the inefficient termination can still occur, and hence their transcription can be coupled (24, 43). Interestingly, in all known magnetotactic *Magnetospirillum* species, *mms36* and *mms48* are always preceded by *mms6-mmsF*, suggesting that this coupled organization might be preserved by natural selection.

We also revealed a very active additional promoter within the *mamXYop* (*PmamX*). However, the lack of reporter expression in the absence of optRBS strongly argues against translation of the produced transcript in the native context, including potential leaderless translation (44). Nonetheless, the knockout of *PmamX* resulted in the

production of aberrant flake-like magnetosomes under nitrate deprivation, which implies that the expression of one or all of *mamX*, *mamZ*, and/or *ftsZm* was affected and, hence, *PmamX* activity is necessary for proper magnetosome biosynthesis under these conditions. At the same time, the adverse effect of this deletion on magnetosome formation was compensated by transfer of *PmamX-mamXzftsZm*. The lack of translation of the generated transcript from *PmamX* on the one hand, and its functional importance on the other hand, suggests that it might represent a noncoding RNA (ncRNA) with a potential regulatory function. However, identification of the exact type and characteristics of the produced RNA species will require further experimentation.

Comparison of the promoter sequences in various MTB suggests that the transcriptional organization of *mamABop* and *mamXYop* revealed in MSR-1 is conserved across the species of *Magnetospirillum*. A notable exception was strain UT-4, in which the promoter sequences were the least conserved. According to Monteil et al. (42), UT-4 possesses the magnetosome genes that are ancestral for *Magnetospirillum*, whereas the evolutionary history of magnetosome operons in other *Magnetospirillum* strains was shaped by repeated loss and regain by horizontal transfer. Therefore, the transcriptional organization of magnetosome operons as in MSR-1 likely evolved not in the common ancestor of magnetospirilla, but after their speciation. At the same time, the lack of conservation outside *Magnetospirillum* suggests independent evolution of transcriptional regulation of the MagOPs in different phylogenetic groups. This is a plausible scenario, considering the long evolutionary distances between the MTB genomes and the evidence that new promoters can evolve rapidly (45, 46).

Besides shedding light on the mechanisms underlying control over magnetosome formation, the insights into the transcriptional architecture of the MagOPs obtained in this study have several important practical implications. First, the high-resolution map of transcription initiation will enable synthetic biology approaches to transcriptionally engineer the magnetosome operons for enhanced and controlled magnetosome production, e.g., through replacing the native promoters of individual transcriptional units by stronger and tunable promoters. Likewise, data gained in this study will facilitate the rational design of synthetic versions of magnetosome operons optimized for the expression in foreign organisms (19, 20), as poor transcription of native magnetosome clusters has proven to be one of the key hurdles for successful transplantation of magnetosome biosynthesis to different bacteria. Second, our study provides a catalog of well-characterized promoters with different strengths for constructing expression cassettes in magnetospirilla and other *Alphaproteobacteria*. In conclusion, our study unveils how a genetically complex pathway is orchestrated at the transcriptional level to ensure the proper assembly of one of the most intricate prokaryotic organelles.

MATERIALS AND METHODS

Bacterial strains and culture conditions. If not specified otherwise, *Magnetospirillum gryphiswaldense* strain MSR-1 (DSM 6361) (47, 48) was routinely cultivated in flask standard medium (FSM, 10 mM HEPES [pH 7.0], 15 mM potassium lactate, 4 mM NaNO₃, 0.74 mM KH₂PO₄, 0.6 mM MgSO₄·7H₂O, 50 μM iron citrate, 3 g/liter soy peptone, 0.1 g/liter yeast extract), in flasks containing 2% (vol/vol) O₂ in the headspace, at 120 rpm agitation (49). Selection for the mutants was carried on solid FSM with 1.5% (wt/vol) agar and 5 μg/ml kanamycin (Km).

E. coli WM3064 strains carrying plasmids were cultivated in lysogeny broth (LB) supplemented with 0.1 mM DL- α,ϵ -diaminopimelic acid (DAP) and 25 μg/ml Km at 37°C, with 180 rpm agitation. Characteristics of the strains used in this study are summarized in Table 1.

RNA isolation, library preparation, sequencing, and mapping to the reference genome. Transcription initiation, expression coverage, and transcription termination were investigated by Cappable-seq, whole-transcriptome shotgun sequencing (WTSS), and 3' end sequencing, respectively. For RNA isolation, cells of MSR-1 were cultivated in 5-liter screw-cap bottles at 25°C. Cells were harvested at mid-growth phase (optical density at 565 nm [OD₅₆₅] = 0.2) by centrifugation at 8,300 × *g* and 4°C for 10 min using a Sorvall RC-5B Plus centrifuge (Thermo Fisher Scientific, Waltham, USA) and flash frozen with liquid nitrogen prior to total RNA isolation. Magnetosome biosynthesis was verified using magnetically induced differential light scattering method C_{mag}, as described previously (50) and transmission electron microscopy (TEM). RNA isolated from biological duplicates using the mirVana RNA isolation kit (Thermo Fisher Scientific, Waltham, USA) was treated by DNase, checked by capillary electrophoresis, pooled together, and subsequently used for all library preparations and sequencing by Vertis Biotechnologie AG (Freising, Germany).

TABLE 1 Bacterial strains and vectors used in this work

| Strain or vector | Characteristics/application | Source/reference |
|---|--|------------------------------------|
| Strains | | |
| <i>Magnetospirillum gryphiswaldense</i> MSR-1 | WT, archetype | Lab collection, DSM 6361 |
| <i>E. coli</i> WM3064 | <i>thrB1004 pro thi rpsL hsdS lacZΔM15 RP4-1360 Δ(arabAD) 567 ΔdapA1341::[erm pir]</i> . Donor strain for transformation by conjugation, α,ϵ -diaminopimelic acid (DAP) auxotroph. | William Metcalf, UIUC, unpublished |
| Vectors | | |
| pBamII-Tn7-P-luxAE | <i>KmR, AmpR, p15A ori, Tn7, tr2, T1, luxABCDE</i> ; a plasmid for the transcriptional fusion of a promoter (P) and the <i>lux</i> operon. Suicide vector, a cassette is introduced by chromosomal insertion mediated by Tn7 into the attTn7 site. | This work |
| pORFM-galK | <i>KmR, npt, galK, tetR, mobRK2</i> ; general vector for GalK counterselection | 55 |
| pBamII-Tn5 | <i>KmR, AmpR, p15A ori, mini-Tn5</i> ; general vector used for complementation experiments. Suicide vector, a cassette is introduced by random chromosomal insertion mediated by mini-Tn5 | Uebe, manuscript in preparation |

For the enrichment of primary 5' ends, a modified version of the Cappable-sequencing technique was used (30). Briefly, 5' triphosphorylated RNA was capped with 3'-desthiobiotin-TEG-guanosine 5' triphosphate (DTBGTP) (New England Biolabs, Ipswich, MA, USA) using the vaccinia capping enzyme (New England Biolabs, Ipswich, MA, USA). The biotinylated RNA was then enriched by reversible binding to a streptavidin column, followed by washing and elution of the 5' fragments. The uncapped control was also applied to the streptavidin column to control for unspecific binding to the column matrix. Afterward, adapter ligation, reverse transcription, and amplification of the cDNA were performed according to the instructions for the TrueSeq Stranded mRNA library (Illumina, San Diego, USA) for both libraries. Single-end sequencing for the two libraries was performed on an Illumina NextSeq 500 system using 1×75 bp read length.

For the WTSS library, rRNA was depleted from the pooled RNA sample using the Ribo-Zero rRNA removal kit for bacteria (Illumina, San Diego, CA, USA). The remaining mRNA was purified using the Agencourt AMPure XP kit (Beckman Coulter Genomics, Chaska, MN, USA) and analyzed by capillary electrophoresis. Fragmentation of mRNA, reverse transcription, adapter ligation, and PCR amplification were performed according to the TrueSeq Stranded mRNA library instructions (Illumina). Single-end sequencing was performed on an Illumina NextSeq 500 system using 1×75 bp read length.

For the 3' end library preparation, a 3' Illumina sequencing adapter was ligated to the 3'-OH ends of the rRNA-depleted RNA sample prior to reverse transcription, cDNA fragmentation, sequencing adapter ligation, and cDNA purification using the Agencourt AMPure XP kit (Beckman Coulter Genomics, Chaska, MN, USA). The paired-end sequencing of the PCR amplified cDNA fragments was performed on an Illumina NextSeq 500 system using 2×75 bp read length.

The sequencing reads of the four library preparations were trimmed for sequencing adapters as well as low-quality bases prior to mapping to the *M. gryphiswaldense* genome (accession no. CP027526) using the CLC Bio's Genomic Workbench software package (Qiagen, Venlo, Netherlands).

Annotation of TSS and TTS. TSS were automatically detected using the Cappable-tools with standard parameters as previously described (30). Briefly, for each position in the genome, the read coverage was normalized to the sequencing depth, resulting in the relative read score (RRS). For TSS identification, the enrichment score was calculated according to the formula $\text{enrichment score} = \log_2(\text{RRS}/\text{RRS}_{\text{control}})$, where $\text{RRS}_{\text{control}}$ is the relative read score in the control library for the same position as in the TSS-enriched library. When the enrichment score was above 1, a putative TSS was annotated. Subsequently, TSS classification was performed based on the localization of the TSS relative to the genome annotation using an in-house script. Subsequently, the putative TSS were curated manually by comparison of read coverage of the TSS to the background, as well as by applying an enrichment score of 1.4 as a threshold. Afterward, the filtered TSS were then evaluated by comparing the putative TSS with the coverage of the other transcriptome sequencing (RNA-seq) data sets using the software ReadXplorer for visualization (62). At least one of the following criteria had to be met for assigning a confident TSS: (i) a read coverage increase in the WTSS data set downstream and (ii) a 3'-end enrichment upstream of the putative TSS. In the cases of TSS 5 and TSS 9 (Fig. 1A), although a conspicuous rise in read coverage could be detected manually in both Cappable-seq and WTSS, they did not pass the applied threshold. Nonetheless, since the promoter associated with TSS 5 (*PmamH*) had already been identified in previous research (11, 32), and TSS 9 could be easily identified in the Cappable-seq and WTSS data sets by manual curation, both TSS were included in the subsequent experimental evaluation.

TTS were manually identified by a significant increase in read coverage above a threshold of 2,500 uniquely mapped reads in the 3' end sequencing data set combined with a decrease in WTSS coverage up to 150 bp downstream of a coding sequence.

Molecular and genetic techniques. Oligonucleotides applied in this study are listed in Table S1 in the supplemental material. To verify and measure the activity of promoters, regions of varying lengths (Table S3) from maximal +450 bp to −112 bp relative to the predicted TSS were PCR amplified and cloned by *Nde*I and *Xho*I restriction sites into a suicide vector pBamII-Tn7-P-luxAE (Table 1) upstream of the *Photobacterium luminescens luxABCDE* operon, which was cloned from pAH328 (51, 52). The vector enables precise and orientation-specific genomic integration of the expression cassette into the *attTn7* site downstream of *glmS* gene by means of the Tn7 transposase (53), (Uebe, manuscript in preparation). Integration of the cassette in the *attTn7* site was verified by PCR with specific primers.

The promoters *PmamH*, *Pmms6*, and *PmamY* were inactivated by replacing 100-bp regions (except *PmamY*, where a 160-bp fragment was exchanged) located immediately upstream of the start codon with an inert artificial sequence of equal length that was free of any regulatory elements (the “promoter-free sequence” [PFS]). In case of the intergenic *Pmms36* and *PmamX*, the regions upstream of the −20 bp position to the start codon were replaced with the PFS, to keep putative natural RBSs. Maintaining the native sequence lengths was important to avoid potential effects caused by shorter distances to the neighbor promoters located upstream or with altered gene expression due to the reduced leader length.

The PFS (5'-CATTACTCGCATCCATTCTCAGGCTGTCTCGTCTCGTCTCGCTGGGAGTTCGTAGACGGAAACAAACGCAGAATCCAAGCGCACTGAAGGTCCTCAATCG-3') was designed as a concatenate of the unique nucleotide sequences UNS1, UNS2, and the first 20 nt of UNS3 that were used previously to generate regulation signature-free homology arms for Gibson assembly (54). The oligonucleotide was inserted by overlapping PCR between two 1- to 1.3-kb sequences flanking the target promoters. The resulting PCR products were phosphorylated by T4 polynucleotide kinase and blunt ligated into the vector for homologous recombination (pORFM-Galk) digested with *EcoRV* (55). The plasmids were transferred into the wild-type MSR-1 by conjugation, as described elsewhere (56). Selection, counterselection, and screening of the deletion mutants were performed essentially as described previously (55). For genetic complementation, the silenced genes and the corresponding missing promoters were inserted randomly into the mutant chromosome by Tn5 transposition. To this end, the *PmamH-mamH*, *Pmms6-mms6-mmsF*, *Pmms36-mms36-mms48*, *PmamY-mamY*, and *PmamX-mamX-mamZ-mamFtsZm* regions were PCR amplified from the MSR-1 WT genomic DNA (gDNA), digested with *Xho*I/*Bam*HI, *Pac*I/*Bam*HI, or *Xho*I/*Sac*I and ligated into a vector derivative of pBam1, pBamII (57), (Uebe, manuscript in preparation). Positive clones were selected by Km resistance and screened by PCR.

Luminescence measurements. At least three randomly selected transconjugants harboring vector pBamII-Tn7-P-luxAE were analyzed in three biological replicates for luminescence. The luminescence signal was detected as arbitrary light units by a multiwell plate reader equipped with a luminometer module (Tecan Infinite M200 PRO) during growth of the cultures in FSM at 28°C and 280 rpm, every 20 min over 200 cycles (72 h). Arbitrary light units were normalized to optical density measured at the wavelength of 565 nm (OD_{565}) to obtain relative light units, according to the formula:

$$RLU = \frac{\text{Light AU}}{OD_{565} \text{ AU}}$$

Maxima of the RLU curves (RLU_{max}) were used to compare promoter activities.

Transmission electron microscopy (TEM). Cells were concentrated from 2 to 3 ml of culture by centrifugation, adsorbed onto carbon-coated copper grids, and washed twice with deionized water. Samples were imaged with a JEOL-1400 Plus TEM (Japan) at 80 kV acceleration. Micrographs were analyzed with tools implemented in the ImageJ software (58).

Analysis of promoter sequence conservation. For each TSS identified by Cappable-seq with the luminescence-confirmed promoter activity, 300 nt upstream of the TSS, a leader sequence and a gene positioned next to TSS, were extracted. Regions homologous to the extracted ones were identified in the genomes of other MTB by blastp (59) of the gene product amino acid sequence (E value cut-off threshold 10^{-5}) and inspected manually. Homologous DNA sequences were aligned by MAFFT with the default parameters (60) and the sequence identity between the regions aligned to the fragment positioned −5 to −50 to the TSS in MSR-1 were calculated.

Statistical analysis. Statistical analysis was carried out by R version 3.6.1 (<http://www.r-project.org>). Significance in comparison of magnetosome size and number was estimated by Kruskal-Wallis test. Violin and box plots were created using the following R packages: ggplot (<https://CRAN.R-project.org/package=ggplot2>), ggpubr (<https://CRAN.R-project.org/package=ggpubr>), dplyr (<https://CRAN.R-project.org/package=dplyr>), and EnvStats (<https://cran.r-project.org/web/packages/EnvStats/index.html>). The bioluminescence and growth curves were plotted using GraphPad Prism software (v. 6.01 for Windows).

Data availability. The data discussed in this publication have been deposited in NCBI's Gene Expression Omnibus (61) and are accessible through GEO Series accession number GSE168986.

SUPPLEMENTAL MATERIAL

Supplemental material is available online only.

FIG S1, TIF file, 0.4 MB.

FIG S2, TIF file, 6.9 MB.

FIG S3, TIF file, 0.8 MB.

FIG S4, TIF file, 0.4 MB.

TABLE S1, PDF file, 0.1 MB.

TABLE S2, PDF file, 0.1 MB.

TABLE S3, PDF file, 0.1 MB.

TABLE S4, PDF file, 0.2 MB.

ACKNOWLEDGMENTS

This study was supported by the European Research Council (ERC) under the European Union's Horizon 2020 research and innovation program (grant no. 692637 to D.S.).

We are grateful to Bachelor students Filiz Kuybu, Tobias Göttische, and Katharina Volk for technical assistance. We also thank Stefan Geimer and Rita Grotjahn for help with electron microscopy, and Susanne Gebhard (University of Bath) for kindly providing the *luxABCDE*-containing vector pAH328.

D.S., M.D., and C.N.R. conceived the study and designed the experiments. C.N.R., M.W., T.B., and J.K. carried out the transcriptome analysis; M.D. and R.U. designed the vectors for the bioluminescence reporter assay; M.D. generated plasmids and carried out the promoter evaluation. M.D. designed the promoter mutagenesis experiment; M.D. and L.B. generated and analyzed the promoter knockout mutants. M.D. analyzed the sequence conservation. M.D., C.N.R., and D.S. wrote the manuscript. All authors read and approved the final manuscript.

REFERENCES

- Faivre D, Schüler D. 2008. Magnetotactic bacteria and magnetosomes. *Chem Rev* 108:4875–4898. <https://doi.org/10.1021/cr078258w>.
- Vargas G, Cypriano J, Correa T, Leão P, Bazylinski DA, Abreu F. 2018. Applications of magnetotactic bacteria, magnetosomes and magnetosome crystals in biotechnology and nanotechnology: mini-review. *Molecules* 23:2438. <https://doi.org/10.3390/molecules23102438>.
- Mickoleit F, Schüler D. 2018. Generation of multifunctional magnetic nanoparticles with amplified catalytic activities by genetic expression of enzyme arrays on bacterial magnetosomes. *Adv Biosyst* 2:1–10. <https://doi.org/10.1002/adbi.201700109>.
- Goldhawk DE, Rohani R, Sengupta A, Gelman N, Prato FS. 2012. Using the magnetosome to model effective gene-based contrast for magnetic resonance imaging. *Wiley Interdiscip Rev Nanomed Nanobiotechnol* 4: 378–388. <https://doi.org/10.1002/wnan.1165>.
- Pekarsky A, Spadiut O. 2020. Intrinsically magnetic cells: a review on their natural occurrence and synthetic generation. *Front Bioeng Biotechnol* 8: 573183. <https://doi.org/10.3389/fbioe.2020.573183>.
- Raschdorf O, Forstner Y, Kolinko I, Uebe R, Plietzko JM, Schüler D. 2016. Genetic and ultrastructural analysis reveals the key players and initial steps of bacterial magnetosome membrane biogenesis. *PLoS Genet* 12: e1006101. <https://doi.org/10.1371/journal.pgen.1006101>.
- Uebe R, Schüler D. 2016. Magnetosome biogenesis in magnetotactic bacteria. *Nat Rev Microbiol* 14:621–637. <https://doi.org/10.1038/nrmicro.2016.99>.
- Müller FD, Schüler D, Pfeiffer D. 2020. A compass to boost navigation: cell biology of bacterial magnetotaxis. *J Bacteriol* 21:1–40. <https://doi.org/10.1128/JB.00398-20>.
- Silva KT, Schüler M, Mickoleit F, Zwiener T, Müller FD, Awal RP, Weig A, Brachmann A, Uebe R, Schüler D. 2020. Genome-wide identification of essential and auxiliary gene sets for magnetosome biosynthesis in *Magnetospirillum gryphiswaldense*. *mSystems* 5:e00565-20. <https://doi.org/10.1128/mSystems.00565-20>.
- Lohße A, Borg S, Raschdorf O, Kolinko I, Tompa E, Pósfai M, Faivre D, Baumgartner J, Schüler D. 2014. Genetic dissection of the *mamAB* and *mms6* operons reveals a gene set essential for magnetosome biogenesis in *Magnetospirillum gryphiswaldense*. *J Bacteriol* 196:2658–2669. <https://doi.org/10.1128/JB.01716-14>.
- Schubbe S, Würdemann C, Peplies J, Heyen U, Wawer C, Glöckner FO, Schüler D. 2006. Transcriptional organization and regulation of magnetosome operons in *Magnetospirillum gryphiswaldense*. *Appl Environ Microbiol* 72:5757–5765. <https://doi.org/10.1128/AEM.00201-06>.
- Raschdorf O, Müller F, Pósfai M, Plietzko J, Schüler D. 2013. The magnetosome proteins MamX, MamZ and MamH are involved in redox control of magnetite biomineralization in *Magnetospirillum gryphiswaldense*. *Mol Microbiol* 89:872–886. <https://doi.org/10.1111/mmi.12317>.
- Rong C, Huang Y, Zhang W, Jiang W, Li Y, Li J. 2008. Ferrous iron transport protein B gene (*feoB1*) plays an accessory role in magnetosome formation in *Magnetospirillum gryphiswaldense* strain MSR-1. *Res Microbiol* 159: 530–536. <https://doi.org/10.1016/j.resmic.2008.06.005>.
- Ullrich S, Kube M, Schübbe S, Reinhardt R, Schüler D. 2005. A hypervariable 130-kilobase genomic region of *Magnetospirillum gryphiswaldense* comprises a magnetosome island which undergoes frequent rearrangements during stationary growth. *J Bacteriol* 187:7176–7184. <https://doi.org/10.1128/JB.187.21.7176-7184.2005>.
- Uebe R, Schüler D, Jogler C, Wiegand S. 2018. Reevaluation of the complete genome sequence of *Magnetospirillum gryphiswaldense* MSR-1 with single-molecule real-time sequencing data. *Genome Announc* 6: e00309-18. <https://doi.org/10.1128/genomeA.00309-18>.
- Zwiener T, Dziuba M, Mickoleit F, Rückert C, Busche T, Kalinowski J, Uebe R, Schüler D. 2021. Towards a 'chassis' for bacterial magnetosome biosynthesis: genome streamlining of *Magnetospirillum gryphiswaldense* by multiple deletions. *Microb Cell Fact* 20:35. <https://doi.org/10.1186/s12934-021-01517-2>.
- Lohße A, Ullrich S, Katzmann E, Borg S, Wanner G, Richter M, Voigt B, Schweder T, Schüler D. 2011. Functional analysis of the magnetosome island in *Magnetospirillum gryphiswaldense*: the *mamAB* operon is sufficient for magnetite biomineralization. *PLoS One* 6:e25561. <https://doi.org/10.1371/journal.pone.0025561>.
- Toro-Nahuelpan M, Giacomelli G, Raschdorf O, Borg S, Plietzko JM, Bramkamp M, Schüler D, Müller FD. 2019. MamY is a membrane-bound protein that aligns magnetosomes and the motility axis of helical magnetotactic bacteria. *Nat Microbiol* 4:1978–1989. <https://doi.org/10.1038/s41564-019-0512-8>.
- Kolinko I, Lohße A, Borg S, Raschdorf O, Jogler C, Tu Q, Pósfai M, Tompa É, Plietzko JM, Brachmann A, Wanner G, Müller R, Zhang Y, Schüler D. 2014. Biosynthesis of magnetic nanostructures in a foreign organism by transfer of bacterial magnetosome gene clusters. *Nature Nanotech* 9:193–197. <https://doi.org/10.1038/nnano.2014.13>.
- Dziuba MV, Zwiener T, Uebe R, Schüler D. 2020. Single-step transfer of biosynthetic operons endows a non-magnetotactic *Magnetospirillum* strain from wetland with magnetosome biosynthesis. *Environ Microbiol* 22:1603–1618. <https://doi.org/10.1111/1462-2920.14950>.
- Raschdorf O, Bonn F, Zeytuni N, Zarivach R, Becher D, Schüler D. 2018. A quantitative assessment of the membrane-integral sub-proteome of a bacterial magnetic organelle. *J Proteomics* 172:89–99. <https://doi.org/10.1016/j.jprot.2017.10.007>.
- Dziuba MV, Baeuerlein E. 1996. Iron-limited growth and kinetics of iron uptake in *Magnetospirillum gryphiswaldense*. *Arch Microbiol* 166:301–307. <https://doi.org/10.1007/s002030050387>.
- Schüler D, Baeuerlein E. 1998. Dynamics of iron uptake and Fe₃O₄ biomineralization during aerobic and microaerobic growth of *Magnetospirillum gryphiswaldense*. *J Bacteriol* 180:159–162. <https://doi.org/10.1128/JB.180.1.159-162.1998>.
- Conway T, Creecy JP, Maddox SM, Grissom JE, Conkle TL, Shadid TM, Teramoto J, Miquel PS, Shimada T, Ishihama A, Mori H, Wanner BL. 2014. Unprecedented high-resolution view of bacterial operon architecture

- revealed by RNA sequencing. *mBio* 5:e01442-14. <https://doi.org/10.1128/mBio.01442-14>.
25. Koide T, Reiss DJ, Bare JC, Pang WL, Facciotti MT, Schmid AK, Pan M, Marzolf B, Van PT, Lo FY, Pratap A, Deutsch EW, Peterson A, Martin D, Baliga NS. 2009. Prevalence of transcription promoters within archaeal operons and coding sequences. *Mol Syst Biol* 5:285. <https://doi.org/10.1038/msb.2009.42>.
 26. Babski J, Haas KA, Näther-Schindler D, Pfeiffer F, Förstner KU, Hammelmann M, Hilker R, Becker A, Sharma CM, Marchfelder A, Soppa J. 2016. Genome-wide identification of transcriptional start sites in the haloarchaeon *Haloferax volcanii* based on differential RNA-Seq (dRNA-Seq). *BMC Genomics* 17:629. <https://doi.org/10.1186/s12864-016-2920-y>.
 27. Mejía-Almonte C, Busby SJW, Wade JT, van Helden J, Arkin AP, Stormo GD, Eilbeck K, Palsson BO, Galagan JE, Collado-Vides J. 2020. Redefining fundamental concepts of transcription initiation in bacteria. *Nat Rev Genet* 21:699–714. <https://doi.org/10.1038/s41576-020-0254-8>.
 28. Liotenberg S, Steunou AS, Picaud M, Reiss-Husson F, Astier C, Ouchane S. 2008. Organization and expression of photosynthesis genes and operons in anoxygenic photosynthetic proteobacteria. *Environ Microbiol* 10:2267–2276. <https://doi.org/10.1111/j.1462-2920.2008.01649.x>.
 29. Cozy LM, Kearns DB. 2010. Gene position in a long operon governs motility development in *Bacillus subtilis*. *Mol Microbiol* 76:273–285. <https://doi.org/10.1111/j.1365-2958.2010.07112.x>.
 30. Ettwiller L, Buswell J, Yigit E, Schildkraut I. 2016. A novel enrichment strategy reveals unprecedented number of novel transcription start sites at single base resolution in a model prokaryote and the gut microbiome. *BMC Genomics* 17:199. <https://doi.org/10.1186/s12864-016-2539-z>.
 31. Dar D, Sorek R. 2018. High-resolution RNA 3'-ends mapping of bacterial Rho-dependent transcripts. *Nucleic Acids Res* 46:6797–6805. <https://doi.org/10.1093/nar/gky274>.
 32. Lang C, Pollithy A, Schüler D. 2009. Identification of promoters for efficient gene expression in *Magnetospirillum gryphiswaldense*. *Appl Environ Microbiol* 75:4206–4210. <https://doi.org/10.1128/AEM.02906-08>.
 33. Naylor LH. 1999. Reporter gene technology: the future looks bright. *Biochem Pharmacol* 58:749–757. [https://doi.org/10.1016/s0006-2952\(99\)00096-9](https://doi.org/10.1016/s0006-2952(99)00096-9).
 34. Borg S, Hofmann J, Pollithy A, Lang C, Schüler D. 2014. New vectors for chromosomal integration enable high-level constitutive or inducible magnetosome expression of fusion proteins in *Magnetospirillum gryphiswaldense*. *Appl Environ Microbiol* 80:2609–2616. <https://doi.org/10.1128/AEM.00192-14>.
 35. Dieudonné A, Prévéral S, Pignol D. 2020. A sensitive magnetic arsenite-specific biosensor hosted in magnetotactic bacteria. *Appl Environ Microbiol* 86:e00802-20. <https://doi.org/10.1128/AEM.00803-20>.
 36. Cambray G, Guimaraes JC, Mutalik VK, Lam C, Mai QA, Thimmaiah T, Carothers JM, Arkin AP, Endy D. 2013. Measurement and modeling of intrinsic transcription terminators. *Nucleic Acids Res* 41:5139–5148. <https://doi.org/10.1093/nar/gkt163>.
 37. Müller FD, Raschdorf O, Nudelmann H, Messerer M, Katzmann E, Piltzko JM, Zarivach R, Schüler D. 2014. The FtsZ-like protein FtsZm of *Magnetospirillum gryphiswaldense* likely interacts with its generic homolog and is required for biomineralization under nitrate deprivation. *J Bacteriol* 196:650–659. <https://doi.org/10.1128/JB.00804-13>.
 38. Lin W, Zhang W, Paterson GA, Zhu Q, Zhao X, Knight R, Bazylinski DA, Roberts AP, Pan Y. 2020. Expanding magnetic organelle biogenesis in the domain Bacteria. *Microbiome* 8:152. <https://doi.org/10.1186/s40168-020-00931-9>.
 39. Lin W, Zhang W, Zhao X, Roberts AP, Paterson GA, Bazylinski DA, Pan Y. 2018. Genomic expansion of magnetotactic bacteria reveals an early common origin of magnetotaxis with lineage-specific evolution. *ISME J* 12:1508–1519. <https://doi.org/10.1038/s41396-018-0098-9>.
 40. Monteil CL, Perrière G, Menguy N, Ginot N, Alonso B, Waisbord N, Cruveiller S, Pignol D, Lefèvre CT. 2018. Genomic study of a novel magnetotactic *Alphaproteobacteria* uncovers the multiple ancestry of magnetotaxis. *Environ Microbiol* 20:4415–4430. <https://doi.org/10.1111/1462-2920.14364>.
 41. Monteil CL, Benzerara K, Menguy N, Bidaud CC, Michot-Achdjan E, Bolzoni R, Mathon FP, Coutaud M, Alonso B, Garau C, Jézéquel D, Viollier E, Ginot N, Florian M, Swaraj S, Sachse M, Busigny V, Duprat E, Guyot F, Lefevre CT. 2021. Intracellular amorphous Ca-carbonate and magnetite biomineralization by a magnetotactic bacterium affiliated to the *Alphaproteobacteria*. *ISME J* 15:1–18. <https://doi.org/10.1038/s41396-020-00747-3>.
 42. Monteil CL, Grouzdev DS, Perrière G, Alonso B, Rouy Z, Cruveiller S, Ginot N, Pignol D, Lefevre CT. 2020. Repeated horizontal gene transfers triggered parallel evolution of magnetotaxis in two evolutionary divergent lineages of magnetotactic bacteria. *ISME J* 14:1783–1794. <https://doi.org/10.1038/s41396-020-0647-x>.
 43. Creecy JP, Conway T. 2015. Quantitative bacterial transcriptomics with RNA-seq. *Curr Opin Microbiol* 23:133–140. <https://doi.org/10.1016/j.mib.2014.11.011>.
 44. Cortes T, Schubert OT, Rose G, Arnvig KB, Comas I, Aebersold R, Young DB. 2013. Genome-wide mapping of transcriptional start sites defines an extensive leaderless transcriptome in *Mycobacterium tuberculosis*. *Cell Rep* 5:1121–1131. <https://doi.org/10.1016/j.celrep.2013.10.031>.
 45. Yona AH, Alm EJ, Gore J. 2018. Random sequences rapidly evolve into de novo promoters. *Nat Commun* 9:1530. <https://doi.org/10.1038/s41467-018-04026-w>.
 46. Urtecho G, Insigne K, Tripp A, Brinck M, Lubock N, Kim H, Chan T, Kosuri S. 2020. Genome-wide functional characterization of *Escherichia coli* promoters and regulatory elements responsible for their function. *bioRxiv* 2020.01.04.894907.
 47. Schleifer KH, Schüler D, Spring S, Weizenegger M, Amann R, Ludwig W, Köhler M. 1991. The Genus *Magnetospirillum* gen. nov. description of *Magnetospirillum gryphiswaldense* sp. nov. and transfer of *Aquaspirillum magnetotacticum* to *Magnetospirillum magnetotacticum* comb. nov. *Syst Appl Microbiol* 14:379–385. [https://doi.org/10.1016/S0723-2020\(11\)80313-9](https://doi.org/10.1016/S0723-2020(11)80313-9).
 48. Schüler D, Köhler M. 1992. The isolation of a new magnetic spirillum. *Zentralbl Mikrobiol* 147:150–151. [https://doi.org/10.1016/S0232-4393\(11\)80377-X](https://doi.org/10.1016/S0232-4393(11)80377-X).
 49. Heyen U, Schüler D. 2003. Growth and magnetosome formation by microaerophilic *Magnetospirillum* strains in an oxygen-controlled fermenter. *Appl Microbiol Biotechnol* 61:536–544. <https://doi.org/10.1007/s00253-002-1219-x>.
 50. Schüler D, Uhl R, Bäuerlein E. 1995. A simple light scattering method to assay magnetism in *Magnetospirillum gryphiswaldense*. *FEMS Microbiol Lett* 132:139–145. <https://doi.org/10.1111/j.1574-6968.1995.tb07823.x>.
 51. Winson MK, Swift S, Hill PJ, Sims CM, Griesmayr G, Bycroft BW, Williams P, Stewart GSAB. 1998. Engineering the *luxCDABE* genes from *Photobacterium luminescens* to provide a bioluminescent reporter for constitutive and promoter probe plasmids and mini-Tn5 constructs. *FEMS Microbiol Lett* 163:193–202. <https://doi.org/10.1111/j.1574-6968.1998.tb13045.x>.
 52. Schmalisch M, Maiques E, Nikolov L, Camp AH, Chevreux B, Muffler A, Rodriguez S, Perkins J, Losick R. 2010. Small genes under sporulation control in the *Bacillus subtilis* genome. *J Bacteriol* 192:5402–5412. <https://doi.org/10.1128/JB.00534-10>.
 53. Choi KH, Gaynor JB, White KG, Lopez C, Bosio CM, Karkhoff-Schweizer RR, Schweizer HP. 2005. A Tn7-based broad-range bacterial cloning and expression system. *Nat Methods* 2:443–448. <https://doi.org/10.1038/nmeth765>.
 54. Torella JP, Lienert F, Boehm CR, Chen J, Way JC, Silver PA. 2014. Unique nucleotide sequence-guided assembly of repetitive DNA parts for synthetic biology applications. *Nat Protoc* 9:2075–2089. <https://doi.org/10.1038/nprot.2014.145>.
 55. Raschdorf O, Piltzko JM, Schüler D, Müller FD, Schüler D, Müller FD, Schüler D, Müller FD. 2014. A tailored *galK* counterselection system for efficient markerless gene deletion and chromosomal tagging in *Magnetospirillum gryphiswaldense*. *Appl Environ Microbiol* 80:4323–4330. <https://doi.org/10.1128/AEM.00588-14>.
 56. Schultheiss D, Schüler D. 2003. Development of a genetic system for *Magnetospirillum gryphiswaldense*. *Arch Microbiol* 179:89–94. <https://doi.org/10.1007/s00203-002-0498-z>.
 57. Martínez-García E, Calles B, Arévalo-Rodríguez M, De Lorenzo V. 2011. pBAM1: an all-synthetic genetic tool for analysis and construction of complex bacterial phenotypes. *BMC Microbiol* 11:38. <https://doi.org/10.1186/1471-2180-11-38>.
 58. Abràmoff MD, Magalhães PJ, Ram SJ. 2004. Image processing with imageJ. *Biophotonics Int* 11:36–42.
 59. States DJ, Gish W. 1994. QGB: combined use of sequence similarity and codon bias for coding region identification. *J Comput Biol* 1:39–50. <https://doi.org/10.1089/cmb.1994.1.39>.
 60. Katoh K, Standley DM. 2013. MAFFT multiple sequence alignment software version 7: improvements in performance and usability. *Mol Biol Evol* 30:772–780. <https://doi.org/10.1093/molbev/mst010>.
 61. Edgar R, Domrachev M, Lash AE. 2002. Gene Expression Omnibus: NCBI gene expression and hybridization array data repository. *Nucleic Acids Res* 30:207–210. <https://doi.org/10.1093/nar/30.1.207>.
 62. Hilker R, Stadermann KB, Doppmeier D, Kalinowski J, Stoye J, Straube J, Winneballd J, Goemann A. 2014. ReadXplorer—visualization and analysis of mapped sequences. *Bioinformatics* 30:2247–2254. <https://doi.org/10.1093/bioinformatics/btu205>.

Article 3

Manuscript 3

The transcriptomic landscape of *Magnetospirillum gryphiswaldense* during magnetosome biomineralization

Cornelius N. Riese, Manuel Wittchen, Valérie Jérôme, Ruth Freitag, Tobias Busche, Jörn Kalinowski and Dirk Schüler.

BMC Genomics (2022) 23:699

doi: 10.1186/s12864-022-08913-x

RESEARCH

Open Access



The transcriptomic landscape of *Magnetospirillum gryphiswaldense* during magnetosome biomineralization

Cornelius N. Riese¹, Manuel Wittchen², Valérie Jérôme³, Ruth Freitag³, Tobias Busche², Jörn Kalinowski² and Dirk Schüler^{1*}

Abstract

Background: One of the most complex prokaryotic organelles are magnetosomes, which are formed by magnetotactic bacteria as sensors for navigation in the Earth's magnetic field. In the alphaproteobacterium *Magnetospirillum gryphiswaldense* magnetosomes consist of chains of magnetite crystals (Fe₃O₄) that under microoxic to anoxic conditions are biomineralized within membrane vesicles. To form such an intricate structure, the transcription of > 30 specific structural genes clustered within the genomic magnetosome island (MAI) has to be coordinated with the expression of an as-yet unknown number of auxiliary genes encoding several generic metabolic functions. However, their global regulation and transcriptional organization in response to anoxic conditions most favorable for magnetite biomineralization are still unclear.

Results: Here, we compared transcriptional profiles of anaerobically grown magnetosome forming cells with those in which magnetosome biosynthesis has been suppressed by aerobic condition. Using whole transcriptome shotgun sequencing, we found that transcription of about 300 of the > 4300 genes was significantly enhanced during magnetosome formation. About 40 of the top upregulated genes are directly or indirectly linked to aerobic and anaerobic respiration (denitrification) or unknown functions. The *mam* and *mms* gene clusters, specifically controlling magnetosome biosynthesis, were highly transcribed, but constitutively expressed irrespective of the growth condition. By Capable-sequencing, we show that the transcriptional complexity of both the MAI and the entire genome decreased under anaerobic conditions optimal for magnetosome formation. In addition, predominant promoter structures were highly similar to sigma factor σ^{70} dependent promoters in other Alphaproteobacteria.

Conclusions: Our transcriptome-wide analysis revealed that magnetite biomineralization relies on a complex interplay between generic metabolic processes such as aerobic and anaerobic respiration, cellular redox control, and the biosynthesis of specific magnetosome structures. In addition, we provide insights into global regulatory features that have remained uncharacterized in the widely studied model organism *M. gryphiswaldense*, including a comprehensive dataset of newly annotated transcription start sites and genome-wide operon detection as a community resource (GEO Series accession number GSE197098).

Keywords: *Magnetospirillum*, Magnetosomes, Operons, Promoters, Transcription, Transcriptome

*Correspondence: Dirk.Schueler@uni-bayreuth.de

¹ Department of Microbiology, University of Bayreuth, Bayreuth, Germany
Full list of author information is available at the end of the article

Background

Magnetosomes, which are formed by magnetotactic bacteria (MTB) as sensors for geomagnetic navigation in their aquatic habitat, represent an example for one of the



most complex organelles found in prokaryotic cells [1–3]. Their unprecedented magnetic properties make bacterial magnetosomes also highly attractive as biomaterial in several biotechnical and biomedical applications, such as magnetic imaging [4] and hyperthermia [5–7], as well as magnetic separation and drug targeting [8–10].

In the well-studied alphaproteobacterium *Magnetospirillum gryphiswaldense* and related MTB, magnetosomes consist of a monocrystalline core of magnetite (Fe_3O_4) bounded by a dedicated proteo-lipid membrane [2, 11]. Magnetosome biosynthesis starts with the invagination of the magnetosome membrane (MM) vesicle, followed by sorting of specific magnetosome proteins into the MM, the accumulation of large amounts of iron within the MM vesicles and the biomineralization of well-ordered crystals of magnetite (Fe_3O_4), and finally, their assembly and positioning into linear chains along the dedicated cytoskeletal network [2, 12].

Magnetosome biosynthesis has been found to be orchestrated by numerous proteins [2], which together build a sophisticated machinery that exerts strict control over each step of magnetosome formation. Most specific functions are encoded by the >30 genes termed *mam* (magnetosome membrane), *mms* (magnetosome particle membrane-specific) and *feoABI* (a magnetosome-specific Fe^{2+} transport system) [2, 13, 14]. These are all clustered in five major operons within a larger genomic magnetosome island (MAI) that extends over ~110kb [14, 15]. Transfer of all five *mam*- and *mms*-operons (MagOPs) from *M. gryphiswaldense*, conferred magnetosome biosynthesis to various foreign, hitherto non-magnetic bacteria, thereby confirming the essential role of this gene set [16, 17]. A recent analysis by RNA-sequencing, bioluminescence reporter assays and promoter knockouts revealed that the transcriptional architecture of magnetosome operons is complex [18]: in microaerobically grown cells, the *mamGFDCop* (2.1kb) and *feoABIop* (2.4kb) operons are transcribed as single transcriptional units, whereas multiple transcription start sites (TSS) were present in the *mms6op* (3.6kb), *mamXYop* (5kb) and the long *mamABop* (>16kb), which comprises 17 genes and encodes all the essential factors for magnetosome biosynthesis [13, 19].

An increasing number of studies indicated that in addition to key functions encoded by the MAI genes, further auxiliary genes encoding generic cellular functions located outside the MAI are required for proper magnetosome biosynthesis. For example, aerobic and anaerobic respiration pathways were shown to participate in magnetite biomineralization, probably by contributing to oxidation of ferrous iron to ferric iron under oxygen-limited conditions [20, 21]. Mutants of *M. gryphiswaldense* that lack enzymes of the denitrification pathway, such as the

periplasmic nitrate reductase (NapAB), Fe^{2+} -nitrite oxidoreductase (NirS) or nitric oxide reductase (NorBC) were severely impaired in magnetite biomineralization [20, 21]. The importance of respiratory pathways was confirmed by a genome-wide transposon mutagenesis screen, in which also further genes with additional auxiliary functions were implicated in magnetosome biosynthesis, such as sulfate assimilation, oxidative protein folding and cytochrome c maturation [22].

In addition to the availability of micromolar amounts of iron [23, 24], the O_2 concentration was found to be the crucial factor affecting magnetite biomineralization in *M. gryphiswaldense* [25, 26]. Magnetite crystals are formed only under microoxic to anoxic conditions, whereas dissolved oxygen concentration (dO_2) >10% air saturation were found to entirely inhibit the formation of magnetosomes [25, 26]. However, the molecular mechanisms and determinants of oxygen regulation and redox control of magnetite biomineralization have remained unclear. Several early studies suggested that the transcription of magnetosome genes comprised in the MagOPs is only weakly affected by oxygen (and iron) [13, 27]. This was also observed in a whole-transcriptomic study by Wang and colleagues, which found that MagOP expression was neither affected by oxygen nor iron. Whereas genes coding for iron regulation, transport and metabolism were differentially expressed under high iron conditions, oxygen mainly affected genes encoding nitrate respiration [28, 29].

However, although these previous studies already revealed valuable insights into the transcriptional organization and the role of oxygen, major parts of the regulation and transcriptional architecture are still unknown. Most importantly, previous studies [18, 28] employed microoxic conditions supporting fastest growth, but sub-optimal magnetosome formation, as indicated by the formation of fewer, less regular and smaller magnetosomes compared to anoxic conditions [25, 26]. Furthermore, the operon architecture and transcriptional organization of genes involved in magnetosome biosynthesis outside the MAI has remained unknown. In addition, given the importance of *M. gryphiswaldense* as a widely studied model organism for biomineralization, organelle formation and magnetotaxis, knowledge about global regulatory features, such as promoter and operon structures within the MAI and in the entire genome is needed.

Here, we studied the transcriptional profiles of *M. gryphiswaldense* during magnetosome biomineralization under anaerobic conditions, favoring highest magnetite biomineralization, compared to oxic conditions entirely inhibiting magnetite synthesis [25, 26]. In addition, we present new candidates for further magnetosome biosynthesis-associated genes, and reveal genome-wide

structures and positions of promoters, operons and other regulatory elements.

Results

Cultivation and RNA-sequencing of *M. gryphiswaldense*

To compare transcriptomic profiles between magnetic and non-magnetic cells, we mainly focused on the analysis of cells grown under two conditions: i) the entire absence of oxygen (0% dO₂) with 10 mM nitrate as electron-acceptor for anaerobic denitrifying growth [20]. These anoxic conditions are known to support optimal magnetosome biosynthesis [20, 25, 26]. For comparison, cells were grown under ii) oxic conditions (95% dO₂), which were shown to entirely suppress magnetosome biosynthesis [24, 25]. In addition, the anaerobic electron acceptor nitrate was replaced by an equimolar amount of ammonium as the nitrogen source (see Fig. 1 for a summary of growth experiments and library construction). For each condition, cells were cultured in triplicates at 28 °C within an oxystat fermenter allowing precise control of all growth parameters [26]. Anoxic cultures reached a final optical density (OD₅₆₅) of approximately 0.5 after 25 h (Fig. S1), and as expected, exhibited the highest magnetic response (C_{mag} , a light-scattering proxy for magnetosome biomineralization [30]) of >0.7 as well as the largest average crystal size (34 nm) with 25 magnetosomes per cell (Fig. 1). For comparison, oxic cultures grew to an OD₅₆₅ of 0.8 after 26 h and did not form magnetite crystals, as indicated by a C_{mag} of nearly 0 and the absence of electron dense particles in electron micrographs in most cells (Fig. 1). Growth was highly consistent between all replicates per condition (Fig. S1).

To minimize putative effects of media depletion, we chose sampling points during early growth, which was OD₅₆₅ 0.1 for anoxic, and OD₅₆₅ 0.2 for oxic conditions. Upon sampling, triplicates from anoxic and oxic conditions were pooled, respectively, and used for genome-wide TSS identification by Cappable-sequencing [31]. In addition, for the genome-wide identification of transcription termination sites (TTSs) as well as elucidation of operon structures, 3'end-sequencing technique [32] and whole transcriptome shotgun sequencing (WTSS) were applied. The WTSS libraries were separately constructed from each replicate of conditions i) 0% dO₂ with 10 mM nitrate and ii) 95% dO₂ for evaluation of differential transcription. For the detection of maximal numbers of operons and termination events, results from two additional conditions were considered: iii) microoxic conditions (1% dO₂, 4 mM nitrate) as used for high yield routine cultivation and magnetosome production [25], iv) as well as oxic conditions (95% dO₂) with 4 mM nitrate as an alternative nitrogen source to separate effects of electron acceptor

from nitrogen-source (Fig. S1). Samples of triplicates from all four growth conditions were pooled and used for WTSS and 3' end-sequencing.

Effects of anoxic growth conditions permitting magnetosome biosynthesis on gene expression

We first compared the genome-wide abundance of transcripts under anoxic and oxic conditions. For the identification of highly differentially expressed genes, the M-value (log₂ of the calculated foldchange) was plotted against the A-value (log₂ of the base mean) as proxy for the expression level of each gene (Fig. 2). From the >4300 genes in total, about 300 were found significantly upregulated.

To capture only the most significantly regulated genes, the M-value threshold of ≥ 4 for stronger and ≤ -3 for downregulated genes were qualitatively chosen from the MA-plot (Fig. 2). Using these thresholds, 41 genes were found highly upregulated in magnetic cells under anoxic conditions and 11 genes downregulated compared to oxic conditions (Table S3).

Highest upregulation of all (319.6 -fold, M-value: 8.32) was detected for *cycA_1*, which encodes a cytochrome c₄-precursor. Further genes highly upregulated (16 to 256-fold, M-value 4–8, see Table S3 for details) in anoxic magnetic cells are linked to various steps of denitrification such as *napABCHG* (nitrate reduction) *nirCDEFGHJLST*, *nrrS* [33] (nitrite reduction), *norBCDQ* (nitric oxide reduction) and *nosZ* (nitrous oxide reduction) [20, 21, 34].

Expression of various oxygen-dependent cytochrome c terminal oxidases was also affected by anoxic conditions: genes *ccoNOQP* encoding the subunits of the *ccb3*-type cytochrome c oxidase [35], were upregulated under anoxic conditions by 2.1, 2.4, 2.2 and 1.6-fold (M-value 1.04, 1.27, 1.12 and 0.66), respectively. In previous studies, an *aa3*-type cytochrome c terminal oxidase was found only active under oxic conditions [35]. Consistently, we found *coxBAC* and *ctaG* encoding this oxidase downregulated by 4.2, 6.7, 5.0 and 6.2-fold (M-value -2.07, -2.75, -2.32 and -2.63), respectively. A third type of cytochrome oxidase, the *bd*-type cytochrome c oxidase, encoded by the genes *cydBA* [35], was actively transcribed under anoxic conditions with an A-value of ca. 7 but genes were not differentially expressed across conditions. Further highly upregulated genes were MSR1_08970 (M-value 5.27) and MSR1_08150 (M-value 8.09), which may putatively encode a cytochrome c and a cytochrome c oxidase, supported by their co-localization with genes of related functions within common operons. However, no heme-binding motif (CXXCH) was found during sequence analysis.

Some of these respiratory genes were previously found to be regulated by the oxygen-sensing transcription factor

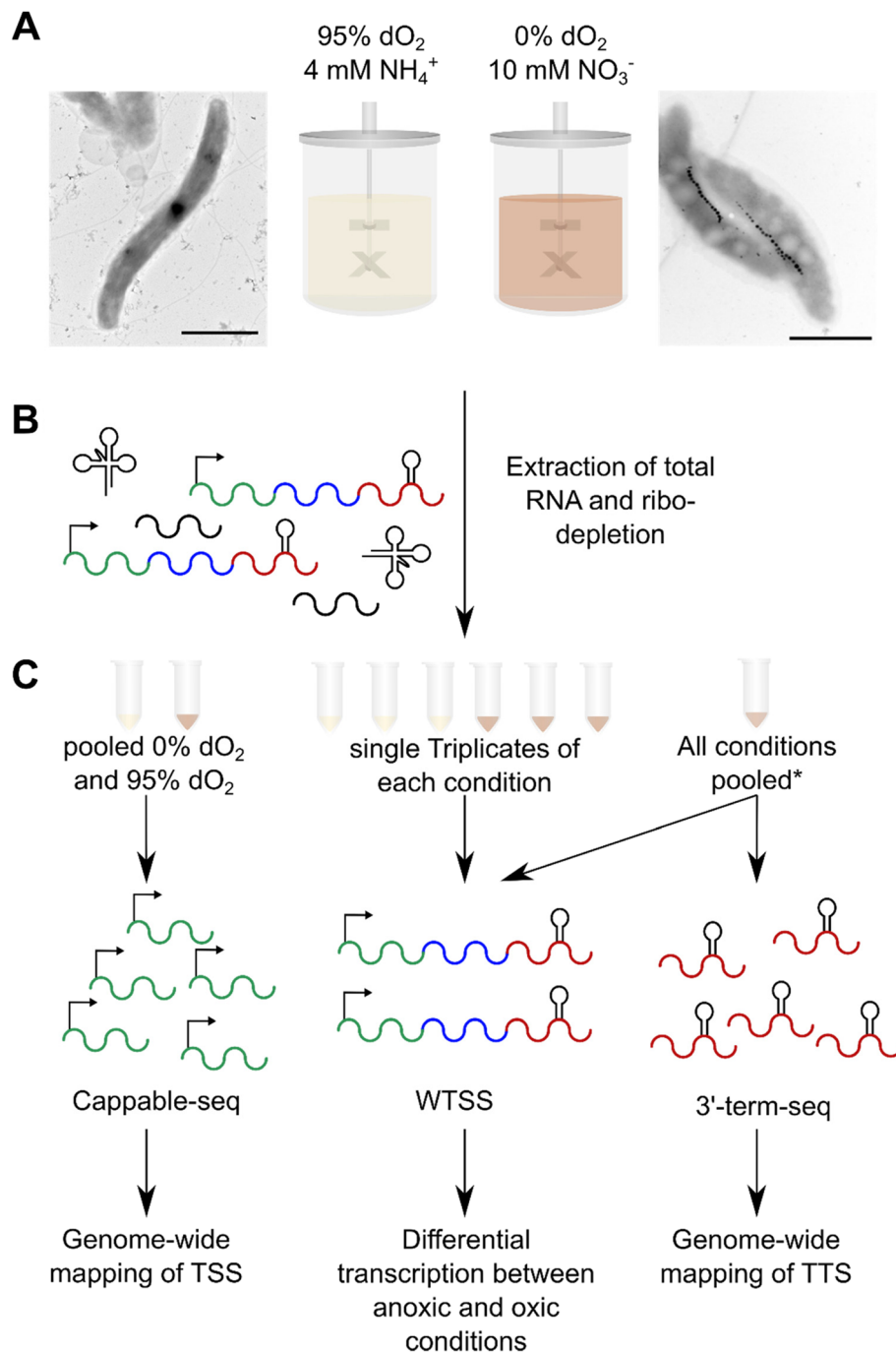
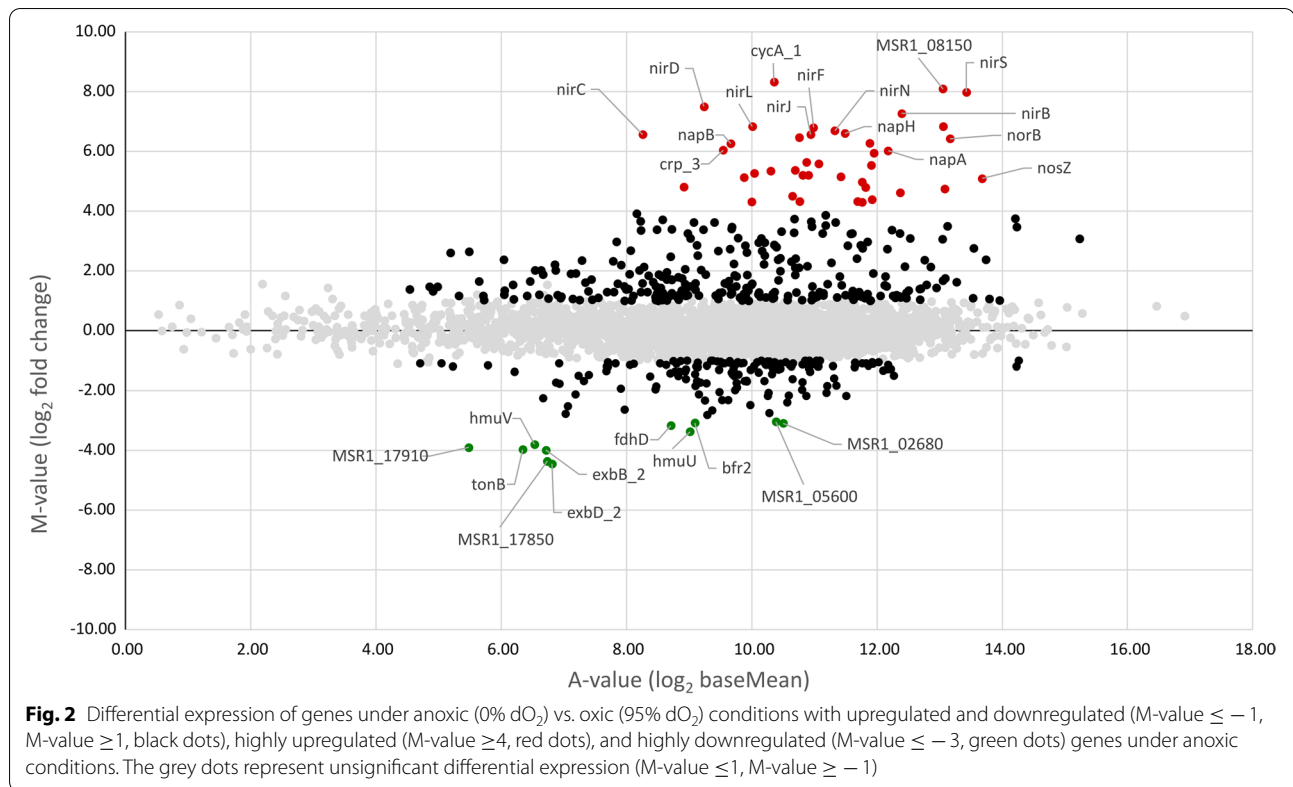


Fig. 1 Overview of the study design. **A** Cultivation of *M. gryphiswaldense* under controlled oxic (95% dO₂) and anoxic (0% dO₂) conditions resulting in nonmagnetic and magnetosome forming cells, respectively, as visible by transmission electron microscopy imaging (scale bar 1 μm). **B** Extraction of the total RNA in technical triplicates, followed by **C** pooling of the samples for the three different library preparations and library preparation prior to RNA-sequencing. * All conditions encompassing anoxic, microoxic and oxic growth with nitrate (NO₃⁻) or ammonium (NH₄⁺) were pooled for this analysis

called MgFnr, which represses denitrification genes with increasing oxygen concentration [36]. We found *Mgfnr* itself to be only weakly regulated (*M*-value -0.44), thus ensuring the presence of this regulator under all growth

conditions. Two other homologues of the *fnr*-family MSR1_08370 and MSR1_08380 were highly upregulated in magnetic cells (*M*-value 6.04 and 2.37), thus



representing additional potential regulators of magnetosome biosynthesis-associated genes.

Because of the involvement of many cytochrome c-like proteins in magnetosome biosynthesis [2, 31, 35, 37, 38], and also their abundance among highly upregulated genes in anoxic magnetic cells, we further focused on genes responsible for cytochrome c biosynthesis and maturation. For example, *resA*, which enables heme to bind by breakage of the disulfide bonds in apo-cytochrome c [39], was highly upregulated by 19.8-fold (M-value 4.31). The genes *ccmG* (disulfide bond formation) and *ccmI* (apo-cytochrome c chaperon) [40] from the operons *ccmABop* and *ccmCDEFGHlop* were weakly, but significantly downregulated by 1.4 and 1.2-fold (M-value -0.51 and -0.26), respectively, whereas *ccmA* was 1.4-fold upregulated (M-value 0.44). Transcription of other genes from these operons remained unchanged between anoxic and oxic conditions. Further genes that are associated with cytochrome c biogenesis and were previously implicated in magnetosome biosynthesis [22] are *dsbA* and *dsbB*, which function in disulfide bond formation during translocation of proteins across the cytoplasmic membrane [41]. However, their transcription was essentially unaffected between anoxic and oxic conditions.

Another highly upregulated gene (49.9-fold, M-value 5.64) was MSR1_19280, which encodes an *HHE cation binding domain* containing protein with unknown function. This domain is found in bacteriohemerythrins known for binding oxygen during import processes, but is also found in proteins that play a part in transcriptional regulation in response to oxygen or nitrate [42, 43]. Several other hemerythrin-like genes were upregulated under anoxic conditions, including MSR1_34750, MSR1_33560 and MSR1_04470 by 4.0, 2.3 and 18.7-fold (M-value 2.00, 1.22 and 4.32), respectively.

Among the most highly downregulated genes under anoxic conditions were *exbD_2* (M-value -4.45), *exbB_2* (M-value -3.99) and *tonB* (M-value -3.97), all of them involved in import of various substrates, including iron siderophores [44]. Likewise, *hmuV* and *hmuU* involved in the import of heme, another putative iron source, were also downregulated 13.9 and 10.3-fold (M-value -3.80 and -3.37), respectively. Since ferrous iron becomes oxidized to insoluble ferric iron in the presence of oxygen, this might lead to the exploitation of alternative iron sources (e.g. siderophores and heme) in anticipation of iron shortage under oxic conditions. On the other hand, the lower transcription of siderophore and heme uptake genes under anoxic conditions suggests only a minor role of these proteins in magnetosome biosynthesis. Other

genes with a function in iron homeostasis are bacterioferritins *bfr1* and *bfr2*, which were previously implicated in magnetosome biosynthesis by Mößbauer spectroscopy [45]; this, however, was questioned more recently by a genetic approach [46]. Here, single and double deletions of *bfr1* and *bfr2* did not impact magnetite formation in *M. gryphiswaldense* [46]. Consistent with the latter *bfr1* and *bfr2* were downregulated under anoxic conditions by -7.0 and -8.5 -fold (M-value -2.81 and -3.08), respectively. However, this interesting observation does not necessarily indicate whether bacterioferritins are involved in magnetosome biosynthesis or not. Since the oxic conditions were likely to impose oxidative stress to the microaerophilic *M. gryphiswaldense*, we expected genes involved in tolerance to reactive oxygen species to be among the differentially transcribed genes (Fig. 2). In fact, *tpx* and *sodB*, coding for putative peroxidases were downregulated under anoxic conditions by 3.2 and 2.3-fold (M-value -1.68 and -1.17), respectively. Additionally, MSR1_07950 coding for rubrerythrin, and *tsA*, a putative peroxidase, were both downregulated by 2.1 and 2.9-fold (M-value -1.04 and -1.52). Furthermore, *rpoE* (σ^{24}) a sigma factor for cell envelope and oxidative stress [47, 48] was downregulated by 2.1-fold (M-value -1.10), whereas the putative peroxide sensing transcription factor encoded by *perR_1* was significantly upregulated by 2.4-fold (M-value 1.26).

Expression of magnetosome gene clusters

The well-established *mam*- and *mms*-gene clusters, which are directly linked to magnetosome biomineralization, were not among the most differentially transcribed genes by applying routinely used thresholds (i.e. M-value ≥ 1 or ≤ -1). However, as indicated by their high A-value, all *mam*- and *mms*-genes were among genes with highest overall expression levels (A-value of 12–14) across all investigated conditions (Fig. 3). Transcription of *mamA-Bop*, which harbors all essential genes for magnetosome biosynthesis [19], was largely unaffected between anoxic and oxic conditions. Strongest upregulation among *mamA-Bop* genes was observed for *mamE*, *mamO* and *mamP* 1.4 (M-value 0.53), 1.6 (M-value 0.67) and 1.4-fold (M-value 0.44), respectively, while *mamH*, *mamJ*, *mamN*, *mamA*, *mamB* and *mamT* showed only low upregulation by 1.2-fold (M-value 0.26–0.3). Only genes from two magnetosome operons were upregulated under anoxia: 1) *mms5* and *mmxF* from the *mms5op* (M-value 1.54 and 0.98) and 2) *mms6*, *mmsF*, *mms36*, and *mms48* from *mms6op* (M-value 1.56, 1.17, 1.09, 0.6) that are all important for magnetite particle size regulation [19, 49–51]. The accessory genes *mamGFDC* [52] were only weakly upregulated ca. 1.4-fold (M-value 0.73, 0.38, 0.49, 0.5).

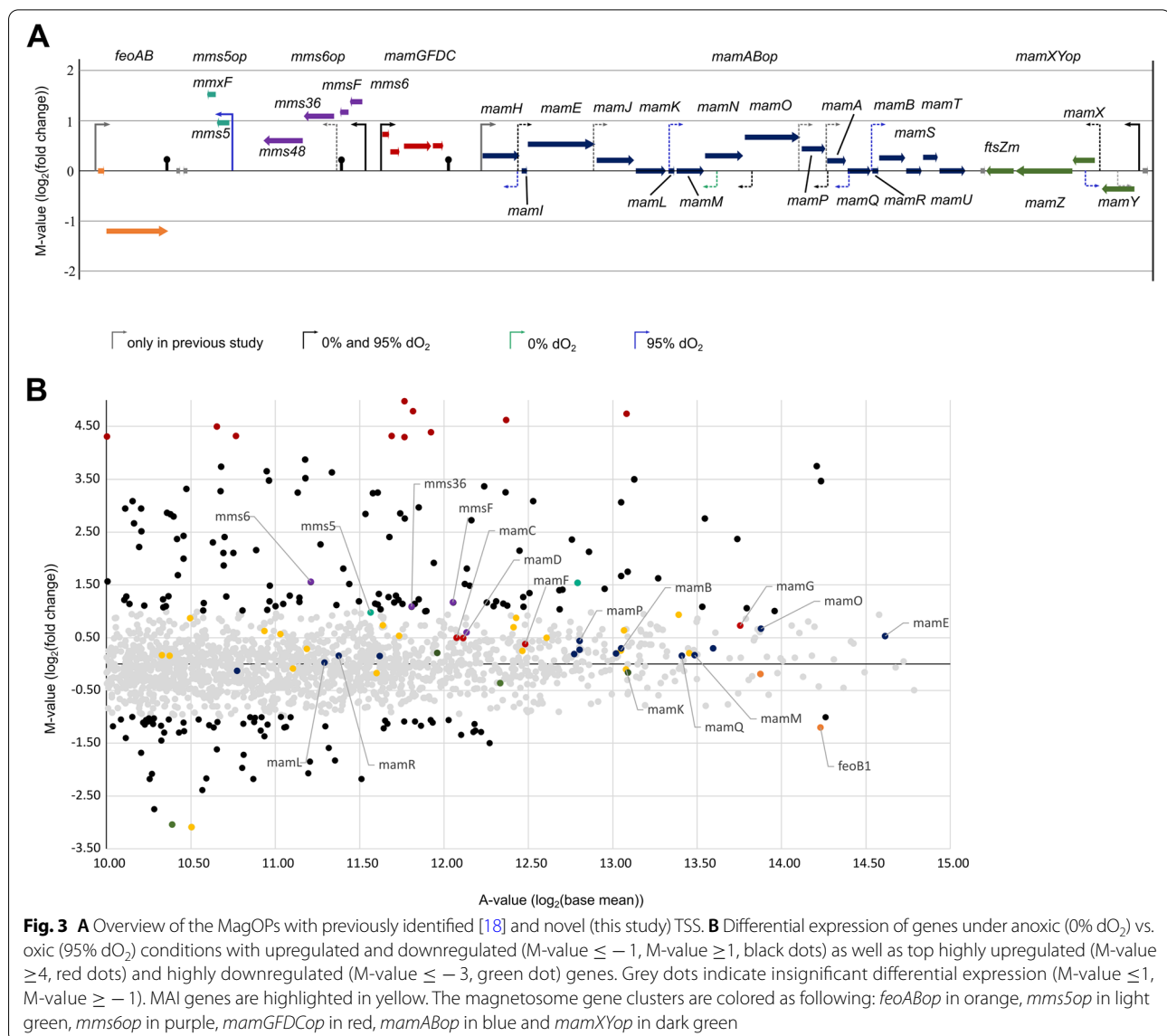
From *mamXYop* genes, no significant differential expression was observed for *mamZ* and *ftsZm*, while *mamY* and *mamX* showed weak, but opposite regulation patterns. Under anoxic conditions *mamY* was 1.3-fold (M-value -0.36) downregulated, whereas *mamX* was upregulated 1.2-fold (M-value 0.21). This seems to be in agreement with their suggested functions, where a possible link between denitrification, the cellular redox potential and biomineralization was suggested for *mamX*, *mamZ* and *ftsZm* [53, 54], while *mamY* was shown to encode a cytoskeletal protein involved in magnetosome chain positioning rather than biomineralization [55]. In addition to the already observed primary promoter upstream of *mamY* (*PmamY*), an intergenic promoter (*PmamX*) between *mamY* and *mamX* was detected under both conditions, which might drive the different transcription of *mamX*, *mamZ* and *ftsZm* [18].

The *feoABIop*, one of the two ferrous iron uptake systems present in *M. gryphiswaldense*, is thought to be mainly responsible for ferrous iron uptake for magnetosome biosynthesis [2, 56]. Under anoxic conditions, *feoB1*, which encodes a ferrous iron transporting transmembrane GTPase, was 2.3-fold downregulated (M-value -1.2), while *feoA1* encoding a Fe^{2+} transport related protein of unknown function [57] remained unchanged.

Genome-wide analysis of promoter architectures

Next, all TSS present under anoxic and oxic conditions were identified with Cappable-seq [31]. After empirical testing, the thresholds providing high specificity as well as reasonable reduction of false positives were set to an enrichment factor of 2.5. By applying this threshold, 5200 and 5002 TSS were identified for oxic and anoxic conditions, respectively, with 2755 (95% dO_2) and 2579 (0% dO_2) TSS exclusively found in each respective condition. Identified TSS were classified as primary TSS upstream of the corresponding coding regions (pTSS), intragenic TSS (iTSS), anti-sense TSS (asTSS) and other TSS (oTSS) not part of any of the classes mentioned before.

Since promoter motifs are most highly preserved in intergenic regions, which do not obey the evolutionary restrictions of protein coding regions, motif analysis was performed with the identified pTSS using the software Improbizer [58]. Under both oxic and anoxic conditions, a conserved TATAaT motif was identified (Fig. 4A). Furthermore, a second motif was recognized with the consensus sequence of cTTGcc. Both motifs are separated by a 11–20bp interspacing region. In most genes, transcription starts with a conserved adenine 6–9bp downstream of the corresponding -10 region. For both conditions, a conserved aaGGAG motif as ribosome binding site (RBS)

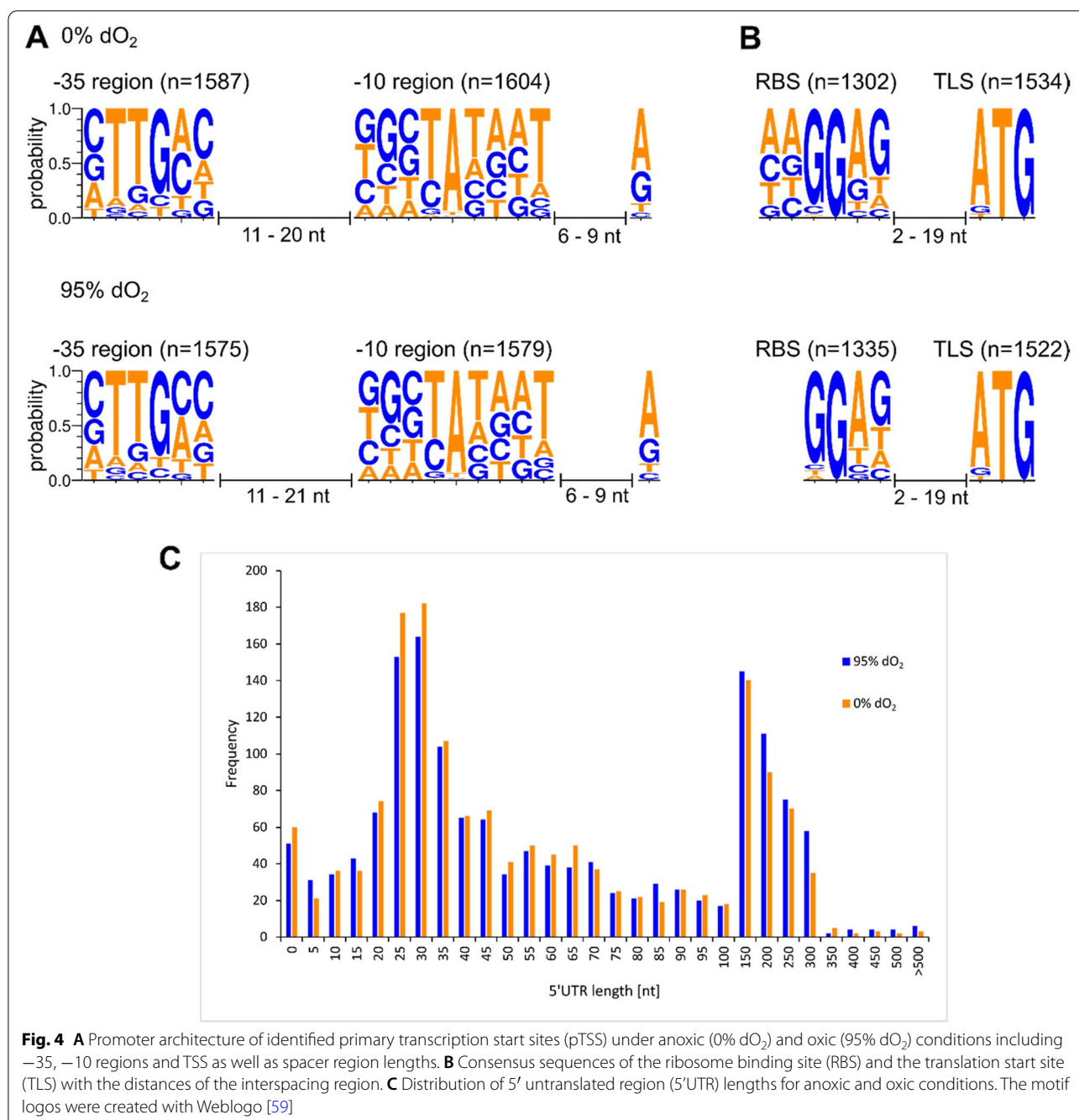


with a 2–19 nt spacer to the start codon was detected (Fig. 4B). Consensus sequences were calculated separately for pTSS within the MAI (inMAI) and the rest of the genome (exMAI). However, no differences were found (Fig. S3).

To further identify putative regulatory elements of translation apart from the RBS, the region between the identified pTSS and the translation start site (TLS), the so called 5'-untranslated region (5'-UTR) was extracted and further analyzed (Fig. S2). From the 1522 (95% dO₂) and 1534 (0% dO₂) extracted 5'-UTRs, 5% (Number of 5'-UTRs under 95% dO₂ 51 and 0% dO₂ 60) were considered as leaderless transcripts (5'-UTR length

0–9 nt), since 5'UTRs below 9 nt are considered too short to harbor an RBS with a corresponding spacer region. Short 5'-UTRs with a length of 25–35 nt were the dominant fraction with 20.8% (317) and 23.4% (353) of the investigated sequences under oxic and anoxic conditions, respectively (Fig. 4C). These 5'-UTRs are sufficiently long to comprise an RBS with the corresponding spacer to the TLS.

A second dominant fraction (406 5'-UTRs under 95% dO₂ (26.7%), and 353 under 0% dO₂ (23.0%)) ranging from 150 to 300 nt in 5'-UTR length was identified. This suggests a high degree of regulation at both the transcriptional and translational level by



cis-regulatory elements such as riboswitches, secondary structures or attenuators since 5'-UTR of these lengths are known to enable such complex structures [60, 61]. Analysis of the genome sequence with the Rfam database [62, 63] identified three putative riboswitches (Table 1), in addition to the previously identified putative regulatory elements in the 5'-UTR [15]. Additionally, one small RNA (sRNA) was identified in the genome.

Elucidation of the global operon architecture

We further investigated genome-wide operon organization by combining Cappable-seq, WTSS as well as 3'-end-sequencing. To enhance the detection of operons and termination events, results from microoxic and oxic conditions, with nitrate as a nitrogen source, were considered, in addition to the main oxic and anoxic conditions. Initial analysis was conducted using the automatic operon prediction tool as part of the ReadXplorer

Table 1 Predicted cis-regulatory elements by using the Rfam database [62, 63]

| Name | Start | Stop | Bit Score | Strand | 0% dO ₂ TSS | 95% dO ₂ TSS |
|--------------------------|-----------|-----------|-----------|--------|------------------------|-------------------------|
| Cobalamin riboswitch | 530,889 | 531,128 | 118.2 | + | 530,905 | 530,801 |
| Guanidine-I riboswitch* | 119,571 | 119,680 | 75.6 | - | | 119,678 |
| SAM riboswitch | 3,457,791 | 3,457,868 | 69.5 | - | 3,457,976 | 3,457,976 |
| Glycine riboswitch | 3,661,824 | 3,661,919 | 68.7 | + | 3,661,819 | 3,661,819 |
| TPP riboswitch | 72,546 | 72,658 | 70.6 | + | 72,467 | 72,558 |
| manganese riboswitch* | 2,189,415 | 2,189,528 | 49 | - | 2,189,523 | 2,189,523 |
| rpsB* | 1,038,575 | 1,038,671 | 46.8 | + | 1,038,568 | 1,038,569 |
| Guanidine-II riboswitch* | 3,082,026 | 3,082,072 | 45.7 | + | 3,082,019 | 3,082,019 |
| Bjrc80 sRNA* | 1,456,741 | 1,456,921 | 43.4 | - | | |

The newly predicted cis-regulatory elements are highlighted by an asterisk

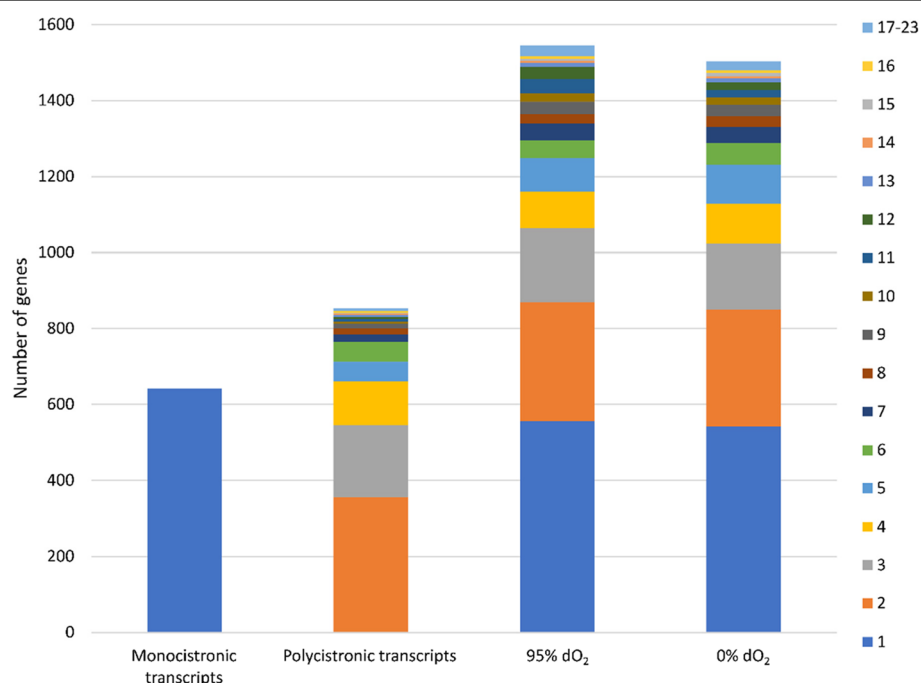


Fig. 5 Distribution of identified operons by gene number. Monocistronic and polycistronic transcripts were identified from the pooled dataset including all tested conditions. Sub-operons were defined by transcription start site (TSS) identification within a primary operon for the respective condition (95 and 0% dO₂). The number of genes within the monocistronic and polycistronic as well as the sub-operons is coded by color

software [64] with the threshold of at least three spanning reads for assigning two neighboring genes into a primary operon (i.e., a polycistronic transcript harboring at least two genes). If additional TSS were located within a presumed primary operon, a sub-operon was assumed. Using this procedure, 643 genes were found expressed as monocistronic transcripts, and 853 as primary operons comprising between 2 and 23 genes, and 3254 genes in total (Fig. 5). The majority (89% / 764 primary operons) of the polycistronic transcripts comprised 2–6 genes with 357 primary operons coding for two genes (41.9%),

followed by transcripts with three genes (22% / 189 primary operons). Among the longest operons was the well-studied *mamABop* with 17 genes involved in magnetosome biosynthesis. Other examples for long operons comprised 16 genes (17kb) encoding NADH-quinone oxidoreductase subunits, and 21 genes encoding ribosomal proteins (9kb).

Different sub-operon profiles were identified in magnetic (anoxic) and non-magnetic (oxic) cells. Under oxic conditions 1545 sub-operons were identified with 814 sub-operons exclusive for this condition. Anoxic datasets

showed 1504 sub-operons of which 836 were exclusively identified under this condition. In both conditions, the majority of sub-operons encompass a single gene (oxic: 36.1% / anoxic: 36.1%), followed by two genes (20.1% / 20.4%), whereas 43.8% / 43.8% of the identified sub-operons consist of more than three genes (Fig. 3).

Within the MAI, 28 monocistronic transcripts and 30 primary operons (including the MagOPs) were identified under all four investigated conditions, the majority of which encompass two genes (21 primary operons). Furthermore, 47 sub-operons dataset were identified within the oxic dataset, whereas only 29 within the anoxic dataset, suggesting a lower transcriptional complexity under anoxic conditions. Whereas the architecture of the two primary *feoAB1op* and *mms5op* did not change, showing two and no sub-operons, respectively, the other MagOPs exhibited condition-dependent changes in TSS numbers resulting in different sub-operonic structures. The smaller primary operons *mms6op* (3 / 2) and *mamGFD-Cop* (2 / 1) showed a decreased complexity by one sub-operon under anoxic conditions. The most striking effect was observed for *mamABop*, in which the number of 36 sub-operons under oxic conditions decreased to only 13 under anoxic conditions. The same was observed in the case of *mamXYop*, where the number of sub-operons decreased from 6 to 3 sub-operons.

Discussion

Here, we employed a combination of various RNA-seq techniques to identify the transcriptional landscape, promoter structure and operon architecture of *M. gryphiswaldense* during anaerobic conditions favoring magnetosome formation. As expected, many of the upregulated genes are directly or indirectly linked to anaerobic respiration and most of these genes (23) have functions in various steps of denitrification. Determinants of aerobic respiration were also among the top upregulated genes in anoxic magnetic cells, such as the *cbb3* oxidase encoded by *ccoNOQP* operon. Besides encoding the primary cytochrome c terminal oxidase for aerobic respiration, *cbb3*-type oxidase was also linked to the redox balance control required for magnetosome biomineralization, which was severely impaired upon deletion [35]. By contrast, the *aa₃*-type cytochrome c oxidase encoded by *coxBAC* and *ctaG* with a suggested function in oxygen detoxification, but no role in magnetosome biosynthesis [35] was significantly downregulated, and the *bd*-type cytochrome c terminal oxidase encoded by *cydBA* did not show any differential expression. Additionally, we also found several genes involved in cytochrome c maturation and disulfide bond formation among upregulated genes. Since several key proteins involved in magnetosome biosynthesis are c-type

cytochromes exhibiting a unique so called “magnetochrome” fold [37, 38], regulation of the cytochrome c maturation system may affect magnetosome biosynthesis directly, in addition to the more indirect effects on many cytochrome c domain containing respiratory enzymes. Indeed, genetic impairment of cytochrome maturation resulted in aberrant magnetite crystal morphologies in a genome wide transposon mutagenesis screen [22]. The genes *dsbA* and *dsbB* are involved in the proper folding of periplasmic proteins through disulfide bond formation [65], but also have a suspected auxiliary function in magnetosomes biosynthesis [22]. For example, several magnetosome proteins, such as MamE/F/G/H/N/P/S/T/X/Z, contain more than two cysteines in their proposed luminal domains [66], rendering them putative substrates of DsbA and DsbB. In our analysis, the constitutive high expression of *dsbA* and *dsbB* (A-value 9–10) would agree with such an important function.

Genes for respiratory functions were also found enriched among the 77 upregulated genes in microoxic (0.5% dO₂) magnetic *M. gryphiswaldense* cells compared to semi-oxically grown cells (30% dO₂) by Wang and colleagues [28]. In the same study, 95 genes, involved in various generic cellular processes, were downregulated under 0.5% dO₂ compared to cells grown under 30% dO₂ [28]. The top upregulated *cycA_1* and putatively transcriptional regulators such as *crp_1* or *crp_3* identified in our study escaped detection in the previous study [28]. Furthermore, motility associated genes found to be highly regulated by Wang et al. [28], were not among the top-upregulated genes in our study. Since overlapping expression of aerobic and anaerobic key genes was observed under microoxic conditions [20], our comparison between highly controlled inhibitory oxic and fully anoxic conditions favoring highest magnetite biomineralization can be expected to reveal more pronounced regulatory differences between magnetic and non-magnetic cells, which likely explains the higher number of differentially expressed genes (300 up-, and 164 downregulated) identified in our study. Among them, several genes with so far unknown function, such as MSR1_19280, MSR1_19290 and MSR1_04470 represent novel candidates for respiration-linked genes, but as such might also be putatively involved in magnetosome biosynthesis because of their high upregulation in magnetic cells.

Hemerythrins were previously implicated in magnetosome biosynthesis because of their known function in oxygen sensing as well as iron transport in other bacteria [43]. In addition, the conspicuously high numbers of genes encoding bacteriohemerythrins present in the genome (26 copies), and in particular within the MAI of *M. gryphiswaldense* led to speculations about a possible function in magnetosome biosynthesis [42, 67]. Thus,

their upregulation in magnetic cells observed in our and a previous study [28] would be consistent with such a function, which however needs to be further investigated.

Regulation of magnetosome genes

A remarkable finding was that the magnetosome specific genes comprised within the *feoAB1op*, *mms5op*, *mms6op*, *mamGFDCop*, *mamABop* and *mamXYop* operons were among the most highly transcribed genes in the cell, comparable to, or even exceeding highly expressed housekeeping genes, such as those coding for DNA-polymerase subunits (*dnaE* and *dnaN*, A-value 12.2 and 12.1), as well as ribosomal proteins (*rplD* and *rplE*, A-values 13.0 and 11.4). The overall weak regulation of the majority of the *mam*- and *mms*-genes confirmed earlier studies, which suggested a constitutive expression of specific magnetosome biosynthesis genes [13, 28]. In addition, previous studies showed that key magnetosome proteins as well as empty magnetosome membrane vesicles were highly abundant in non-magnetic cells in which magnetite biomineralization was entirely suppressed by aerobic cultivation [13, 68]. Expression of the large *mamABop* encoding key functions in magnetosome membrane formation, assembly and crystal nucleation, remained largely unchanged at high expression levels between our tested conditions. Only *mms6op*, *feoAB1op* and *mms5op*, which are not essential, but have redundant or accessory function in iron transport or magnetite crystal size regulation, were upregulated in magnetic cells. The high and constitutive expression of magnetosome genes indicates that magnetosome biosynthesis is among the key cellular functions under all conditions. Thus, the absence of magnetite crystals in oxic cells cannot be explained by the lack or poor transcription of magnetosome specific proteins but instead possibly by abiotic direct oxidation of the cellular ferrous iron, thus disturbing the proper $\text{Fe}^{2+}/\text{Fe}^{3+}$ ratio required for magnetite precipitation, which cannot be compensated by the cellular reductase activities. Alternatively, or in addition, highly aerobic conditions may damage oxygen-sensitive cofactors important for the magnetite biomineralization, such as Fe-S-cluster containing respiratory enzymes, as observed by Imlay and colleagues in *E. coli* [69, 70].

Oxic conditions cause increasing transcriptional complexity

We found substantial differences in the number and position of TSSs between anoxic and oxic conditions, and to some degree, also between each of those and a previous study [18]. A higher number of TSSs (5200) was identified in oxic, non-magnetic cells vs. 5002 in anoxic magnetic cells. A possible reason for the increased number of TSS in oxic cells could be the compensation of instability

of long transcripts induced by reactive oxygen species, thus possibly ensuring transcription from additional sites within the operon. However, since we identified only a 4% difference in TSS-number between conditions with pooled replicates, it might be worth to clarify oxygen impact on transcriptional organization in future studies. Within the MAI, anoxic conditions also resulted in fewer TSSs than detected in the previous study [18], whereas under oxic conditions most of the previously detected TSSs were confirmed [18]. The absence of the previously detected intergenic TSS upstream of *mms36* [18] suggests that this TSS is only active under the rather undefined oxygen conditions used in the previous study [18], resulting in cells at diverse stages of growth.

Comparative analysis of global promoter structure

Under both anoxic and oxic conditions, conserved motifs at -35 (cTTGcc) and -10 regions (TATAaT) separated by an interspacing region of 11–20bp were detected. A similar promoter architecture was also identified in the σ^{70} -dependent promoters in other Alphaproteobacteria such as *Gluconobacter oxydans* [71], and with sequence similarity to the -35 (TTGACA) and -10 (TATAAT) motifs characteristic for the *E. coli* house-keeping sigma factor σ^{70} [72]. Thus, the vast majority of *M. gryphiswaldense* primary promoters during the investigated growth phase conditions is likely σ^{70} -dependent as well. The identification of conserved promoter structures also has practical implications. For instance, the *PmamDC₄₅* promoter driving transcription of the *mamGFDCop* shows a canonical σ^{70} promoter architecture with TTCGC for -35 region and TAAATT for -10 region separated by an approximately 20bp spacer, and a 6bp spacer to the corresponding TSS [13]. The high similarity between *PmamDC₄₅* sequence to the promoter motifs that we found to exhibit highest activity confirms that the *PmamDC₄₅* represents an appropriate promoter for high expression in *M. gryphiswaldense* [10, 53, 73].

Within the 5'-UTR we found a conserved aaGGAG motif serving as an RBS with in average 8 nt as spacer to the corresponding start codon in both oxic and anoxic datasets. This architecture resembles the optimized RBS (AGGAG followed by an 8 nt spacer) for expression in *M. gryphiswaldense*, which has been experimentally identified [10, 73]. Noteworthy, longer 5'-UTRs were more common in transcripts from oxic conditions, whereas significantly shorter 5'-UTRs were found under anoxic conditions. This may suggest a higher potential for regulation by cis-regulatory elements and is consistent with the increased transcriptional complexity in oxic cells, possibly suggesting an overall increased regulatory potential under these conditions. Our analysis of 5'-UTR for regulatory RNA structures, based on

the Rfam database, predicted new riboswitches in addition to the previously annotated ones in the most recent version of the *M. gryphiswaldense* genome [15]. New elements with a clear regulatory function, such as a glycine-riboswitch upstream of the glycine degradation system (*gcvTHPAPB*-operon), but also elements with so far unknown function were detected such as the BjrC80 sRNA upstream of hypothetical proteins. Although some new cis-regulatory elements were found, they only represent a relatively small fraction (2.5% of 5'-UTR length 150–300 nt under anoxic conditions) compared to the high number of long 5'-UTRs (26.7 [95% dO₂]/23% [0% dO₂]), suggesting that most regulators remain unidentified. Taken together, it seems that expression regulation under the tested conditions in *M. gryphiswaldense* is based to a significant degree on cis-regulatory elements like riboswitches as sensors for environmental cues, as suggested by the 5'-UTR length.

Conclusions

The transcriptome under conditions of highest magnetosome biosynthesis revealed an interplay between generic metabolic processes, such as anaerobic respiration, as well as increased biosynthesis and maturation of cytochrome c proteins and hemerythrins; some of these pathways have already been implicated in magnetosome biosynthesis. In addition, in highly magnetic cells, the transcriptional complexity is reduced compared to oxic, nonmagnetic cells. Furthermore, magnetosome genes mostly exhibit a constitutively high expression, which is only weakly affected by growth conditions.

Our study sheds light on the genome-wide complex transcriptional organization during magnetosome biosynthesis as a model for the formation of an intricate prokaryotic organelle with relevance for the research at system level. Furthermore, the insights can be used for engineering promoters as well as entire cellular pathways, thereby enabling rational design of synthetic magnetosome operons for targeted magnetosome production.

Materials and methods

Bacterial strains, culturing conditions and cell sampling

Magnetospirillum gryphiswaldense strain MSR-1 (DSM 6361) [74, 75] was cultivated in flask standard medium (FSM) comprising 10 mM 2-[4-(2-hydroxyethyl) piperazin-1-yl] ethanesulfonic acid (HEPES) (pH 7.0), 15 mM potassium lactate, 4 mM NaNO₃, 0.74 mM KH₂PO₄, 0.6 mM MgSO₄ × 7H₂O, 50 μM iron citrate, 3 g L⁻¹ soy peptone and 0.1 g L⁻¹ yeast extract.

Cells used for RNA isolation and cDNA library preparation were cultivated in a stirred-tank 3 L bioreactor (BioFlo™ 320, Eppendorf Bioprocess, Jülich, Germany) equipped with an InPro3253i (Mettler-Toledo,

Columbus, USA) pH probe and an InPro6850i (Mettler-Toledo, Columbus, USA) O₂ sensor, according to the previously established oxystat fermentation regime [26]. Briefly, the seed-train encompassed two passages in 10 mL FSM in 15 mL conical centrifugation tubes at room temperature for 40 h after inoculation from 4 °C stock cultures. Afterwards, stepwise scale-up was performed in screw-capped bottles with subsequent cultivation in 30 mL preculturing medium (FSM with 150 μM iron citrate and 1 g L⁻¹ soy peptone) at room temperature for 40 h followed by a second preculturing step with 300 mL preculturing medium at 28 °C for 16 h with slightly unscrewed lid for air exchange. For the second step, the incubation was performed at 120 rpm in an orbital shaking incubator, which were then used for inoculation of the bioreactor.

Oxystat fermentations were conducted under oxic (95% dO₂), microoxic (1% dO₂) and anoxic (0% dO₂) in large-scale medium (LSM) comprising 15 mM potassium lactate, 4 mM NaNO₃, 0.74 mM KH₂PO₄, 0.6 mM MgSO₄ × 7H₂O, 150 μM iron citrate, 3 g L⁻¹ soy peptone and 0.1 g L⁻¹ yeast extract. For anaerobic fermentations, the medium was supplemented with additional sodium nitrate to 10 mM to further prolong the main growth phase. Prior to inoculation of the microoxic and anoxic processes, oxygen was gassed out with nitrogen. During microoxic and oxic fermentations dO₂ was controlled by automated adjustment of agitation (100–300 rpm) and airflow (0–10 SLPM) with compressed air [26]. For anoxic conditions, the medium was continuously sparged with 0.2 standard liter per minute (SLPM) nitrogen to prevent oxygen diffusion into the system and agitation was kept constant at 100 rpm.

Cells were harvested during main growth phase by pumping 400 mL of the fermentation broth through an ice cooled silicon tube for quick cooling to 4 °C. Subsequently the cells were pelleted at 8300 g and 4 °C for 10 min using a Sorvall RC-5B Plus centrifuge (Thermo Fisher Scientific, Waltham, USA) and shock-frozen with liquid nitrogen. The cell pellets were then shipped on dry ice to Vertis Biotechnologie AG (Freising) for RNA isolation, library preparation and sequencing.

Cell growth and magnetic response

Both optical density (OD) as measure for cell growth and magnetic response were measured with an Ultrospec2000 pro spectrophotometer at 565 nm. The magnetic response was measured according to Schüler et al., 1995 [30]. Briefly, cells were magnetically aligned perpendicular and vertical to the light beam of a photometer resulting in a change of the OD₅₆₅. The ratio of maximal and minimal scattering intensities subtracted by 1 (C_{mag})

represents the magnetic response of the cells as estimation for magnetosome biomineralization.

RNA isolation, cDNA library preparations and sequencing

The RNA isolation, cDNA library preparation and sequencing were performed by Vertis Biotechnologie AG (Freising). Different RNA-seq techniques were employed, such as 3'-end sequencing [32], whole transcriptome shotgun sequencing (WTSS) and Cappable-sequencing [31].

For the elucidation of genome wide transcription initiation, expression coverage and transcription termination, Cappable-seq [31], whole transcriptome shotgun sequencing (WTSS) and 3'-end sequencing [32] techniques were applied, respectively.

Total RNA was isolated from samples using the mirVana RNA isolation kit (Thermo Fisher Scientific, Waltham, USA) followed by a DNase treatment step. RNA quality was checked by capillary electrophoresis.

For the identification of transcription start sites (TSS), the extracted RNA of the oxic and anoxic triplicates were pooled resulting in two pooled RNA samples for primary 5'-end enrichment by using a modified version of the Cappable-sequencing technique [31]. Briefly, 5' triphosphorylated RNA was capped with 3'-desthiobiotin-TEG-guanosine 5' triphosphate (DTBGTP) (New England Biolabs, Ipswich, USA) facilitated by the vaccinia capping enzyme (New England Biolabs, Ipswich, USA). For enrichment of the primary 5'-ends, the biotinylated RNA was applied to a streptavidin column, washed and eluted. An uncapped control was also applied to the column to check for unspecific binding to the column matrix. Subsequently, the sequencing adapter ligation, reverse transcription and PCR amplification of the cDNA were performed according to TrueSeq Stranded mRNA library instructions (Illumina, San Diego, USA).

The WTSS library preparation was performed for biological triplicates of the four investigated conditions and a pooled RNA sample of all extracted RNAs. The ribosomal RNA was then depleted by an in-house protocol (Vertis Biotechnologie AG, Freising, Germany) for the 13 RNA samples. The remaining mRNA was purified using the Agencourt AMPure XP kit (Beckman Coulter Genomics, Chaska, USA) and quality checked by capillary electrophoresis. Fragmentation of the mRNA, reverse transcription, adapter ligation and PCR amplification were performed according to TrueSeq Stranded mRNA library instructions (Illumina, San Diego, USA).

For the 3'-end library preparation a 3' Illumina sequencing adapter was ligated to the 3'-OH ends of the rRNA depleted RNA sample prior to reverse transcription, cDNA fragmentation, sequencing adapter ligation

and cDNA purification using the Agencourt AMPure XP kit (Beckman Coulter Genomics, Chaska, USA).

All cDNA libraries (in total 15 libraries) were single-end sequenced on an Illumina NextSeq 500 system (Illumina, San Diego, USA) using 1×75 bp read length.

Bioinformatic methods

Read mapping and visualization

The sequencing reads from all 15 libraries were trimmed for sequencing adapters and low-quality bases before mapping to the current *M. gryphiswaldense* genome (Accession No. CP027526) using the CLC Bio's Genomic Workbench software package (Qiagen, Venlo, Netherlands) with a mapping efficiency between 93 to 98% (Table S1). The resulting datasets were then visualized and investigated with ReadXplorer [64].

Transcriptional start site detection and motif analysis

Transcriptional start sites (TSS) were automatically detected with the Cappable-seq tools [31]. Briefly, the relative read score (RRS) is calculated for both Cappable-seq datasets by normalizing the read coverage for each base in the reference genome to the sequencing depth. Subsequently, the enrichment score for the corresponding position is calculated according to the formular enrichment score = $\log_2(\text{RRS}/\text{RRS}_{\text{control}})$, where $\text{RRS}_{\text{control}}$ is the relative read score in the control library at the same genomic position as in the TSS enriched library. After empirical testing, the optimal threshold for highly specific TSS detection was determined with 2.5 for both datasets (oxic and anoxic conditions). Afterwards, the identified TSS were classified based on the localization in the genome by using an automated in-house script.

For identification of the conserved σ^{70} -promoter motives, sequences 70bp upstream of the assigned pTSSs were extracted and taken as input for the motif-analysis software Improbizer [58]. To identify the consensus sequence of the ribosome binding site (RBS) the region 20bp upstream of the translation start site (TLS) assigned to a pTSS was analyzed by Improbizer.

The identified consensus sequences for the -10 and -35-region were visualized with WebLogo 3 [59].

Elucidation of operon structure

The operon detection was performed with the automated prediction tool implemented in ReadXplorer [64]. When at least three reads connecting two coding sequences were counted the corresponding genes were assigned into a primary operon. This process was continued for the following genes until no more genes could be assigned to that operon.

Sub-operons were assigned, when a TSS (pTSS or iTSS) was identified within a primary operon.

Differential gene expression analysis

Prior to differential expression analysis, the reads of the replicates were normalized by transcripts per kilobase million (TPM) [76] and checked by Pearson correlation coefficient (R^2) to ensure the suitability for comparison. All replicates among each condition show R^2 -values above 0.8 indicating the high consistency among the different experiments (Table S2). Differential expression analysis was conducted with the whole transcriptome datasets cells grown under different growth conditions described under 'Bacterial strains, culturing conditions and cell sampling'. The reads mapped to genes of three biological replicates per condition were counted by the implemented tool in the ReadXplorer software and tested for differential expression with DESeq2 [77] using default settings. In case the false discovery corrected p -value was below 0.01, the corresponding gene was considered as differentially expressed under the compared conditions.

Supplementary Information

The online version contains supplementary material available at <https://doi.org/10.1186/s12864-022-08913-x>.

Additional file 1: Figure S1. Cell growth and magnetic response (C_{mag}) under **A)** anoxic (dO₂ 0%, 10 mM nitrate), **B)** oxic (dO₂ 95%, 4 mM ammonium), **C)** microoxic (dO₂ 1%, 4 mM nitrate), **D)** oxic with nitrate (dO₂ 95%, 4 mM nitrate) conditions. (Scale bar 1 μ m). Growth (black and grey lines) and C_{mag} (colored lines) were depicted for each replicate (circles, diamonds and triangles). The black arrow indicates the sampling timepoint for the RNA-seq experiments.

Additional file 2: Table S3. List of top 41 up- and downregulated genes under anoxic in comparison to oxic conditions.

Additional file 3: Figure S3. Comparison between promoter motives of TSS located within (inMAI) and outside (exMAI) of the magnetosome island, cultivated under anoxic (0% dO₂) and oxic (95% dO₂) conditions. The motif logos were created with Weblogo [58].

Additional file 4: Figure S2. Distribution of classified transcription start sites (TSS) under anoxic (0% dO₂) and oxic (95% dO₂) conditions in the whole genome (pTSS, primary TSS; aTSS, antisense TSS; iTSS, intragenic TSS; oTSS; other TSS).

Additional file 5: Table S1. Mapping statistics of the different RNA-seq datasets including the three library preparation techniques, namely Cappable-seq, whole transcriptomic shotgun sequencing and term-seq sequencing.

Additional file 6: Table S2. Pearson correlation coefficients R^2 of the biological replicates.

Acknowledgments

We thank Matthias Völkl for contributing some of the produced data as part of his Master's theses at the Department of Microbiology and the Chair for Process Biotechnology (University of Bayreuth).

Authors' contributions

DS and CNR conceived the study. CNR, RF and VJ designed and performed the fermentation experiments for sample preparation. CNR, MW, TB, JK carried out the transcriptome analysis. CNR and DS wrote the manuscript. All authors read and approved the final manuscript.

Funding

Open Access funding enabled and organized by Projekt DEAL. We gratefully acknowledge financial support from the Deutsche Forschungsgemeinschaft (INST 91/374–1 LAGG to D.S.), the European Research Council (ERC) under the European Union's Horizon 2020 research and innovation program (Grant No.692637 to D.S.) and the Federal Ministry of Education and Research (BMBF) (Grant MagBioFab to R.U. and D.S.).

Availability of data and materials

The data discussed in this publication have been deposited in NCBI's Gene Expression Omnibus and are accessible through GEO Series accession number GSE197098, <https://www.ncbi.nlm.nih.gov/geo/query/acc.cgi?acc=GSE197098>.

Declarations

Ethics approval and consent to participants

Not applicable.

Consent for publication

Not applicable.

Competing interests

The authors declare that they have no competing interests.

Author details

¹Department of Microbiology, University of Bayreuth, Bayreuth, Germany.

²Center for Biotechnology (CeBITec), University of Bielefeld, Bielefeld, Germany.

³Chair for Process Biotechnology, University of Bayreuth, Bayreuth, Germany.

Received: 23 February 2022 Accepted: 23 September 2022

Published online: 10 October 2022

References

- Lefèvre CT, Bazylinski DA. Ecology, diversity, and evolution of magnetotactic bacteria. *Microbiol Mol Biol Rev.* 2013;77:497–526.
- Uebe R, Schüler D. Magnetosome biogenesis in magnetotactic bacteria. *Nat Rev Microbiol.* 2016;14:621–37.
- McCausland HC, Komeili A. Magnetic genes: studying the genetics of biomineralization in magnetotactic bacteria. *PLoS Genet.* 2020;16:e1008499.
- Mériaux S, Boucher M, Marty B, Lalatonne Y, Prévéral S, Motte L, et al. Magnetosomes, biogenic magnetic nanomaterials for brain molecular imaging with 17.2 T MRI scanner. *Adv Healthc Mater.* 2015;4:1076–83.
- Hergt R, Hiergeist R, Zeisberger M, Schüler D, Heyen U, Hilger I, et al. Magnetic properties of bacterial magnetosomes as diagnostic and therapeutic tools. *J Magn Magn Matter.* 2005;293:80–6.
- Alphandéry E, Guyot F, Chebbi I. Preparation of chains of magnetosomes, isolated from *Magnetospirillum magneticum* strain AMB-1 magnetotactic bacteria, yielding efficient treatment of tumors using magnetic hyperthermia. *Int J Pharm.* 2012;434:444–52.
- Gandia D, Gandarias L, Rodrigo I, Robles-García DR, Garaio E, García JA, et al. Unlocking the potential of magnetotactic bacteria as magnetic hyperthermia agents. *Small.* 2019;15:1902626.
- Vargas G, Cypriano J, Correa T, Leão P, Bazylinski DA, Abreu F. Applications of magnetotactic bacteria, magnetosomes and magnetosome crystals in biotechnology and nanotechnology: Mini-review. *Molecules.* 2018;23:2438.
- Mickoleit F, Jérôme V, Freitag R, Schüler D. Bacterial magnetosomes as novel platform for the presentation of immunostimulatory, membrane-bound ligands in cellular biotechnology. *Adv Biosys.* 2020;4:1900231.
- Mickoleit F, Lanzloth C, Schüler D. A versatile toolkit for controllable and highly selective multifunctionalization of bacterial magnetic nanoparticles. *Small.* 2020;16:1906922.
- Schüler D, Monteil CL, Lefèvre CT. *Magnetospirillum gryphiswaldense*. *Trends Microbiol.* 2020;28:947–8.
- Barber-Zucker S, Keren-Khadmy N, Zarivach R. From invagination to navigation: the story of magnetosome-associated proteins in magnetotactic bacteria. *Protein Sci.* 2015;25:338–51.

13. Schübbe S, Würdemann C, Heyen U, Wawer C, Peplies J, Glöckner FO, et al. Transcriptional organization and regulation of magnetosome operons in *Magnetospirillum gryphiswaldense*. *Appl Environ Microbiol*. 2006;72:757–65.
14. Ullrich S, Kube M, Schübbe S, Reinhardt R, Schüler D. A hypervariable 130 kb genomic region of *Magnetospirillum gryphiswaldense* comprises a magnetosome island, which undergoes frequent rearrangements during stationary growth. *J Bacteriol*. 2005;187:7176–84.
15. Uebe R, Schüler D, Jogler C, Wiegand S. Reevaluation of the complete genome sequence of *Magnetospirillum gryphiswaldense* MSR-1 with single-molecule real-time sequencing data. *Genome Announc*. 2018;6:e00309–18.
16. Kolinko I, Lohße A, Borg S, Raschdorf O, Jogler C, Tu Q, et al. Biosynthesis of magnetic nanostructures in a foreign organism by transfer of bacterial magnetosome gene clusters. *Nat Nanotech*. 2014;9:193–7.
17. Dziuba MV, Zwiener T, Uebe R, Schüler D. Single-step transfer of biosynthetic operons endows a non-magnetotactic *Magnetospirillum* strain from wetland with magnetosome biosynthesis. *Environ Microbiol*. 2020;22:1603–18.
18. Dziuba M, Riese CN, Wittchen M, Borgert L, Busche T, Kalinowski J, et al. *mSystems*. 2021;6:e00893–21 Epub 2021 Sep 14.
19. Lohße A, Borg S, Raschdorf O, Kolinko I, Tompa É, Pósfai M, et al. Genetic dissection of the *mamAB* and *mms6* operons reveals a gene set essential for magnetosome biogenesis in *Magnetospirillum gryphiswaldense*. *J Bacteriol*. 2014;196:2658–69.
20. Li Y, Katzmann E, Borg S, Schüler D. The periplasmic nitrate reductase nap is required for anaerobic growth and involved in redox control of magnetite biomineralization in *Magnetospirillum gryphiswaldense*. *J Bacteriol*. 2012;194:4847–56.
21. Li Y, Bali S, Borg S, Katzmann E, Ferguson SJ, Schüler D. Cytochrome cd1 nitrite reductase NirS is involved in anaerobic magnetite biomineralization in *Magnetospirillum gryphiswaldense* and requires NirN for proper d1 heme assembly. *J Bacteriol*. 2013;195:4297–309.
22. Silva KT, Schüler M, Mickoleit F, Zwiener T, Müller FD, Awal RP, et al. Genome-wide identification of essential and auxiliary gene sets for magnetosome biosynthesis in *Magnetospirillum gryphiswaldense*. *mSystems*. 2020;5:1–20.
23. Schüler D, Baeuerlein E. Iron-limited growth and kinetics of iron uptake in *Magnetospirillum gryphiswaldense*. *Arch Microbiol*. 1996;166:301–7.
24. Schüler D, Baeuerlein E. Dynamics of iron uptake and Fe₃O₄ biomineralization during aerobic and microaerobic growth of *Magnetospirillum gryphiswaldense*. *J Bacteriol*. 1998;180:159–62.
25. Heyen U, Schüler D. Growth and magnetosome formation by microaerophilic *Magnetospirillum* strains in an oxygen-controlled fermentor. *Appl Microbiol Biotechnol*. 2003;61:536–44.
26. Riese CN, Uebe R, Rosenfeldt S, Schenk AS, Jérôme V, Freitag R, et al. An automated oxystat fermentation regime for microoxic cultivation of *Magnetospirillum gryphiswaldense*. *Microb Cell Factories*. 2020;19:206.
27. Würdemann C, Peplies J, Schübbe S, Ellrott A, Schüler D, Glöckner FO. Evaluation of gene expression analysis using RNA-targeted partial genome arrays. *System Appl Microbiol*. 2006;29:349–57.
28. Wang X, Wang Q, Zhang Y, Wang Y, Zhou Y, Zhang W, et al. Transcriptome analysis reveals physiological characteristics required for magnetosome formation in *Magnetospirillum gryphiswaldense* MSR-1. *Environ Microbiol Rep*. 2016;8:371–81.
29. Wang Q, Wang X, Zhang W, Li X, Zhou Y, Li D, et al. Physiological characteristics of *Magnetospirillum gryphiswaldense* MSR-1 that control cell growth under high-iron and low-oxygen conditions. *Sci Rep*. 2017;7:2800.
30. Schüler D, Uhl R, Baeuerlein E. A simple light-scattering method to assay magnetism in *Magnetospirillum gryphiswaldense*. *FEMS Microbiol Lett*. 1995;132:139–45.
31. Ettwiller L, Buswell J, Yigit E, Schildkraut I. A novel enrichment strategy reveals unprecedented number of novel transcription start sites at single base resolution in a model prokaryote and the gut microbiome. *BMC Genomics*. 2016;17:1–14.
32. Dar D, Shamir M, Mellin JR, Koutero M, Stern-Ginossar N, Cossart P, et al. Term-seq reveals abundant ribo-regulation of antibiotics resistance in bacteria. *Science*. 2016;352:aad9822.
33. Bartnikas TB, Wang Y, Bobo T, Veselov A, Scholes CP, Shapleigh JP. Characterization of a member of the NnrR regulon in *Rhodobacter sphaeroides* 2.4.3 encoding a heme-copper protein. *Microbiol*. 2002;148:825–33.
34. Li Y. Redox control of magnetosome biomineralization. *J Oceanol Limnol*. 2021. <https://doi.org/10.1007/s00343-021-0422-5>.
35. Li Y, Raschdorf O, Silva KT, Schüler D. The terminal oxidase cbb3 functions in redox control of magnetite biomineralization in *Magnetospirillum gryphiswaldense*. *J Bacteriol*. 2014;196:2552–62.
36. Li Y, Sabaty M, Borg S, Silva KT, Pignol D, Schüler D. The oxygen sensor MgFnr controls magnetite biomineralization by regulation of denitrification in *Magnetospirillum gryphiswaldense*. *BMC Microbiol*. 2014;14:153.
37. Siponen MI, Adryanczyk G, Ginet N, Arnoux P, Pignol D. Magnetochrome: a c-type cytochrome domain specific to magnetotactic bacteria. *Biochem Soc Trans*. 2012;40:1319–23.
38. Arnoux P, Siponen MI, Lefevre CT, Ginet N, Pignol D. Structure and evolution of the magnetochrome domains: no longer alone. *Front Microbiol*. 2014;5:117.
39. Erlenstsson LS, Acheson RM, Hederstedt L, Le Brun NE. *Bacillus subtilis* resA is a thiol-disulfide oxidoreductase involved in cytochrome c synthesis. *J Biol Chem*. 2003;278:17852–8.
40. Sanders C, Turkarslan S, Lee D-W, Daldal F. Cytochrome c biogenesis: the Ccm system. *Trends Microbiol*. 2010;18:266–74.
41. Hatahet F, Boyd D, Beckwith J. Disulfide bond formation in prokaryotes: history, diversity and design. *Biochim Biophys Acta*. 2014;1844:1402–14.
42. French CE, Bell JML, Ward FB. Diversity and distribution of hemerythrin-like proteins in prokaryotes. *FEMS Microbiol Lett*. 2007;279:131–45.
43. Alvarez-Carreño C, Alva V, Becerra A, Lazcano A. Structure, function and evolution of the hemerythrin-like domain superfamily. *Protein Sci*. 2018;27:848–60.
44. Jordan LD, Zhou Y, Smallwood CR, Lill Y, Ritchi K, Yip WT, et al. Energy-dependent motion of TonB in the gram-negative bacterial inner membrane. *PNAS*. 2013;110:11553–8.
45. Faivre D, Böttger L, Matzanke B, Schüler D. Intracellular magnetite biomineralization in bacteria proceeds via a distinct pathway involving membrane-bound ferritin and ferrous iron species. *Angew Chem Int Ed*. 2007;46:8647–52.
46. Uebe R, Ahrens F, Stang J, Boettger JK, L, Schmidt C, Matzanke B and Schüler D. Bacterioferritin of *Magnetospirillum gryphiswaldense* is a heterotetraicosameric complex composed of functionally distinct subunits but is involved in magnetite biomineralization. *mBio*. 2019;30:e02795–18.
47. Dartigalongue C, Missiakas D, Raina S. Characterization of the *Escherichia coli* σ^E regulon. *J Biol Chem*. 2001;276:20866–75.
48. Rhodius VA, Suh WC, Nonaka G, West J, Gross CA. Conserved and variable functions of the σ^E stress response in related genomes. *PLoS Biol*. 2006;4:e2.
49. Arakaki A, Webbs J, Matsunaga T. A novel protein tightly bound to bacterial magnetite particles in *Magnetospirillum magnetotacticum* strain AMB-1. *J Biol Chem*. 2003;278:8745–50.
50. Rawlings AE, Bramble JP, Walker R, Bain J, Galloway JM, Staniland SS. Self-assembled MmsF proteinosomes control magnetite nanoparticle formation in vitro. *Proc Natl Acad Sci U S A*. 2014;111:16094–9.
51. Arakaki A, Yamagishi A, Fukuyo A, Tanaka M, Matsunaga T. Co-ordinated functions of mms proteins define the surface structure of cubo-octahedral magnetite crystals in magnetotactic bacteria. *Mol Microbiol*. 2014;93:554–67.
52. Scheffel A, Gärdes A, Grünberg K, Wanner G, Schüler D. The major magnetosome proteins MamGFDC are not essential for magnetite biomineralization in *Magnetospirillum gryphiswaldense*, but regulate the size of magnetosome crystals. *J Bacteriol*. 2008;190:377–86.
53. Raschdorf O, Müller FD, Pósfai M, Plietzko JM, Schüler D. The magnetosome proteins MamX, MamZ, and MamH are involved in redox control of magnetite biomineralization in *Magnetospirillum gryphiswaldense*. *Mol Microbiol*. 2013;89:872–86.
54. Müller FD, Raschdorf O, Nudelmann H, Messerer M, Katzmann E, Plietzko JM, et al. The FtsZ-like protein FtsZm of *M. gryphiswaldense* likely interacts with its generic FtsZ homolog and is required for biomineralization under nitrate deprivation. *J Bacteriol*. 2014;196:650–9.
55. Toro-Nahuelpan M, Giacomelli G, Raschdorf O, Borg S, Plietzko JM, Bramkamp M, et al. MamY is a membrane-bound protein that aligns magnetosomes and the motility axis of helical magnetotactic bacteria. *Nat Microbiol*. 2019;4:1978–89.
56. Rong C, Zhang C, Zhang Y, Qi L, Yang J, Guan G, et al. FeoB2 functions in magnetosome formation and oxidative stress protection in *Magnetospirillum gryphiswaldense* strain MSR-1. *J Bacteriol*. 2012;194:3972–6.

57. Lau CKY, Krewulak KD, Vogel HJ. Bacterial ferrous iron transport: the *feo* system. *FEMS Microbiol Rev.* 2015;40:273–9.
58. Ao W, Gaudet J, Kent WJ, Muttumu S, Mango SE. Environmentally induced foregut remodeling by PHA-4/FoxA and DAF-12/NHR. *Science.* 2004;305:1743–6.
59. Crooks GE, Hon G, Chandonia J-M, Brenner SE. WebLogo: A sequence logo generator. *Genome Res.* 2004;14:1188–90.
60. Winkler WC, Breaker RR. Regulation of bacterial gene expression by riboswitches. *Ann Rev Microbiol.* 2005;59:487–517.
61. Meyer MM. The role of mRNA structure in bacterial translational regulation. *WIREs RNA.* 2017;8:e1370.
62. Kalvari I, Nawrocki EP, Argasinska J, Quinones-Olvera N, Finn RD, Bateman A, et al. Non-coding RNA analysis using the Rfam database. *Curr Protoc Bioinformatics.* 2018;62:e51.
63. Kalvari I, Nawrocki EP, Ontiveros-Palacios N, Argasinska J, Lamkiewicz K, Marz M, et al. Rfam 14: expanded coverage of metagenomic, viral and microRNA families. *Nucleic Acids Res.* 2020;49:D192–200.
64. Hilker R, Stadermann KB, Doppmeier D, Kalinowski J, Stoye J, Straube J, et al. ReadXplorer—visualization and analysis of mapped sequences. *Bioinformatics.* 2014;30:2247–54.
65. Landeta C, Boyd D, Beckwith J. Disulfide bond formation in prokaryotes. *Nat Microbiol.* 2018;3:270–80.
66. Nudelman H, Zarivach R. Structure prediction of magnetosome associated proteins. *Front Microbiol.* 2014;5:9.
67. Frankel RB, Bazylinski DA. Magnetosomes and magneto-aerotaxis. *Contrib Microbiol.* 2009;16:182–93.
68. Raschdorf O, Forstner Y, Kolinko I, Uebe R, Pitzko JM, Schüler D. Genetic and ultrastructural analysis reveals the key players and initial steps of bacterial magnetosome membrane biogenesis. *PLoS Genet.* 2016;12:e1006101.
69. Imlay JA. The molecular mechanisms and physiological consequences of oxidative stress: lessons from a model bacterium. *Nat Rev Microbiol.* 2013;11:443–54.
70. Khademian M, Imlay JA. How microbes evolved to tolerate oxygen. *Trends Microbiol.* 2020;29:428–40.
71. Kranz A, Busche T, Vogel A, Usadel B, Kalinowski J, Bott M, et al. RNAseq analysis of α -proteobacterium *Gluconobacter oxydans* 621H. *BMC Genomics.* 2018;19:24.
72. Ruff EF, Record MT, Artsimovitch I. Initial events in bacterial transcription initiation. *Biomolecules.* 2015;5:1035–62.
73. Borg S, Hofmann J, Pollithy A, Lang C, Schüler D. New vectors for chromosomal integration enable high-level constitutive or inducible magnetosome expression of fusion proteins in *Magnetospirillum gryphiswaldense*. *Appl Environ Microbiol.* 2014;80:2609–16.
74. Schleifer KH, Schüler D, Spring S, Weizenegger M, Amann R, Ludwig W, et al. The genus *Magnetospirillum* gen. nov. description of *Magnetospirillum gryphiswaldense* sp. nov. and transfer of *Aquaspirillum magnetotacticum* to *Magnetospirillum magnetotacticum* comb. nov. *Syst Appl Microbiol.* 1991;14:379–85.
75. Schüler D, Köhler M. The isolation of a new magnetic spirillum. *Zentralbl Mikrobiol.* 1992;147:150–1.
76. Li B, Ruotti V, Stewart RM, Thomson JA, Dewey CN. RNA-Seq gene expression estimation with read mapping uncertainty. *Bioinformatics.* 2009;26:493–500.
77. Love MI, Huber W, Anders S. Moderated estimation of fold change and dispersion for RNA-seq data with DESeq2. *Genome Biol.* 2014;15:550.

Publisher's Note

Springer Nature remains neutral with regard to jurisdictional claims in published maps and institutional affiliations.

Ready to submit your research? Choose BMC and benefit from:

- fast, convenient online submission
- thorough peer review by experienced researchers in your field
- rapid publication on acceptance
- support for research data, including large and complex data types
- gold Open Access which fosters wider collaboration and increased citations
- maximum visibility for your research: over 100M website views per year

At BMC, research is always in progress.

Learn more biomedcentral.com/submissions



Danksagung

An erster Stelle möchte ich mich ganz besonders bei Prof. Dr. Dirk Schüler für die Betreuung und Unterstützung während der Doktorarbeit bedanken. Die Freiheiten, die ich genießen durfte, haben es mir ermöglicht sowohl fachlich, als auch persönlich zu wachsen.

Ich möchte mich auch bei Prof. Dr. Ruth Freitag für die Übernahme des Zweitgutachtens und die produktive Zusammenarbeit bedanken. Dr. Valérie Jérôme möchte ich in diesem Zuge ebenfalls für die produktive und angenehme Zusammenarbeit danken. Ich habe während dieser Kooperation vieles über Produktionstechnik im Labor- und Pilotmaßstab lernen dürfen. Insbesondere hat mich die GMP-Vorlesung auf die vielfältigen Karrierechancen in der Pharmaziebranche aufmerksam gemacht, in welcher ich mich nun sehr gut aufgehoben fühle.

Prof. Dr. Jörn Kalinowski und Dr. Tobias Busche von der Universität Bielefeld möchte ich für die erfolgreiche Kooperation im Bereich der Transkriptomanalyse danken. Insbesondere möchte ich Dr. Manuel Wittchen danken, der mir mit Rat und Tat zur Seite stand und mir sehr geholfen hat, die Datenflut zu ordnen.

Prof. Dr. Anna Schenk und Dr. Sabine Rosenfeldt danke ich für die Einführung in die Kleinwinkel-Röntgenstreuung und die fruchtbare Zusammenarbeit. Mir hat die Thematik sehr viel Freude bereitet, da ich über den eigenen Tellerrand hinausschauen und Einblicke in die physikalische Chemie erlangen konnte.

Selbstverständlich möchte ich mich auch beim gesamten „Magnetolab“ für die schöne Zeit und bedanken. Insbesondere möchte ich meinen Kollegen Prof. Dr. René Uebe, Dr. Marina Dziuba und Dr. Frank Mickoleit für die wissenschaftlichen Diskussionen und die hervorragende Zusammenarbeit danken, ohne die diese Arbeit nicht möglich gewesen wäre. Besonderer Dank gebührt Matthias Völkl, Sophia Tessaro, Alexander Knöchel, Paul Jorzik und Dennis Weigel, die durch ihre Abschlussarbeiten zu dieser Dissertation beigetragen haben.

Bei meiner Familie möchte ich mich ganz besonders für die Unterstützung während der Dissertation bedanken. Insbesondere meiner Mutter Renate Riese und meiner Schwester Carolin Riese gebührt besonderer Dank für die Aufmunterung und Unterstützung in den stressigen Phasen der Arbeit.

Ich widme diese Arbeit meinem Vater Franz-Wolfgang Riese, der schon früh meine Begeisterung für die Biologie geweckt hat und meinem Großvater Dr. Heino Schaefer, der mich stets auf meinem Weg unterstützte.

(Eidesstattliche) Versicherungen und Erklärungen

(§ 8 Satz 2 Nr. 3 PromO Fakultät)

Hiermit versichere ich eidesstattlich, dass ich die Arbeit selbstständig verfasst und keine anderen als die von mir angegebenen Quellen und Hilfsmittel benutzt habe (vgl. Art. 64 Abs. 1 Satz 6 BayHSchG).

(§ 8 Satz 2 Nr. 3 PromO Fakultät)

Hiermit erkläre ich, dass ich die Dissertation nicht bereits zur Erlangung eines akademischen Grades eingereicht habe und dass ich nicht bereits diese oder eine gleichartige Doktorprüfung endgültig nicht bestanden habe.

(§ 8 Satz 2 Nr. 4 PromO Fakultät)

*Hiermit erkläre ich, dass ich Hilfe von gewerblichen Promotionsberatern bzw. –
vermittlern oder ähnlichen Dienstleistern weder bisher in Anspruch genommen
habe noch künftig in Anspruch nehmen werde.*

(§ 8 Satz 2 Nr. 7 PromO Fakultät)

*Hiermit erkläre ich mein Einverständnis, dass die elektronische Fassung der
Dissertation unter Wahrung meiner Urheberrechte und des Datenschutzes einer
gesonderten Überprüfung unterzogen werden kann.*

(§ 8 Satz 2 Nr. 8 PromO Fakultät)

*Hiermit erkläre ich mein Einverständnis, dass bei Verdacht wissenschaftlichen
Fehlverhaltens Ermittlungen durch universitätsinterne Organe der
wissenschaftlichen Selbstkontrolle stattfinden können.*

.....
Ort, Datum, Unterschrift